Republic of Iraq

Ministry of Higher Education and Scientific Research

University of Kerbala

Collage of Engineering

Department of Civil Engineering

Numerical Study of Optimum Pier Shape for Safe Bridge

A thesis
Submitted in Partial Fulfilment of the Requirements of University of Kerbala for the Degree of Master of Science in Infrastructure Engineering

By

Halah Kais Jalal

B.Sc. in Civil Engineering, (2016)

Supervised by

Prof. Dr. Waqed H. Hassan

September 2019   **Muharram 1441**

بِسْمِ اللَّهِ الرَّحْمٰنِ الرَّحِيمِ

يَرْفَعِ اللَّهُ الَّذِينَ آمَنُوا مِنكُمْ وَالَّذِينَ أُوتُوا الْعِلْمَ دَرَجَاتٍ

صدق الله العلي العظيم

(المجادلة: من الآية 11)

SUPERVISOR CERTIFICATE

I certify that the thesis entitled " **Optimum Hydraulic Design of Pier for Safe Bridges"** prepared by **Halah Kais Jalal**, has been carried out completely under our supervision at College of Engineering, University of Kerbala, in partial fulfillment of the requirements for the Degree of Master of Science in Infrastructure Engineering.

Signature:

Prof. Dr. **Waqed H. Hassan**

Date: /   / 20

LINGUISTIC CERTIFICATE

I certify that the thesis entitled " **Optimum Hydraulic Design of Pier for Safe Bridges"** which has been submitted by **Halah Kais Jalal** has been proofread and its language has been amended to meet the English style.

Signature:

Name: Muhammad Abdulredha

Proofreader

Civil Engineering / Collage of Engineering / Department University of Kerbala

Date: /   / 20

CERTIFICATE OF EXAMINATION COMMITTEE

As members of the Final Examination Committee, we certify that we have read the Thesis prepared by **"Halah Kais Jalal"**, entitled **"Numerical Study of Optimum Pier Shape for Safe Bridge"** and recommend that it be accepted as fulfilling the Thesis requirement for the Degree of Master of Science in Infrastructure Engineering.

Supervisor
Signature: Waqed H. H
Prof. Dr. Waqed H. Hassan
Date: / 3 / 2020

Member
Signature: Riyadh Alsaadi
Dr. Riyadh J. M. Al-Saadi
Date: / 3 / 2020

Member
Signature: Fadil M. Duhir
Prof. Dr. Fadhil M. Duhir
Date: / 3 / 2020

Chairman
Signature:
Prof. Dr. Basim K.Nile
Date: / 3 / 2020

Approval of Head of Civil Engineering Department

Signature:
Dr. Raid R. A. Almuhanna
Date: / 3 / 2020

Approval of Deanery of the College of Engineering, University of Kerbala

Signature: L. Sh.Rasl
Asist.Prof.Dr. Laith Shakir Rasheed
Date: / 3 / 2020

Dedication

This thesis is dedicated to my parents who supported me mentally and emotionally throughout my study process. They were the driving force behind my passion to learn and expand my knowledge and I will be eternally grateful to them.

To my friends who were there to listen and support me throughout my study. I would like also thank my aunt and cousin who supported me during writing process.

ACKNOWLEDGEMENT

Above all and beyond, I would like to thank Allah, who gave me the desire and ability to complete this work in spite of the constrains along the way.

Firstly, I would like to express my sincere thanks and deepest gratitude to **Prof. Dr. Waqed H. Hassan,** the supervisor of my research, who I had the excellent luck and the honor of being under his supervision, for his continuous encouragement and invaluable guidance throughout this thesis.

Finally, I would like to show my gratitude to my family for their support and help along the way.

Halah Kais Jalal

2019

Abstract

Local scouring around bridge piers has been identified as one of the main causes of bridges failure around the world, which is significantly affecting the total construction and maintenance costs. Research on local scour around the pier of bridges have shown the lack of understanding the effects of the main parameters such as a pier shape on local scour depth. Thus, the main goal of this study is to investigate the effects of bridge piers' shape on local scour to determine the optimum pier shape that gives minimum scouring. In addition, an empirical equation has been developed to predict scour depth based on parameters obtained from dimensional analysis in terms of shape factor, flow intensity, flow depth, pier width and angle of attacks by employing gene expression programming (GEP) and statistic non-linear regression using Statistical Package for Social Sciences (SPSS). Various shapes of piers are used in this study including circular, square, rectangular, elliptic, oblong, octagonal, hexagonal, ogival and lenticular to decrease the influences of local scour around bridge piers. A computational fluid dynamic -based simulation to compute the depth of local scour around piers using Flow-3D model is used in this study. The effectiveness of the model evaluated and validated using experimentally obtained data from Melville 1975. 729 runs were performed for each pier shapes at three different values of flow intensity V/V_C (0.55, 0.76, 1), fluid depth ratio y/b (0.2, 0.98, 2.95), pier width ratio b/B (0.11, 0.15, 0.2) and angle of attacks (0, 30°, 45°). All these runs were simulated in non-cohesive bed sediment under clear water scour conditions.

The outcome of comparing numerical results of predicting scour depth around circular pier with laboratory experiment of Melville 1975 shows that the numerical model validates a good agreement with experimental model with the

maximum percentage of error between the experimental and the numerical models of 10%. Models results revealed that maximum scour depth observed at rectangular shape while minimum depth of scour occurred at lenticular shape. The results obtained by the simulation on four pier shapes namely circle, square, elliptical and lenticular that have the same volume of concrete and surface area, also showed that minimum depth of scour was observed around the lenticular pier with about 70% lower than square pier shape. Based on the results, it can be said that lenticular pier provides optimum hydraulic design of pier. Additionally, the scour depth increases with increasing flow intensity, flow depth, pier width and angle of attacks.

Based on the simulation results, the equation obtained using GEP model performed better predicting to scour depth than SPSS model with coefficient of determination (R^2) and root mean squares error (RMSE) of 0.89 and 0.152, respectively. The empirical equation derived to predict the scour depth based on shape factor, flow intensity, flow depth, pier width and angle of attacks. Sensitivity analysis results suggests that the flow depth has a major influence in predicting the local scour in comparison to the other input parameters.

Table of Contents

Table of Contents

Table of Contents

List of Figures

List of Figures

List of Figures

List of Figures

List of Figures

List of Figures

List of Tables

List of Symbols

Symbols	Description	Dimensions
B	Flume width	L
b	Upstream Pier width (Diameter)	L
b_b	Bottom base width of tapered pier.	L
bT	Top base width of tapered pier	L
C_*	Dimensionless clay content	-
$C_{b,i}$	Volume fraction of species i in the bed material	-
ds	Maximum depth scour	L
d_{50}	Median particle size which is taken as the representative particle size	L
d_i	diameter of sediment	L
d_{sms}	Maximum scour depth for jet scour in cohesionless sediment	L
d_{smc}	Maximum scour depth for jet scour in cohesive sediment	L
Fr	Froude number	-
Fp	Pier Froude number	-
g	Magnitude of the acceleration of gravity g	LT^{-2}
h	Flow depth	L
K_d	Particle size factor	-
K_I	Flow Intensity factor	-
K_G	Channel geometry factor	-
K1	Correlation factor for pier shape	-
K2	Correlation factor for angle of attacks	-
K3	Correlation factor for bed conditions	-
K4	Coefficient based on armoring by large particles in bed material	-

List of Symbols

Symbol	Description	Dimensions
Ks	Pier shape factor	-
Kyw	Flow depth-foundation size	L
Kyb	Flow depth-pier size	L
k	Turbulent kinetic energy	L^2T^{-2}
L	Pier length	L
μ_t	Turbulent eddy viscosity	$ML^{-1}T^{-1}$
μ_f	Dynamic viscosity of fluid	$ML^{-1}T^{-1}$
Ns	Sediment number	-
P	Pressure	$ML^{-1}T^{-2}$
PI	Plasticity index	-
$q_{b,i}$	Volumetric bed-load transport rate	-
R_s	Nikuradse roughness of the bed surface	
S_0	Channel bed slope	-
s_{ij}	Strain rate tensor	-
t	Time	T
u_i	Fluid velocity component in i direction	LT^{-1}
$ú_i$	Fluctuation of fluid velocity in i direction	-
$\overline{ú_i ú_j}$	Reynolds stress tensor	-
V	Mean velocity of approach flow	LT^{-1}
V_c	Mean velocity at threshold motion of sediment for approach flow	LT^{-1}
V^*	Shear velocity of initiation of sediment motion	LT^{-1}
V^*c	Critical threshold shear velocity	LT^{-1}
v	Fluid kinetic viscosity	L^2T^{-1}

List of Symbols

Symbol	Description	Dimensions
v_t	Turbulence viscosity	$ML^{-1}T^{-1}$
W	Antecedent moisture content %	-
W_*	Antecedent moisture content required to saturate the soil sample	-
X	Pier spacing	L
y	Flow depth	L
y_{se}	Maximum equilibrium scour depth	L
θ	Pier alignment (angle of attack)	degree
Φ_i	Dimensionless bed-load transport rate	-
θ_i	Local shields parameter	-
$\theta_{cr,i}$	Dimensionless critical shield parameter	-
σg	Geometric standard deviation of sediment size distribution	-
δ_{ij}	Kronecker delta	-
α_i	Entrainment parameter	-
ρ	Fluid density	ML^{-3}
ρ_i	Density of the sediment species i	ML^{-3}
ρ_f	Fluid density	ML^{-3}
ε	Dissipation rate of turbulent kinetic energy	-

Abbreviations

CFD	Computational Fluid Dynamics
ETs	Expression Trees
FAVOR	Fractional Area/Volume Obstacle Representation
FD	Finite Difference
FE	Finite Element
FEM	Finite Element Method
FV	Finite Volume
GEP	Gene Expression Programming
LES	Large Eddy Simulation
PDFs	Partial Differential equations
RIS	Root Insertion Sequence
RNC	Random Numerical Constant
RNG	Renormalized Group
SPSS	Statistical Package for Social Sciences
VOF	Volume of Fluid

<div align="center">

Chapter One

Introduction

</div>

1.1 Background

The topic of rivers' flow and its related problems such as flooding, transportation of sediments, riverbed deformation and scouring are considered as one of the major issues in a country development. The riverbed deformation is the key interest for infrastructure and hydraulic engineers. The presence of hydraulic structures like bridges which obstructs the flow causes flow contraction and scouring around piers and abutments (Melville, 1975).

Large bridges cost billions of dollars, which justifies rigorous scour depth prediction, both for safety and economic reasons. Under-predicted or over-predicted scour depth may lead to bridge failure or costly bridge construction (Yang, 2005).

While there is still a great deal of uncertainty and controversy regarding scour prediction, it is probably true that many bridges have failed due to scouring and most of these failures have resulted from complete oversight of the scour problem. Scour prediction models already existed and forms of scour prevention and protection for safe bridge resulted are costly.

Recently, the advances in computing technologies and numerical modeling of hydraulic structures is becoming widely used in the engineering field. These models frequently replaced the former industry standard of scaled physical modeling due to certain advantages associated with numerical modeling. Numerical models are less expensive than physical models as they require less space, materials and construction which can be easily modified to accommodate design changes. The application of the numerical simulation is similar in many ways to the set-up of experiment models. All required for simulations are a

computer, a software, and an engineering know-how to interpret the results (Gacek, 2007).

A scientific research is also required before a universal formula can be produced for a particular site can be confidently selected. The lack records from actual bridge sites could be compared to those obtained in the various prediction methods effective in solving the problem of piers' scouring (Little, 1977).

1.2 Problem Statement

The increase in flood waves resulted from river discharge increment due to the climate change leads to erosion of the soil near the bridge pier. This poses a dramatic impact on the construction structure of the pier and bridge and affects the total construction and maintenance costs.

1.3 Research Aim

The main aim of this research is to contribute to the understanding and characterization of local scour around bridge piers. This could help in selecting the optimum piers' shape and results in minimizing value of scour depth. This can be achieved through studying the effect of flow intensity, depth and angle of attacks as well as the piers' shape.

1.4 Methodology

The approach is to review previous methods concerning piers' scour, scouring formation modeling, and numerical modelling evaluation. The following steps are followed to achieve the aim of this study:

- Calibrating Flow-3D software model with experimentally obtained data from scientific researcher.
- Utilizing the calibrated model to investigate the effect of multiple factors including flow intensity, flow depth, pier shape, etc. on scour depth.

- Using gene expression programming software GeneXpro Tools to correlate the resulted scour depth with various variables.
- Comparing the predicted model with regression model obtained from SPSS statistical software.

1.5 Scope and Limitations

Due to the difficulty of constructing a laboratory model for all pier shapes and sizes, a 3D finite volume numerical model was adopted for this thesis. The following are the limitations of this model:

1. The model is not valid for cohesive soils including silts and clays.
2. The model should be applied with caution with excessively large grains due to the limited validity of the sediment theory used in the model, the median grain size of sand used in the models is 0.385mm.
3. In order to obtain accurate results, a fine mesh was applied in the model which requires large computation times (approximately 200 hours per run).
4. The parameters limitation used in this thesis for flow intensity is (0.55-1), flow depth ratio is (0.2-2.95), pier width ratio is (0.11-0.2) and for angle of attacks and pier shape factor are (0°-45°) and (0.71-1.26) respectively.

1.6 Thesis Layout

This thesis consists of six chapters, which are outlined as follows:

- Chapter one presents a brief introduction to the topic.
- Chapter two describes the current understanding of scouring aspect. It also shows previous studies that are related with the main topic. Review regarding experimental and numerical modeling is included.

- Chapter three shows this research methodology of numerical simulation, which include the complete process starting from basic modelling up to the post processing.

- Chapter four illustrate the statistical analysis using GeneXpro Tools and SPSS software packages.

- Chapter five shows the results and discussion of the numerical simulation and the statistical analysis.

- Chapter six outlines the conclusions obtained from the numerical analysis as well as recommendations for future studies.

Chapter Two

Literature Review

2.1 Introduction

Researchers from all over the world have extensively studied the problem of scouring from different points of view and under different conditions. It is well documented that the main cause of concern about the stability of bridge foundation is the occurrence of scour around its piers. This chapter attempts to present a review of relevant literature. The chapter begins with general review of bridge scour definitions, types and regimes. Local scour parameters are also presented in brief. The effects of pier shape and angle of attack on local scour are discussed. In addition, equilibrium scour depth definitions and developing of scour depth formulas are reviewed. Finally, former studies on the numerical modeling of local scour around bridge piers are presented.

2.2 Definition of Scour

Previous studies and engineers have provided many definitions for the scour processes Melville, (1975) defined scouring as the enlargement of a flow section by the removal of the material composing the boundary through the action of the fluid in motion. Breusers et al. , (1977) stated scouring as a natural phenomenon caused by the flow of water in rivers and streams. The erosive action of flowing water has caused scouring phenomenon, which removes and erodes materials from the bed the banks of streams as well as from the vicinity of bridge piers and abutments. The term scouring is another name for extreme erosion according to Annandale, (1995). It is a term generally used to describe severe localized erosion of bed material that happen

when the erosive force of water overrides the capability of bed material to afford it. The range of the resulting scour relies upon whether the bed material consists of cohesive, non-cohesive or rock material (Mohamed, 2005). Previous studies showed that scour can either be caused by the normal flow or flood events. Normal flow can lower the channel bed, however, scouring is most assisted during a peak flow in which the flow velocity is higher. In other words, scour can occur under any flow condition that makes the bed mobile within the vicinity of the obstruction. The rate of scouring is much higher with larger flow events. The amount of reduction below an assumed natural level (generally the level of the river bed prior to the commencement of scour) is termed as the scour depth. A scour hole is defined as the void or depression left behind when sediment is washed away from a stream or river bed (Alabi, 2006). Scouring around a bridge pier will reach its maximum where no more bedding material can be eroded from the scour hole. This is called the maximum scour depth and depends upon the flow which can be reached at different times (Raleigh, 2015)**.**

2.3 Type of Scour

Scouring at piers is an important problem for infrastructure engineering. Scour, collision and overloading are the three major causes of bridge failures according to Xiong et al., (2016). Scouring has been acknowledged as a severe hazard to the performance of bridge piers. Three types of scour generally occur at a bridge site namely general scour, contraction scour and local scour**.** On the other hand, Cheremisinoff, (1987) divided scour into two major types which are general scour and localized scour. Figure 2.1 shows the subdivisions of scouring types according to Melville and Coleman, (2000).
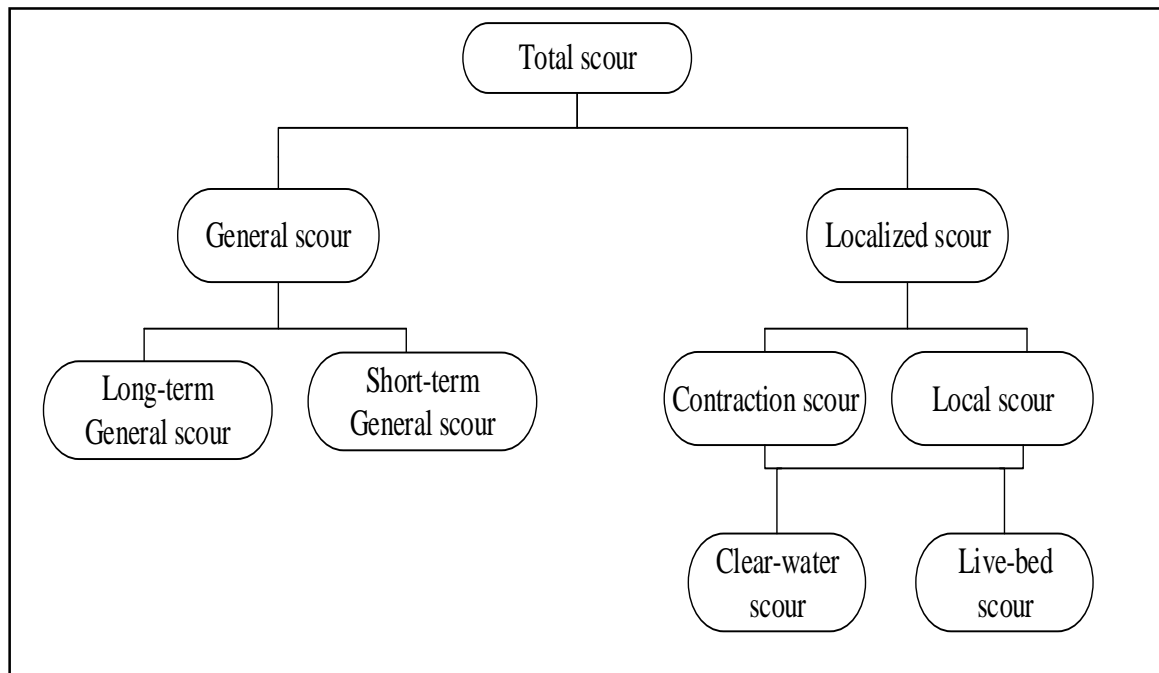
Figure (2-1): Classification of scour (Melville and Coleman, 2000)

2.3.1 General scour

General scour refers to the bed elevation changes resulted from lateral instability of the waterway. This type of scour develops regardless of the presence of the bridge structure (Bridge Sour Manual, 2005). General scour can occur naturally in river channels by aggradation and degradation of the river bed which lowers the channel bed along the longitudinal profile (Alabi, 2006). General scour can further be divided into long-term and short- term scour based on the temporal development of the scour (Cheremisinoff, 1987). Short-term scour occurs in response to a single or several closely spaced floods. Long-term scour develops over a significantly longer time period, usually several years (Melville and Coleman, 2000).

2.3.2 Localized scour

In contrast to general scour, localized scour is directly attributed to the existence of a bridge or other riverine structures. This type is subdivided to contraction and local scour.

2.3.2.1 Contraction scour

Contraction scour can be caused by a decrease in channel width, either naturally or by the presence of a bridge as shown in Figure 2.2. With the decrease in flow area of a stream, the average flow velocity increases and bed shear stress leading to an increase in the erosive forces acting upon the channel bed (Richardson, 2001). Eroded bed material moves from the contracted section until equilibrium**.** When the estimated depths of contraction scour are too large, the bridge crossing length must be increased in order to reduce scour (Hirshfield, 2015).
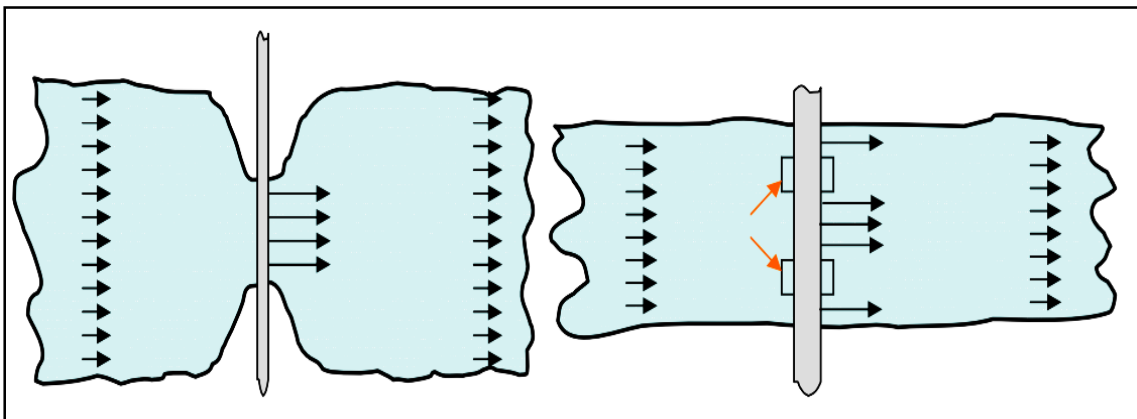
Figure (2-2): Two manmade features that create a contracted section in a channel (Bridge Scour Manual, 2005).

2.3.2.2 local scour

Local scour is the third type of scouring that occurs when water flows around a structure located in or near an erodible sediment bed, the increased forces on the sediment particles near the structure may remove sediment from the vicinity of the

structure (Bridge Scour Manual, 2005). In such a scouring, downward flow is induced at the upstream end of the pier and leads to a localized erosion around the pier. local scour around bridge piers or abutments is commonly recognized as one of the major causes of bridge failures at river crossing. Local scour has led to massive lose on life and economy, and resulted in serious impact on local transportation (Liu et al, 2017), localized scour can occur as either clear-water scour or live-bed scour.. Clear- water scour occurs for mean flow velocities up to the threshold velocity for bed sediment movement, i.e., $V \leq V_c$. The maximum local scour depth is reached when the flow can no longer remove bed material from the scour area. Live-bed scour occurs when there is general sediment transport by the river and this type of scour occurred for $V > V_c$ (Melville and Chiew, 1999).The equilibrium scour depth is attained when the time-averaged transport of the bed material into scour hole equals that removed from it (Melville and Coleman, 2000).

2.4 Local Scour Mechanism

The flow pattern near a pier in a uniform open channel flow is complicated and increases in complexity as the scour hole around the pier develops (Bozkus and Osman, 2004). The main mechanisms that causes scour at piers are the down-flow at the upstream face of the pier and subsequent horseshoe vortices that form at the base of the scour hole (Muzzammil et al., 2004). The down-flow reaches the channel bed and transports sediment away from the pier base creating a scour hole. When the down-flow reaches the channel bed it interacts with the oncoming flow and a complex vortex system develops (Hirshfield, 2015). The vortex then extends downstream along the sides of the pier. The down-flow reaches its maximum strength just below the natural bed level. The down- flow impinging on the bed is the main scouring agent (Melville and Raudkivi, 1977).

The approach flow velocity on the upstream side of the pier is reduced to zero, called the stagnation point. This causes a pressure increment at the pier face. As the velocity decreases from the surface to the bed, the stagnation pressure on the face of the pier also decreases accordingly i.e. downward pressure gradient. The pressure gradient arising from the decreased pressure forces the flow down the face of the pier resembling a vertical jet. The strong vortex motion caused by the existence of the pier entrains bed sediments within the vicinity of the pier base (Lauchlan and Melville, 2001). As the scour develops, the increase in local flow depth reduces the strength of the erosive action at the bed; as a result, the rate of scour decreases and eventually reaches equilibrium.

2.5 Formation of Vortexes Around Bridge Pier

Formation of vortexes is the basic mechanism leading to local scour at piers or abutments. The accumulation of water on the upstream face and subsequent acceleration of the flow around the nose of the pier or the abutment leads to formation of vortexes. A scour hole develops when the transport rate of sediment away from the local region is greater the transport rate into the region. As the depth of scouring increases, the strength of the vortexes is reduced, thus, diminishing the transport rate. As equilibrium is reestablished, scouring ceases and the scour hole will not enlarge further. A typical vortex around a pier is:

1- Horseshoe vortex
2- Wake vortex.
3- Bow wave
4- Trailing vortex

These vortices are responsible for creating holes close to piers. This kind of erosion is damaging many bridges (Hamidi and Siadatmousavi, 2017). The types of vortexes around piers are illustrated in Figure 2.3.
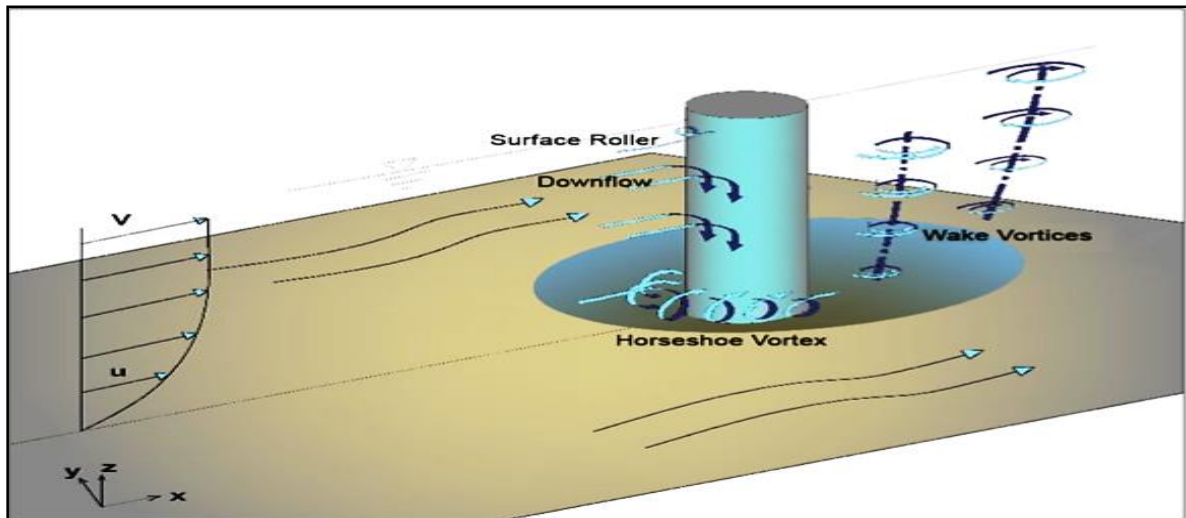
Figure (2-3): Flow and scour pattern around a cylindrical pier
(Jahangirzadeh et al. , 2014).

2.5.1 Horseshoe vortex

The horseshoe vortex is the result of a three-dimensional separation of the boundary layer which rolls up into a vortex ahead and along the sides of the cylinder pier (Melville, 1975). Part of the flow approaching piers is deflected downwards to the bed and rolls up to create what is often described as a "horseshoe vortex" around the front face of the structure. This vortex is often referred to as horseshoe vortex because of its great similarity to a horseshoe. Shen et al. , (1969) describes the horseshoe vortex system in detail. The horseshoe vortex is initiated by the stagnation pressure gradient on the leading edge of the structure resulting from the bottom boundary layer of the approaching flow. That is, the variation in flow velocity from zero at the bed to the value at the surface causes a variation in stagnation pressure on the leading edge of the structure. The largest stagnation pressure occurs at the elevation of the highest velocity. The combination of the horseshoe vortex with down-flow controls the scour mechanism.

11

2.5.2 Wake vortex

The separation of the flow at piers' sides produces the so called wake-vortices (Alabi, 2006). Wake vortices are transferred downstream by the approach flow and acts somewhat like a vacuum cleaner in removing river bed materials, which are then carried downstream by the down-flow and horseshoe vortex (Melville, 1975). The wake-vortex system is formed by the rolling up of the unstable shear layers generated at the surface of the pier, and detached from either side of the pier at the separation line (Breusers et al. , 1977). Both the horseshoe and wake vortices erodes sediment from the pier base. In many cases, the materials which is removed by these vortexes are redeposited immediately downstream of the pier (Richardson, 2001). The strength of the wake vortices is reduced with distance downstream leading to a common sediment deposition downstream of piers (Hirshfield, 2015).

2.5.3 Bow wave

Bow waves are generated when the upward flow forms a circulation near the free surface (Melville and Raudkivi, 1977). It is noted that a bow wave does not dominate piers' scour mechanism unless the flow depth is too shallow which is equal to the sum of the diameters of a horseshoe vortex and a bow wave. As the flow depth decreases, the horseshoe vortex and the bow wave interfere with each other (Lee, 2006); the bow wave causes the horseshow vortex to become weaker and leads to a reduction in scour depth (Hirshfield, 2015). The bow wave at piers is illustrated in Figure 2.4. Where y_{se} is the maximum equilibrium scour depth and y is the average flow depth.
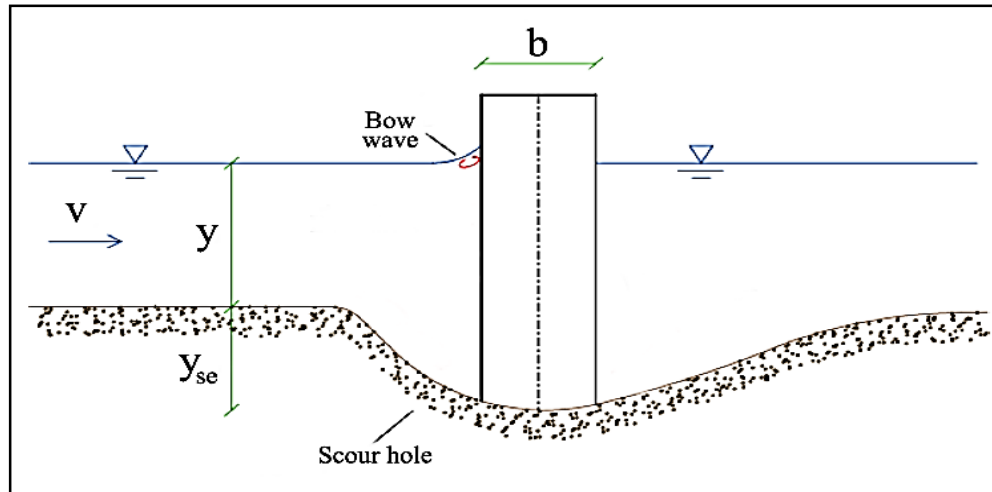
Figure (2-4): Schematic drawing of bow wave at bridge pier (Melville and Coleman, 2000).

2.5.4 Trailing vortex

Trailing-vortex system usually occurs only on completely submerged piers. It composes one or more discrete vortices attached to the top of a pier and extending downstream. These vortices are formed when finite pressure difference exists between two surfaces meeting at a corner normally at the top of a pier (Breusers et al. , 1977).

2.6 Factors Affecting Local Scour

The following parameters have been recognized as factors influencing the depth of scour near a pier:

2.6.1 Width of the pier

The width of piers has a direct impact on the depth of the scour. With the increase in piers' width, the velocity of flow in the bridge opening increases to maintain continuity and leads to increase in scour depth (Richardson, 2001).The influence of pier size has been discussed by Shen et al., (1969), Breusers et al., (1977). These researchers concluded that horseshoe vortex shape and strength are

the main cause of scouring which are functions of piers' size. The larger the pier the deeper the scour hole and the longer the time taken for its development for a given shear stress ratio.

2.6.2 Effect of flow intensity on scour

Flow intensity is defined as the ratio of the shear velocity (V^*) to the critical shear velocity (V^*_c) or the ratio of the mean velocity of approach flow (V) to the critical mean velocity (V_c) (Melville and Sutherland, 1988).Under clear-water conditions, the local scour depth in uniform sediment increases almost linearly with flow intensity to a maximum at threshold velocity (Melville and Chiew, 1999). The maximum scour depth is reached when the ratio V^*/V^*_c equals to 1 or V/V_c equals 1. The corresponding maximum scour depth is called the threshold peak. According Breusers et al. , (1977)**,** no scour occurs when flow intensity $V/V_c \leq 0.5$, while clear water scour conditions happens for both uniform and nonuniform sediments when the flow intensity ranges $0.5 \leq V/V_c \leq 1.0$. The investigators Chabert and Engeldinger, (1956), Ettema (1980), Laursen and Toch, (1956), Breusers et al. (1977) and Chiew, (1984) found that the scour depth increases almost linearly with V, and if $V/V_c \geq 1.0$ (live-bed scour) or scour with sediment movement**.** As the velocity exceeds the threshold velocity, the local scour depth in uniform sediment decreases first and then increases again to a second peak. These changes are relatively small providing the threshold peak is not exceeded and the sediment is uniform. The second peak occurs at the transition flatbed stage of sediment transported on the channel bed and is termed the live-bed peak. The scour depth changing with flow intensity are explained in terms of the balance between sediment input to and output from the scour hole. The general conclusion was that the maximum local scour depth in uniform sediments occurs at the threshold condition for clear-water scour conditions (Alabi, 2006).

2.6.3 Effect of flow depth on scour

Flow depth is usually referred to as flow shallowness and is examined by relating flow depth (y) to the pier width (b). The effect of water depth on scour is a controversial subject.

Ettema, (1980) explained that, for shallow flows, the surface roller (or bow wave) forms ahead of the bridge pier which interferes with the scour action of the horseshoe vortex because of the opposite senses of rotation. When the flow depth increases, the interference of the surface roller with the down-flow and horseshoe vortex is reduced and the effect of flow depth becomes insignificant. Richardson, (2001) stated that Flow depth has a direct effect on scour depth. For pier scour, an increase in flow depth can increase scour depth by a factor of 2 or more.

Melville, (2008) explained that flow shallowness y/b represents the effect of the depth of flow in relation to the pier width. For deep flows compared to the pier width, that is for narrow piers, the scour depth increases proportionately with pier width and is independent of y. Conversely, for shallow flows compared to the pier width, the scour depth increases proportionately with y and is independent of b; while for intermediate depth flows, ds depend on both y and b. These trends are shown schematically in Figure 2.5 and Table 2.1. Ashtiani and Kordkandi, (2013) stated that the scour depth becomes independent of the flow depth when the ratio of the flow depth to pier width greater than 4.

Table (2-1): Classification of local scour processes at bridge piers (Melville, 2008)

No.	Pier Class	y/b	Pier Scour Dependence
1	Narrow pier	y/b>1.4	ds α b
2	Intermediate width pier	0.2≤ y/b≤ 1.4	ds α $\sqrt{yb}$
3	Wide pier	y/b<0.2	ds α y
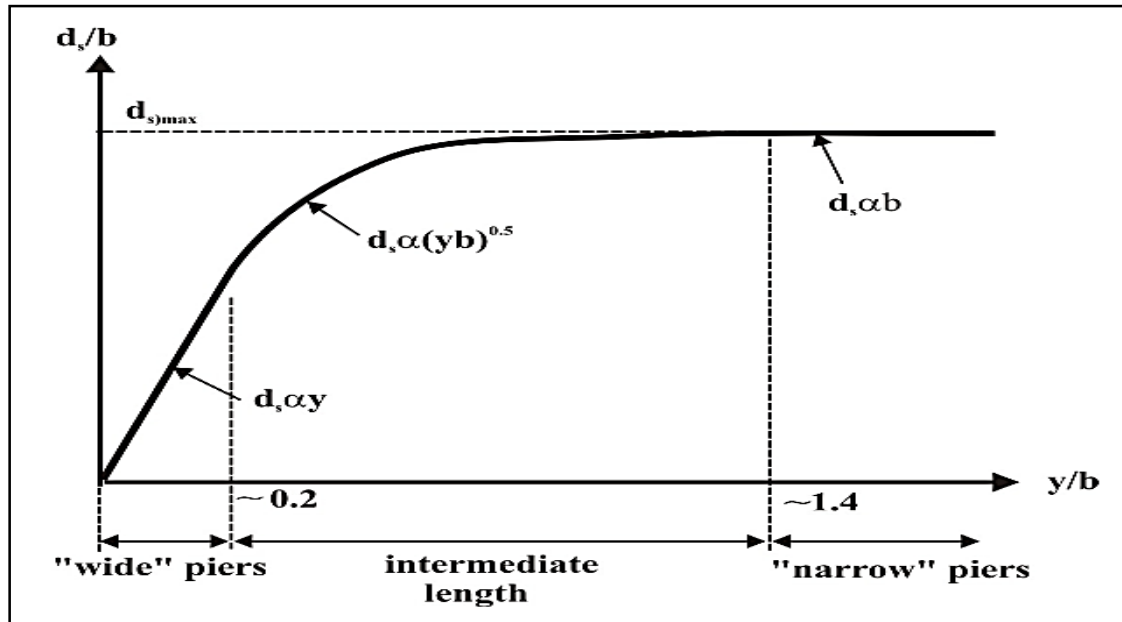
Figure (2-5): Local scour depth variation with flow shallowness (Melville, 2008)

2.6.4 Effect of sediment size on scour depth

The influence of particle sizes and density of the sediment material are often expressed as a function of the critical flow velocity for the initiation of sediment motion. Breusers and Raudkivi, (1991) studied the effect of sediment size on local depth of scour at a bridge pier. The experiments were conducted under clear-water conditions and using a pier of diameter 102 mm and a flume 1.5 m in width under clear-water conditions. It was observed that a sediment of d50 ≤ 0.7 mm leads to a formation of ripples, whereas sediment of d50 ≥ 0.7 mm do not cause ripples. According to Raudkivi and Ettema, (1977) , for non- ripple-forming sediments (d50

16

≥ 0.7 mm), experiments can be run successfully with a flow condition of $V^* \sim$ $0.95V^*_c$ without the upstream bed being disturbed by the approach flow. Whereas, with finer sands (d50 < 0.7 mm), a flatbed cannot be maintained for the same flow condition.

It was concluded by Breusers and Raudkivi, (1991) that ripples usually developed at shear velocities V^* above $0.6V^*_c$ for sediment of size, d50 < 0.7 mm. Thus, clear-water conditions were not maintained long enough for the finer sands to reach the same maximum scour depth. However, an exception occurs if the geometric standard deviation of the sand size σg > 1.3 while the sediment acts as a uniform sediment if the σg < 1.3. In this range of geometric standard deviation, the sediments were not uniform and the coarser grains protect the channel surface but were not large enough to protect against the scour hole where the agitation was higher. Then, clear-water scour depths of the same order as observed with non-ripple-forming sediments could be reached.

2.6.5 Effect of sediment coarseness on scour

The ratio of the pier width (b) to the mean grain size of the sediment material (d50) is defined as relative sediment coarseness (b/d50) (Melville and Coleman, 2000). Figure 2.6 shows the local scour depth versus sediment coarseness ratio, where D is pier diameter, Z is scour depth and Z_{max} is maximum scour depth.
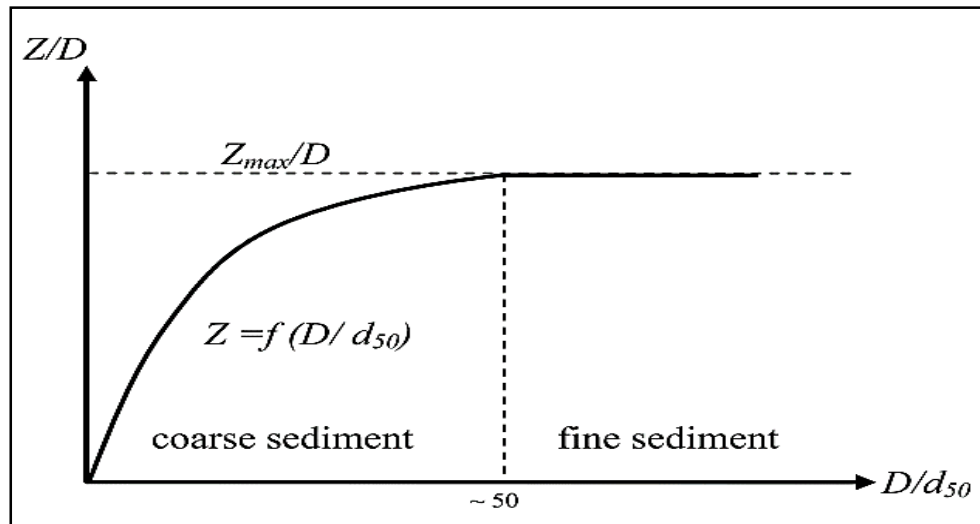
Figure (2-6): Local pier scour depth versus sediment coarseness (Melville and Coleman, 2000)

As shown in figure 2.6, the scour depth is affected by sediment coarseness up to a maximum at $D/d50 = 25 - 50$ and seemingly becomes independent when $D/d50$ ratio exceeds 50.

Ettema, (1980) explained that, for smaller values of the sediment coarseness ratio, individual grains are relatively large to the groove excavated by the down-flow and erosion is impeded because the porous bed dissipates some of the energy of the down-flow. For $D/d50 < 8$, the individual grains are so large relative to the pier that scour is mainly happened due to entrainment at the flanks of the pier (Melville and Coleman, 2000). Recently, Lee and Sturm, (2009) studied the effect of sediment size on local scour depending on laboratory and field data. Their results showed that after the scour depth reached a peak value at $D/d50 = 25$, it decreased again as the sediment coarseness increased**.**

2.6.6 Effect of pier shape and alignment on scour depth

The shape of piers is one of the important factors that play a vital role in the creation and the strength of the vortex system. Bridge piers are constructed of

various shape. The most common shapes used are circular, rectangular, square, rectangular with chamfered end, oblong, elliptic, lenticular and Joukowski. Figure 2.7 shows a schematic illustration of some pier shapes.
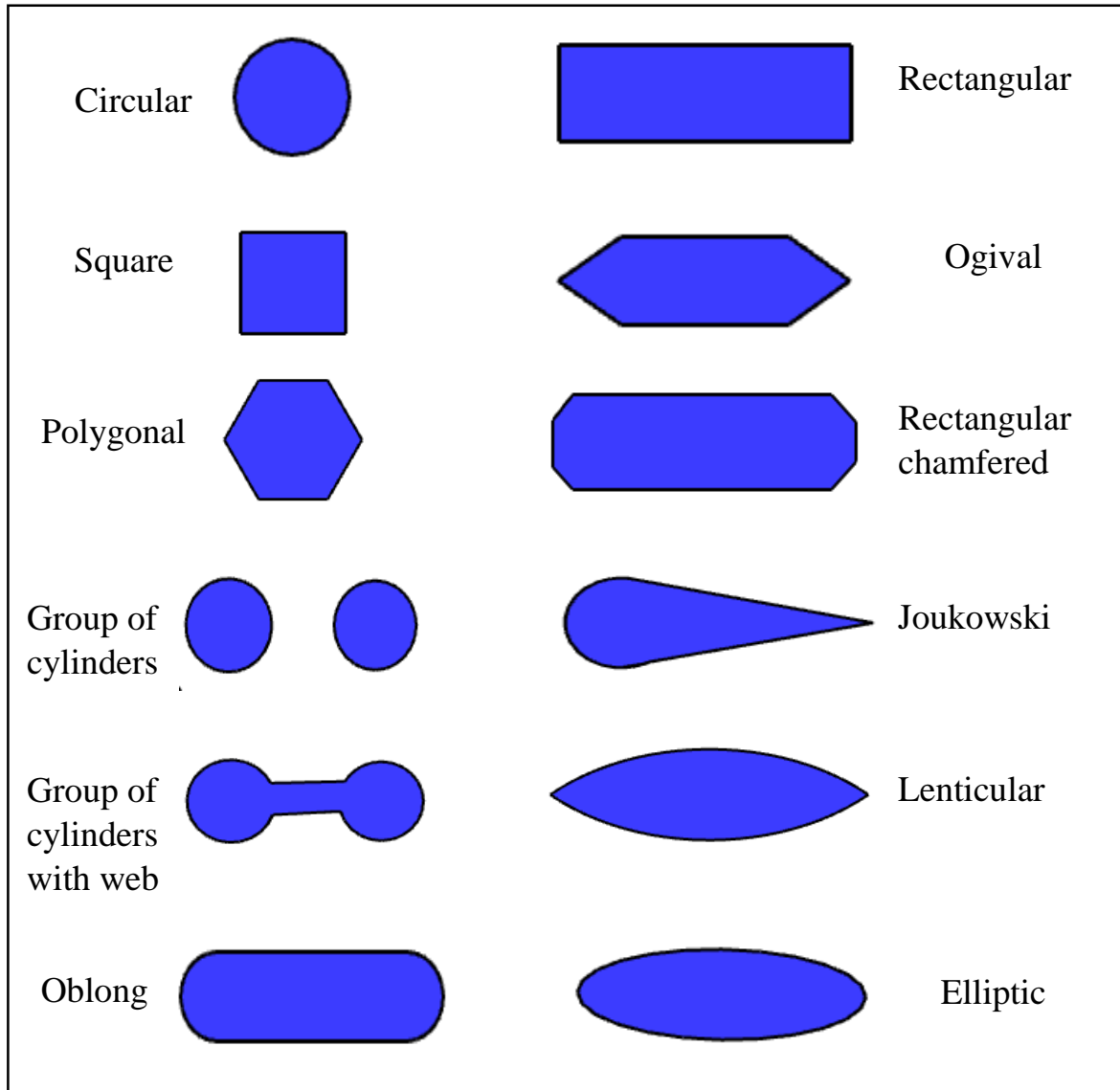
Figure (2-7): Schematic illustration of some common pier shapes (Alabi, 2006)

The effect of pier shape has been reported by many researchers e.g. Laursen and Toch, (1956), Breusers et al. , (1977), Breusers and Raudkivi, (1991) and Melville and Coleman, (2000). Shen et al., (1969) classified pier shapes in two categories namely blunt-nosed and sharp-nosed piers. Blunt-nosed piers create a

strong horseshoe-vortex system; thus the maximum scour depth occur at the pier nose. The upstream pier shape should have a strong influence on the scour depth and the length of the pier and downstream pier shape should have a minimum effect if the blunt- nosed pier is aligned with flow, where the horseshoe-vortex system is very weak and the maximum scour depth occurs near the downstream end.

The geometry of piers is categorizes according width, length, shape and the alignment with flow (Melville, 1975). There are two types of piers including simple piers and complex piers. Simple piers are piers having constant section throughout their depth. Complex piers are piers with piled foundations, caissons, slab footings and tapered piers (Melville, 2008). The shape of piers greatly influenced the amount of scour. With a pier, streamlining the front end reduces the strength of the horseshoe vortex and reduces scour depth. Streamlining the downstream end of piers reduces the strength of the wake vortices. Shape and alignment effects on local scour are given as multiplying correction factors. In practice, shape factors are only important if axial flow can be ensured. Even a small angle of attack will eliminate any benefit of pier shape. Table 2.2 presents some recommended values for the pier shape effect regarding the circular pier shape.

The effect of pier alignment (angle of attack) has been studied by few researchers e.g. Tison, (1940), Chabert and Engeldinger, (1956), Laursen and Toch, (1956), Neill, (1973), Melville, (1975) and Breusers et al. , (1977). The angle of flow attack refers to the angle between the direction of flow and the direction of pier (Hoffmans, and Verheij, 1997). The effect of attack angle of the flow, is clearly shown to be one of most significant factors affecting local scour around bridge piers in Table 2.3, in which (l/b) is the ratio of pier length to width and (θ) is the angle of attack of the approach flow velocity (Lee, 2006). Multiplying factors for angle of attack for different pier length-width ratios proposed by Laursen and Toch, (1956)

are commonly used. In general, angle of attacks greater than 5-10º is to be avoided (Breusers and Raudkivi, 1991). In practice, the angle of attack at bridge crossings may change significantly during floods for braided channels, and it may change progressively over a period of time for meandering channels (Melville and Coleman, 2000).

Table (2-2): Recommended values for the pier shape factors regarding to the circular pier shape (Melville and Coleman, 2000)

Shape	l/b	Tison, 1940	Laursen et al.,1956	Chabert et al., 1956	Garde, 1961	Laursen,1963	Dietz, 1972	Neill, 1973	Maatooq, 1999
					Pier shape factor				
Circular	1	1.0	1.0	1.0	1.0	1.0	1.0	1.0	
Round nose	4		1.0		1.0	1.0	0.85	1.0	0.87
Rectangular	4		1.11		1.11	1.11	-	1.33	
Sharp nose	4	-	-	-	-	-	0.76	0.8	
Lenticular Nose	4	0.59		0.73		0.76			
Elliptical	4		0.83			0.83	0.8		
Joukowski	4			0.86		0.86			
Rectangular chamfered	4						1.01		

Table (2-3): Correlation factor for flow alignment (Kθ) for a bridge pier
(Richardson and Davis, 2001)

θ l/b	Flow alignment (Kθ)				
	0	15	30	45	90
4	1	1.5	2	2.3	2.5
8	1	2	2.75	3.3	3.9
12	1	2.5	3.5	4.3	5

2.6.7 Effect of contraction ratio on local scour depth

The equilibrium depth of local scour at a pier is affected by the contraction ratio. For the purpose of experimental investigations, the width of an experimental flume should be at least eight times the pier size for clear-water scour conditions so that sidewall effects are minimized (Shen et al. , 1969). For live-bed scour, the flume width should be at least 10 times the pier size for scour depths not to be reduced due to bed features being modified as they propagate through the constriction (Alabi, 2006). Raudkivi and Ettema, (1983) suggested that the ratio of flume width to pier diameter should be less than 6.25.

2.6.8 Time effect on local scour depth

The definition of time to scour adopted for a given test plays an important role in the results obtained and also in the conclusions reached by Fanzetti et al, (1982). They also observe that, if care is not taken, the definition of time to equilibrium scour depth can affect the results such that the same experiment carried out under the same experimental conditions. However, different timeframe can yield a different conclusion (Alabi, 2006). Under clear- water conditions, scour depth develops gradually with time following a first order exponential relation towards the equilibrium clear-water scour depth. For live-bed conditions, scour depth increases rapidly with the time reaching maximum value in short duration. Then scour depth

fluctuates over time around a mean value called equilibrium live-bed scour depth (Chabert and Engeldinger, 1956; Raudkivi, 1977 and Melville and Chiew, 1999). The equilibrium scour depth under live-bed is about 10% less than under clear-water conditions (Graf, 1996). Figure 2.8 shows scour depth development with time. The time required to achieve the equilibrium depends on the scale of these experiments. This is a very important point because the results obtained after short run time may give scour depths smaller than the equilibrium scour depth. The data obtained in small-scale laboratory experiments after short run time of 10 to 12 hours can lead to scour depths less than 50% of the equilibrium depth of scour (Melville and Chiew, 1999).

Several researchers (e.g. Heidarpour et al., 2003; Zarrati et al., 2004; Mia and Nago, 2003 and Sheppard et al., 2004) have come up with different definitions of time to equilibrium scour depth as it takes a very long time for an equilibrium condition to be attained. Ettema, (1980) defined the time to equilibrium scour as the time at which no more than 1 mm of incremental scour was realized within a timeframe of four hours. Sheppard et al., (2004) and Melville and Chiew, (1999) stopped their experiments when the change in the scour depth did not exceed 5% of the pier diameter during a 24-hour period.
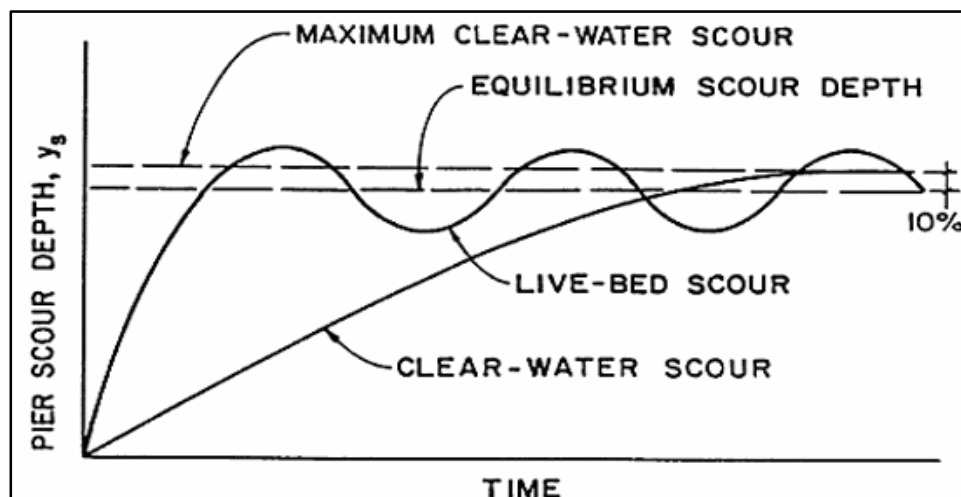
Figure (2-8): Scour depth as a function of time (Breusers and Raudkivi 1991)

2.7 Equilibrium Scour Depth

Equilibrium scour depth refers to the condition of balance wherein the amount of material removed from the scour hole is equaled by the amount of material supplied by the normal transport of the approaching flow (Laursen and Toch, 1956). Equilibrium can also be defined as the asymptotic state of scour reached as the scouring rate becomes very small or insignificant. An equilibrium between the erosive capability of the flow and the resistance to motion of the bed materials is progressively attained through erosion of the flow boundary. The occurrence of a non-equilibrium condition, however, has also been reported by many researchers. Because an equilibrium clear-water scour condition is approached asymptotically with time, Melville and Chiew, (1999) opined that it can take an infinite amount of time for the equilibrium scour hole to develop. Melville and Chiew, (1999) observed that an apparent equilibrium scour hole may continue to deepen at a relatively slow rate long after equilibrium conditions were thought to exist.

2.8 Previous Studies

2.8.1 Experimental Work

A number of literatures are reported on scour around pier. Here some of the important literatures, which are directly related to the present study, are reviewed and discussed

Tison, (1940), Tison, (1961) and Chabert and Engeldinger, (1956), discussed the influence of various variables on local scour depth around bridge pier. The main variables were pier shape, flow velocity and angle of attack. This study state that increase in velocity leads to an increase in scour depth and maximum scour depth was obtained at velocities near the threshold velocity (V_c), whereas scour started at about half the threshold velocity ($V=0.5*V_c$). Maximum scour depth is observed at

the upstream nosed of rectangular pier and at the sides of the lenticular shape. The length of rectangular pier has no influence on scour depth when the pier is aligned with the flow.

Melville, (1975), experimentally study the problem of local scouring at a circular cylinder in sandy material under threshold conditions. The experimental results have shown that although scour is initiated by the high local shear stresses which result from flow acceleration about the cylinder, the subsequent development of the scour hole is due to the establishment of a strong down-flow ahead of the cylinder. Additional measurements have shown that the horseshoe vortex, increases dramatically in size and strength as the scour hole forms.

Melville and Sutherland, (1988), presented a design method for the estimation of equilibrium depths of local scour at bridge piers. The method is based upon envelope curves drawn to experimental data derived mostly from laboratory experiments. The laboratory data include wide variations in flow velocity and depth, sediment size and gradation, and pier size, shape, and alignment. According to the method, this depth is reduced using multiplying factors where clear-water scour conditions exist, the flow depth is relatively shallow, and the sediment size is relatively coarse.

Abdul-Nour, (1990), used laboratory experiments to study the behavioral pattern of the relationship between scour depth and spacing between bridge piers under different conditions including the variation of flow velocity, sediment size, and pier shape. In general, experimental result showed that the scour depth increased with the decrease in pier spacing. The maximum increase ranged between 10%-28% compared with the scour depth at the single pier for almost the same condition.

Hosny, (1995), presented the systematic experimental study of local scour around cylinders in cohesive soils. Remolded natural clays used in this study and it

was found that the equilibrium scour depth in cohesive soils is considerably less than that in non-cohesive soils and a small percent of clay (around 10% or more) dominates the properties of soil mixture.

Maatooq, (1999), found some equations for local scour around bridge pier using dimensionless terms with experimental work and calculate the shape factor K_s for rectangular round nose pier equal to 0.87 and also showed that it should be specified if piers group is to be used instead of a solid pier, this group must consist of 4 piers with 45° orientation.

Ansari et al., (2002), studied experimental results on temporal variation of scour around circular bridge piers founded in cohesionless and cohesive sediments under steady clear water flows were reported. The difference between scour patterns in cohesionless and cohesive sediments was brought out. Ansari et al., (2002) Considered the horseshoe vortex to be the prime agent causing scour and developed a procedure for computing the temporal variation of scour depth in cohesive sediments.

Khsaf, (2010), study the local scour around the piers of Al-Kufa bridge and the effect of the space between the piers on the depth of equilibrium scour. Dimensional analysis technique was used and from the collected data filed measurements, empirical formula was derived. It was found that the predicated scour depth from the formula performs well as compared to the observed scour depth. It was found that no mutual influence on maximum scour depth occurs for spacing ratio in Al-Kufa bridge piers, and the scour depth in middle pier was greater than the others.

By Khwairakpam et al., (2012), a series of clear water scour experiments have been conducted in a tilting flume with a circular pier under different conditions of densimetric Froude number and inflow depths. It was observed that the entire scour

geometry (scour depth, length, width, area and volume) depended on the densimetric Froude number (FD50) and inflow depth (h).

Günala and Ismael, (2016), examined experimentally turbulent flow field around downstream-facing round nosed pier in a scoured bed. Experiments were carried out under live-bed condition. Result shows that the time-average, velocity field, turbulent intensities and turbulent kinetic energy at different depths and distances differs from that at the original bed level. These results are benefiting for validation of three-dimensional flow model and turbulence close to the bridge pier.

Al-Shukur and Obeid, (2016), discuss the effect of pier shape under different flow velocities. The test program was done on ten different shapes, Circular, Rectangular, Octagonal, Chamfered, Hexagonal, Elliptical, Sharp nose, Joukowsky, Oblong, streamline to investigate the effect of the bridge pier's shape on local scour and conclude the best shape that gives minimum depth of scour. The results showed that the rectangular pier gives the largest scour depth, while the streamline shape gives the lowest scour depth.

Nimnim and Al-khaqani, (2017), study the effects of many parameters on the maximum depth of scour and scour pattern around piers. This study considered the effects of upstream flow conditions, shape of pier, side slope angles, and type of soil. Three cross sections for pier (circular, elliptical and oblong) were used for different velocities and discharges to find the scour depth. It has been observed that for circular cross section pier, the maximum reduction for the scour depth at the upstream of the pier with a side slope of 15° for the soil of d50=0.25 mm was about 63.64% and for the soil of d50=0.66 mm was about 54.55%.

2.8.1.1 Developing scour depth formulas

Numerous equations have been proposed in the literature for estimation of the depth of local scour at bridge piers as represented in Table 2.4. Most of them are determined from laboratory studies and verified from few field observations. Laboratory research has been the primary tools in defining the relations among variables affecting the depth of pier scours in recent years.

Table (2-4): Summarizes some of the most commonly used and cited local pier scour equations.

No.	Author & Reference	Formula	Eq.	Notes
1	**Chitael, 1960**	$\dfrac{ds}{y} = 6.65\ Fr - 0.51 - 5.49\ Fr^2$	(2-1)	-
2	**Bata, 1960**	$\dfrac{ds}{y} = 10(\ Fr^2 - \dfrac{3b}{y})$	(2-2)	Bata conclude that the effect of sediment size on scour depth was less significant than that of Froude number
3	**Neill ,1964**	$ds = 1.5\ (\dfrac{y}{b})^{0.3}$	(2-3)	Neill gave equation to Laursen and Toch, 1956 curve for pier under zero angle of attack
4	**Colfman, 1971**	$\dfrac{ds}{b} = 1.49(\dfrac{V^2}{gy})^{0.1}$	(2-4)	For circular pier under conditions of continuous sediment transport
5	**Breusers, 1977**	$\dfrac{ds}{b} = 2\ ks\ k\theta\ \left(2\dfrac{V}{Vc} - 1\right) \tanh\ (\dfrac{y}{b})$	(2-5)	$0.5 \leq \dfrac{v}{vc} \leq 1.0$ ks = 1.0 for circular and rounded piers = 0.75 for stream-lined shapes = 1.3 for rectangular piers
6	**Jain ,1981**	$\dfrac{ds}{b} = 1.84\ (\dfrac{y}{b})^{0.3} Fr^{0.25}$	(2-6)	-

7	**Abdul-Nour,1990**	$\dfrac{ds}{b}$ $= 1.143(\text{Fr})^{1.531}\ \left(\dfrac{d_{50}}{b}\right)^{-0.369}\left(\dfrac{x}{b}\right)^{-0.114}$	(2-7)	a formula that represented the laboratory results for the cylindrical pier in terms of Froude number (Fr), pier diameter (b), sediment size (d_{50}), and the pier spacing (x).
8	**Melville, 1997**	$d_s = K_{yw}K_IK_dK_sK_\theta K_G$	(2-8)	The K-factors were evaluated by fitting envelope curves to existing data for piers and abutments and a new extensive data set for abutments. $K_{yw} = K_{yb}$ for pier $K_{yw} = K_{yL}$ for abutment
9	**Richardson, 2001, Colorado State University equation CSU**	$ds = 2\ ks\ K_\theta\ k3\ k4\ b^{0.65}\ y^{0.35}\ \text{Fr}^{0.43}$	(2-9)	
10	**Maatooq, 1999**	$\dfrac{d_s}{b} = 0.519 + 2.5\left(\dfrac{V}{V_c} - 0.57\right)\dfrac{y}{b}$	(2-10)	For clear water condition, with all range of flow depth
		$\dfrac{d_s}{b} = 0.5\left(\dfrac{y}{b}\right)\left(\dfrac{V}{V_c}\right)^{4.35}(\text{Fr})^{-1.83}$	(2-11)	For clear water with relative flow depth less than unity
		$\dfrac{d_s}{b} = 0.135(\text{Ns})^{2.9}(\text{Fp})^{0.01}(\text{Fr})^{0.01}$	(2-12)	For clear water with relative flow depth greater than unity
		$\dfrac{d_s}{b} = 1.2\left(\dfrac{y}{b}\right)^{1.5}(\text{Fr})^{1.95}(\text{Fp})^{-1.65}$	(2-13)	For convince if flow condition is not to be regarded .
11	**Ansari ,S. A, Kothyari ,U. C. and Rangaraju ,K. G. (2002)**	for PI=0 $\dfrac{d_{smc}}{d_{sms}} = 1.51\left(\dfrac{W}{W_*}\right)^{0.35}\left(\dfrac{C_*}{\varnothing_*}\right)^{0.2}$	(2-14)	Equations (2-14) and (2-15) had been developed for the estimation of the maximum scour depth

		for PI ≥ 4 $$\frac{d_{smc}}{d_{sms}} = \frac{6.02 - 10.82\left(\frac{W}{W_*}\right) + 5.41\left(\frac{W}{W_*}\right)^2}{\left(\frac{C_*}{\emptyset_*}\right)^{0.2}}$$ for PI=0 $$\frac{d_{smc}}{d_{sms}} = 1.51\left(\frac{C_*}{\emptyset_*}\right)^{0.2}$$ for PI ≥ 4 $$\frac{d_{smc}}{d_{sms}} = 0.5\left(\frac{C_*}{\emptyset_*}\right)^{-0.2}$$	(2-15) (2-16) (2-17)	around a bridge pier founded in cohesive sediments. Equations (2-16) and (2-17) had been suggested in which full saturation is assumed.
12	**Sheppard et.al ,2004**	$$\frac{ds}{b} = 2.5 \, f1 \, f2 \, f3$$ $$f1 = \tanh\left(\frac{y}{b}\right)^{0.4}$$ $$f2 = \left\{1 - 1.75\left(\ln\frac{v}{vc}\right)^2\right\}$$ $$f3 = \left(\frac{b}{d50}\right) / \left\{0.4\left(\frac{b}{d50}\right)^{1.2} + 10.6\left(\frac{b}{d50}\right)^{-0.13}\right\}$$	(2-18)	Equation is valid for $0.47 < \frac{v}{vc} < 1$
13	**Khsaf , 2010**	$$\frac{d_s}{b} = 0.29\left(\frac{y}{b}\right)^{0.51} Fr^{0.19}$$	(2-19)	-
14	**FHWA-HIF, 2012 HCI**	$$\frac{ds}{y} = 2 \, k1 \, k2 \, k3 \left(\frac{b}{y}\right)^{0.65} Fr^{0.43}$$ In terms of $\frac{ds}{b}$	(2-20)	For round nose piers aligned with the flow IF fr$\leq$0.8 ds $\leq$ 2.4 times the pier width IF Fr > 0.8 ds $\leq$ 3 times the pier width

		$$\frac{ds}{b} = 2\ k1\ k2\ k3\ \left(\frac{y}{b}\right)^{0.65} Fr^{0.43}$$	(2-21)	and critical velocity $vc = 6.19\ y^{1/6} d^{1/3}$
15	**Khwairakpam and Mazumdar, 2012**	$$ds = \left\{0.744\left(\frac{h}{b}\right) - 0.367\right\}FD50$$ $$+ \left\{-2.438\left(\frac{h}{b}\right)\right.$$ $$\left. + 2.683\right\}$$	(2-22)	The equation is a function of densimetric Froude number and inflow depth.

2.8.2 Numerical modeling work

In recent years, with the ever-increasing capabilities of computer hardware and software, computational fluid dynamics (CFD) has been widely used to determine fluid flow behavior in industrial and environmental applications. Some progression of using numerical simulation approaches to modeling bridge pier scour have been conducted using the two dimensional depth-averaged Navier-Stokes equations extended to turbulent flow using first-order closure techniques with comparisons of the numerical results with experimental data (Vincent et al., 1993). This approach obviously does not consider the full 3D characteristics of flow causing the bridge pier scour.

Olsen et al. (1993), predicted local scour developing processes using a three-dimensional flow and sediment transport model. However, their model may not able to consider all cases of scour, and it is not well-suited to calculate the maximum depth of scour around a bridge pier because the transient terms in the Navier-Stokes equations are neglected.

Mendoza, (1993), suggested that the standard k-ε model is not adequate to simulate the 3D flow field around a circular pier after the numerical calculations for the flow field and the corresponding shear stress of bed computed with the standard

k-ε model compared with the experimental data from Melville, (1975). A great disparity was found in comparison with experimental data.

Ali et al., (1997), used the renormalized group (RNG) k-ε model to predict the flow field and shear stress of bed around piers and their calculations were compared with experimental results. The calculated flow fields showed quantitatively a good agreement with the experimental results, while there was only one fair agreement in the comparison of the bed shear stresses.

Richardson and Panchang, (1998), used a computational fluid dynamics model called Flow-3D to simulate the flow occurring at the base of a cylindrical bridge pier within a scour hole. Comparing the simulated with the experimental results by Melville and Raudkivi, (1977), they found that the 3D hydrodynamic model well simulates the complex flow patterns around the bridge pier.

Chang et al., (1999), used a large-eddy simulation (LES) model to solve the flow equations around a bridge pier with a fixed bed and no scour. They applied this adjusted shear stress to Van Rijn, (1984) bed-load formula to calculate the sediment transport and tested their results against the time series data of Ettema, (1980). They found their results in good agreement with the data, supporting the method of applying flatbed sediment transport formula with an adjusted shear stress value to model the scour hole development with time.

Sumer et al., (2002), used finite volume hydrodynamic model with k-ε turbulence modeling to simulate the 3-D flow around a pier. Sumer et al., (2002) were able to capture all the main features of the scour process and their equilibrium scour depth agreed fairly well with measurements. Equilibrium was reached in approximately 2.5 hours, but computation time for the model was 2.5 months on an Alpha 21264 workstation (equivalent to a 1.5 GHz Pentium 4 PC). This makes

Sumers' model impractical for prototype size calculations where the time to equilibrium is approximately several weeks.

Ali et al., (2002), used FLUENT to predict the three-dimensional flow field around a circular cylinder for rigid beds. There was satisfactory agreement between the bed shear stresses predicted by FLUENT and those calculated from the experimental velocities near the bed. However, FLUENT is not capable of predicting turbulent bursts which can make significant contributions to the sediment motion from the bed. FLUENT is not able to simulate the increase in the water surface, with which most numerical calculations are conducted assuming that the free surface is represented by a smooth closed-lid.

Salaheldin et al., (2004), examined the performance of several models of turbulence in simulating 3-D flow field around circular piers utilizing a CFD solver FLUENT. Several types of k-ε model and Reynolds stress model (RSM) used for closure of turbulence. The computed velocity and shear stress of bed were compared with the results of some experiments in the literature like Melville, (1975), Dargahi, (1987) and Ahmed and Rajaratnam, (1998). It appeared that the standard and the RNG k-ε models were adequate for simulating the flow field around piers, but overestimate the near bed velocity. Reportedly, the RSM gave the most acceptable results of velocity, bed shear stress and level of water in the flat bottom case, and of velocity and level of water in the equilibrium scour case.

Vasquez and Walsh, (2009), used (CFD) model Flow-3D to simulate of local scour in complex bridge piers under tidal flow. Qualitative simulations of an idealized 3-pile group under clear-water tidal flow using Flow-3D showed that the scour depth decreases under tidal conditions with flow reversal, compared to that of unidirectional flow with the same peak velocity. Those numerical results agree with experimental data.

Obeid, (2016), used CFD code to simulate the 3D flow and local scouring around bridge piers. The RNG κ-ε turbulence model is used. Simulated results include scour depth around six different shapes of bridge piers and velocity distribution around piers. Comparison of the results between the numerical model and experimental model for prediction scour depth and maximum velocity, respectively, is considered a good result.

Hamidi and Siadatmousavi, (2017), Used Sediment Simulation In Intakes with Multiblock option (SSIIM) numerical model for flow field and bed transport equations. Two turbulence models k-ε and k-ω were employed for computing eddy viscosity of flow field. It showed that the k-ε turbulence model had superior performance than k-ω model when bed level changes from model were compared with measured data. Although model was successful in reproducing the scour depth in front of piers for side by side piers, it overestimated the bed scour depth between the piles.

2.9 Summary

In preparation for this research study, previous literature was reviewed. Most of them only considered the effect of flow parameters on the scour depth, while some of them investigated the behavior of pier shapes on scouring. Despite, Obeid, (2016) used different pier shapes and study its effect on scour depth under different range of flow intensities, but this problem did not study enough under different parameters effecting on scour depth. Hence, it is essential to study both the shape and flow effects on local scour depth. In the current study, Melville, (1975) model is used for verification purpose with the numerical model. The effect of pier shapes under different conditions study numerically and developed an empirical formula to predict scour depth.

Chapter Three

Numerical Simulation by Flow-3D Theory

3.1 Overview

This chapter presents the scientific theory relevant to the construction and design of numerical model for incompressible fluids, Computational Fluid Dynamic (CFD) theory as well as a review explain the selection of Flow-3D for numerical simulation. The first section will examine the selection of physical model at different conditions to verify the accuracy of Flow-3D in simulation scour around bridge pier. The second section will review simulation law of the Navier-Stokes equations and methods of solutions including turbulence models and sediment scour model, with particular emphasis on the Reynolds-average and Navier-Stokes equations and renormalized group (RNG) model. While, the following sections describe the details of the simulations including the geometry of both the numerical model and the mesh as well as the initial conditions and boundary conditions.

3.2 CFD Theory

CFD is a computer solution of the governing equations for fluid flow problems, by use of modified Navier-Stokes equation (Potter et al., 2002) i.e. the equations that summarize the law of conservation of mass of the bulk fluid and Newton's second law of motion which, with the inclusion of the continuity equation, govern fluid motion (Date, 2005). The fluid behavior, like velocity distribution and turbulence kinetic energy etc., can be obtained through Computational Fluid Dynamics software like Flow-3D, FLUENT, and PHOENIX. These softwares are developed to solve fluid behavior by solving partial differential equations based on the conservation of mass, conservation of energy etc.

Using CFD software is in many ways similar to setting up an experiment, so the original concept of this numerical simulation can be used as an alternative instead of design and construction a physical model using expansive appurtenance instruments like velocimeter. Numerical model can be applied to different environmental conditions including those that could not be modeled under normal laboratory conditions. It has been widely accepted that a good numerical model can certainly be complementary to model tests and can assist engineers in identifying the most crucial cases for which model tests may be conducted. This is an attractive idea to solve complicated problem and large model studies for which there is no need of extra workers or existing large setup to determining the actual results.

Over the years, three discretization methods commonly used in CFD have been developed; these are the finite difference, finite volume and finite element methods. The oldest method for the numerical solution of partial differential equations (PDEs), is finite difference (FD) method introduced by Euler in the 18th century (Gacek, 2007). The starting point in CFD is the differential form of the conservation of mass and momentum equations and requires the solution domain to be covered by a grid. At each grid point, PDEs are approximated in terms of the nodal values of the functions, the result of which is one algebraic equation per grid node that contains its variable value along with unknowns from a certain number of neighboring grids (Ferziger and Perić, 2002).

The finite volume (FV) method differs from the FD method where the starting point of the FV method is the integral form of the conservation equations which are subdivided into a finite number of control volumes and solved. This is done by placing a node at the centroid of each control volumes where the values of variables are to be calculated. Interpolation is then used to calculate the values of variables at the surface of the control volumes in terms of the nodal values. The finite volume

method can accommodate any grid type and is suitable for complex geometries. It is also the simplest to be understood and programed and is often used by engineers since all terms that need to be approximated have a physical meaning (Gacek, 2007).

The finite element method (FEM), which has its origins in solid mechanics and structural analysis (Chen et al., 2002), is similar to the FV method since the solution domain is broken into a set of finite volumes or elements. These elements are often unstructured and in 2D are triangles and quadrilaterals, while in 3D, are tetrahedral and hexahedral in shape (Ferziger and Perić, 2002). The finite element (FE) method is distinguished from the FV method by the multiplying of equations by a weight function before they are integrated over the entire domain.

Using the same methodology for the definition of the grid structure needed by the various methods described above, it becomes possible to define a set of PDEs to be discretized following the specifications of the selected discretization method in order to solve for the free surface and obstacles (e.g. bridge piers, gates etc.) found in open channel flow problems. Two popular models for these respective purposes are the volume of fluid (VOF) method and the fractional area/volume obstacle representation (FAVOR) method.

3.2.1 Volume of Fluid (VOF) method

Flow-3D software use volume of fluid (VOF) method to simulate the free surface flow. To obtain accurate free surface condition for VOF method, it is necessary that three requirements are provided in the software:

1. Fraction variable F is calculated for each cell. If F=1, it indicates the cells are fully filled with fluid, if F=0 it indicates that cell is empty.

2. The accurate free surface is very important to obtained. Since, fraction variable F is calculated for every cell it is possible to obtain free surface accurately.

3. Boundary conditions are the other important concern for VOF method. There are six boundary conditions in the software and it can choose an appropriate boundary condition with the several choices.

3.2.2 Fractional Area/Volume Obstacle Representation (FAVOR) method

FAVOR is a very powerful method introduced by Hirt and Sicilian, (1985) for incorporating geometry effects into the governing equations. However, it is like all discrete methods affected by the resolution of the computational grid. This is because the preprocessor generates area fractions for each cell face in the grid by defining the angles of the face within a specific geometry. If all four corners of a cell face are within geometry, the entire face is defined to be inside geometry. Also, if all corners are located outside, it is assumed that the entire face is outside the geometry. When some corners of the face are inside geometry and some outside, the geometry intersection is calculated by the edges of the face. The area fractions of these intersection points are then calculated by assuming straight-line connections between intersection points within the face. The straight-line assumption presents a small error in the fractional region when the geometric boundary is curved within the cell. Approximation corresponds to the other assumptions in the development of the equations and improves as the grid resolution is refined.

The implication of this construction is that the features that are smaller than the cell size is not resolved. More specifically, any piece of a geometry that extends across a cell face but does not including a corner of that cell face is not recognized by the area fraction generator. be recorded unless it covers at least one grid vertex,

as illustrated for the circle in the lower right corner of the mesh as shown in Figure 3.1.
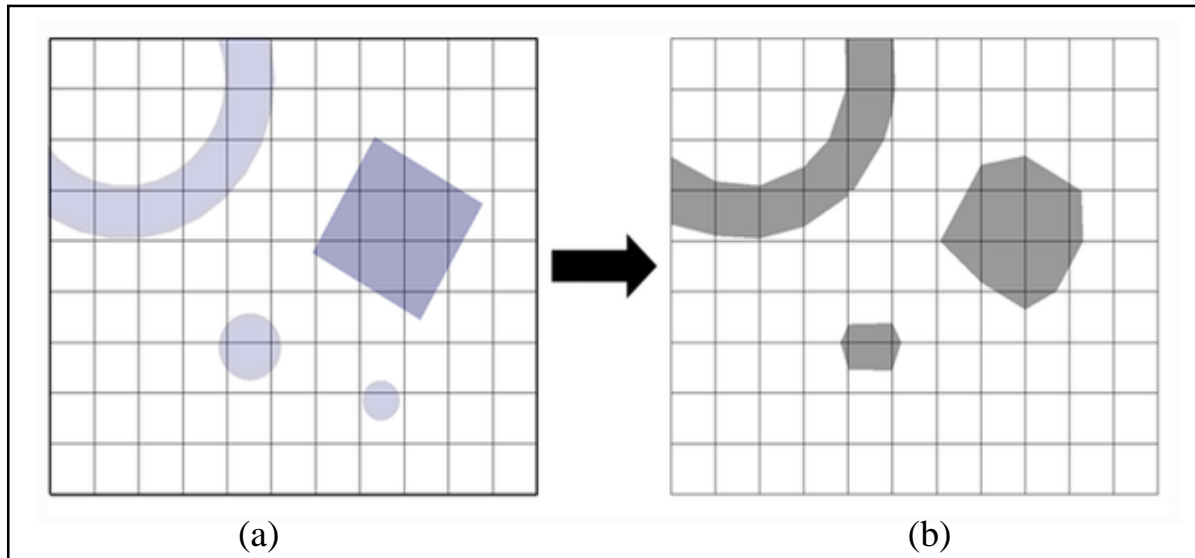
Figure (3-1): (a) Object definition and (b) Object created (FLOW-3D manual, 2014).

For some geometries and mesh resolutions, it is possible that the geometry may intersect a cell face more than once. In this case, the corresponding cell edge is assumed to be either fully inside the object or fully outside. The representation is improved as the mesh resolution is increased the cell size is decreased (FLOW-3D manual, 2014).

3.3 Physical Model

To validate the effectiveness of the present method, numerical simulations of flow and bed deformation around a bridge pier were compared with physical model. The physical model was tested to check the ability of the Flow-3D for the prediction of local scour depth and velocity profile around bridge pier.

3.3.1 Description of experimental model by Melville, 1975

Experiment to study the development of scour hole around bridge pier models was conducted in glass flume. The flume used was 19 m long, 45.6 cm wide and 44 cm deep. A cylinder with a diameter (b) of 5.08 cm was used as a bridge pier, giving a contraction ratio, B/b (where B = flume width and b = cylinder diameter) equal to about 9. The bed material involved was relatively uniform sized sand with a median grain size (d_{50}) of 0.385 mm, height 12.7 cm and density of 2650 kg/m^3. The angle of repose of the sand was measured in the saturated condition and was found to be 32°. The approaching mean flow velocity is 0.25 m/s. The water is discharged at a rate of 0.01712 m^3/s with a water depth of 15 cm. Figure 3.2 shows a sketch of the experiment setup.
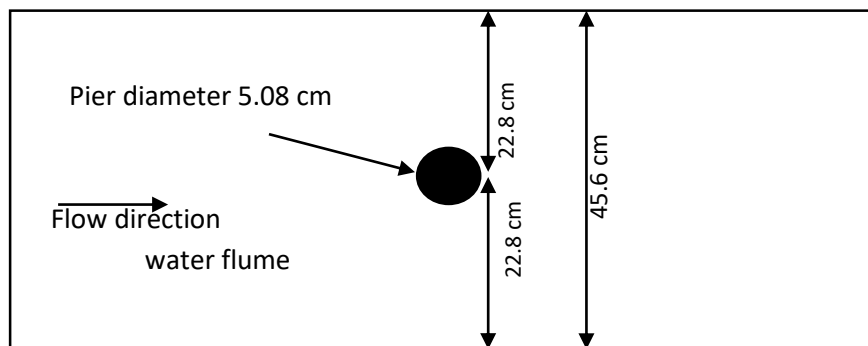
Figure (3-2): Plan view of Melville experimental setup (Melville, 1975)

3.4 Numerical Model

Flow-3D is a commercially available CFD package created by Flow Science Inc., which uses both the VOF and FAVOR methods for determining the location of the free surface and the location of obstacles respectively. Flow-3D employs specially developed numerical techniques to solve the equations of motion for fluids to obtain transient, three-dimensional solutions to multi-scale, multi-physics flow problems (FLOW-3D manual, 2014).

Flow-3D used to simulate the scour process around the bridge piers and has a powerful capacity to investigate the behavior of liquids and gases specializing in the solution of transient, free-surface problems and sediment transport. It uses a non-hydrostatic finite difference model to solve the 3D Navier-Stokes equations.

This numerical model starts with a computational mesh. This computational mesh consists of a number of cells; these cells subdivide the physical space into small volumes with several nodes associated with each such volume. The nodes are used to store values such as pressure, temperature and velocity. The mesh is actually the numerical space that replaces the original physical space. The computational mesh can illustrate the complex boundaries of the solution domain by the application of the FAVOR method, which allows a rectangular computational cell to be partially blocked by an obstacle. Sharp free surface (e.g. hydraulic jumps, free jets in air) are modeled by VOF method.

Flow-3D has a powerful capacity to deal with the scour issues. However, its sediment transport model is based on an empirical formula and this model increases the cost of computational time. Thus, the simulation for some cases cannot be finished within a reasonable time. The CFD code provides an economic way to predict potential results. However, most programs cannot handle scour models in hydraulics because of the complex pattern of the scour procedure under flow conditions (Obeid, 2016).

The purpose of the numerical simulation in this study is to accurately model fluid flow and sediment scour around bridge pier. The following sections describe in detail the physical model tests, which provided the verification data for the computational model, whose methods and constraints are also described.

3.4.1 Governing equations

The equations governing the motion of a viscous fluid namely the continuity equation and the momentum conservation equations are known as Navier- Stokes equations. The Navier-Stokes equations for a viscous incompressible Newtonian fluid take the form (Gacek, 2007):

$$\frac{\partial u_i}{\partial t} + u_j \frac{\partial u_i}{\partial x_j} = -\frac{1}{\rho}\frac{\partial p}{\partial x_i} + \frac{\partial \sigma_{ij}}{\partial x_j} \qquad (3-1)$$

Continuity equation

$$\frac{\partial u_i}{\partial x_i} = 0 \qquad (3-2)$$

In the Reynoldes averaged Navier-Stokes approach, the Navier-Stokes equations are averaged over a time interval or across a grouping of equivalent flows. The goal of this approach is to obtain the mean effect of turbulent quantities (Drikakis, 2003). The Reynoldes Averaged Navier-Stokes (RANS) equations for a viscous incompressible Newtonian fluid are:

$$\frac{\partial \bar{u}_i}{\partial t} + \bar{u}_j \frac{\partial \bar{u}_i}{\partial x_j} = -\frac{1}{\rho}\frac{\partial \bar{p}}{\partial x_i} + \frac{\partial \bar{\sigma}_{ij}}{\partial x_j} - \frac{\partial \left(\overline{\acute{u}_i \acute{u}_j}\right)}{\partial x_j} \qquad (3-3)$$

Where:

$$\sigma_{ij} = 2v s_{ij} \qquad (3-4)$$

$$s_{ij} = \frac{1}{2}\left(\frac{\partial u_i}{\partial x_j} + \frac{\partial u_j}{\partial x_i}\right) \qquad (3-5)$$

$$\overline{\acute{u}_i \acute{u}_j} = v_t \left(\frac{\partial \bar{u}_i}{\partial x_j} + \frac{\partial \bar{u}_j}{\partial x_i}\right) - \frac{2}{3}\delta_{ij}k \qquad (3-6)$$

Where u_i is the fluid velocity component in i direction, $\acute{u}_i$ is the fluctuation of fluid velocity in i direction, P is the pressure, s_{ij} is the strain rate tensor, $\overline{\acute{u}_i \acute{u}_j}$ is the Reynolds stress tensor, ρ is the fluid density, v is the fluid kinetic viscosity, v_t

is the turbulence viscosity, k is the turbulent kinetic energy, and δ_{ij} is the Kronecker delta ($\delta_{ij} = 1$, $i = j$; $\delta_{ij} = 0$, $i \neq j$).

3.4.2 Turbulence model

Turbulence is a three-dimensional unsteady viscous flow phenomenon that occurs at high Reynolds numbers. It is characterized by rapid and highly localized fluctuations in flow parameters such as velocity components, pressure, temperature, species concentration etc.

In Flow-3D, there are six turbulence models available: the Prandtl mixing length model, the one-equation, the two-equation $k - \varepsilon$, renormalized group RNG model, $k - \omega$ models, and a large eddy simulation (LES) model. The principal goal of any turbulence model is to provide a mechanism for estimating the influence of turbulent fluctuations on mean the flow quantities. Yakhot and Orszag, (1986) introduced the RNG-based $k - \varepsilon$ model. The main characteristic of this model is that the numerical constants in the $k - \varepsilon$ model are directly obtained from the renormalization group theory, and are in good agreement with the standard $k - \varepsilon$ model. The RNG model uses equations similar to the equations for the $k - \varepsilon$ model. However, equation constants that are found empirically in the standard $k - \varepsilon$ model are derived explicitly in the RNG model. Generally, the RNG model has wider applicability than the standard $k - \varepsilon$ model. In particular, the RNG model is known to accurately describe low intensity turbulence flows and flows having strong shear regions. The governing equations are as follows (FLOW-3D manual, 2014): Continuity equation:

$$\frac{\partial \rho}{\partial t} + \frac{\partial u_i}{\partial x_i} = 0$$

$$(3-7)$$

k-equation:

43

$$\frac{\partial k}{\partial t} + u_j \frac{\partial k}{\partial x_i} = T_{ij} \frac{\partial u_i}{\partial x_j} + \frac{\partial}{\partial x_j}\left[\frac{1}{\rho}\left(\mu + \frac{\mu_t}{\sigma_k}\right)\frac{\partial k}{\partial x_j}\right] - \varepsilon$$

(3 − 8)

$\mathcal{E}$-equation:

$$\frac{\partial \varepsilon}{\partial t} + u_j \frac{\partial \varepsilon}{\partial x_i} = C_{1\varepsilon}\frac{\varepsilon}{k}T_{ij}\frac{\partial u_i}{\partial x_j} + \frac{\partial}{\partial x_j}\left[\frac{1}{\rho}\left(\mu + \frac{\mu_t}{\sigma_\varepsilon}\right)\frac{\partial \varepsilon}{\partial x_j}\right] - C_{2\varepsilon}\rho\frac{\varepsilon^2}{k}$$

(3 − 9)

Where: k is the Reynolds-averaged kinetic energy

ε is the dissipation rate of turbulent kinetic energy

μ_t is the turbulent eddy viscosity

$$k = \frac{1}{2}\overline{\acute{u}_i\acute{u}_j}$$

(3 − 10)

$$\varepsilon = v\overline{\left(\frac{\acute{u}_i}{\partial x_k}\right)\left(\frac{\acute{u}_i}{\partial x_k}\right)}$$

(3 − 11)

$$\mu_t = \frac{C_\mu \rho k^2}{\varepsilon}$$

(3 − 12)

$$T_{ij} = \frac{\mu_t}{\rho}\left(\frac{\partial u_i}{\partial x_j} + \frac{\partial u_i}{\partial x_j}\right) - \frac{2}{3}\rho k \delta_{ij}$$

(3 − 13)

Where: C_μ , $C_{1\varepsilon}$, $C_{2\varepsilon}$, σ_k and σ_ε are all dimensionless user-adjustable parameters, and have a values of 0.085, 1.42, 1.39, 0.7179 and 0.7179, respectively (FLOW-3D manual, 2014). The RNG model is used in this study. There are three reason for using the RNG model that are:

1- This model is well suited for the modeling of turbulent flow over bridge pier.

2- This model is considered as the most accurate and strong model available in the software for scour simulations.

3- RNG model may perform better for scour simulations due to its suitability in cases where a large amount of turbulence is created and caused by the flow of the fluid through the control structure (FLOW-3D manual, 2014).

3.4.3 Sediment scour model

The sediment scour model assumes multiple non-cohesive sediment species with different properties including grain size, mass density, critical shear stress, angle of repose and parameters for entrainment and transport. For example, medium sand, coarse sand and fine gravel can be categorized into three different species in a simulation. It estimates the motion of sediment by predicting the erosion, advection and deposition of sediment. It does so by:

- Computing the suspended sediment transportation.
- Computing the sediments' settling due to gravity.
- Computing the entrainment of the sediment due to bed shearing and flow perturbations.
- Computing the bed-load transportation, whereby sediment grains roll, hop or slide along the packed sediment bed.

In Flow-3D, this is done by considering two states in which sediment can exist: suspended and packed sediment. Suspended sediment is typically of low concentration and advects with fluid flow. Packed sediment exists at the critical packing fraction which can be defined by the user (default value is 0.64) (FLOW-3D manual, 2014). Only a thin surface layer of grains of the packed sediment (in the thickness of a few grain diameters) can move in the form of bed-load transportation.

Sediment is entrained by the process which turbulent eddies remove the grains from the top of the packed bed and carry it into suspension. It occurs when the bed shear stress exceeds a threshold value (critical shear stress). Because it is not possible

to compute the flow dynamics about each individual grain of sediment, an empirical model must be used. The model used here is based on Mastbergen and Van Den Berg, (2003) work. Also, Soulsby-Whitehouse, (1997) equation can be used to predict the critical Shields parameter, or a user-defined parameter can be specified. By default, the critical Shields parameter is 0.05 simulations (FLOW-3D manual, 2014). The first step to computing the critical Shields parameter is to calculate the dimensionless parameter $d_i{}^*$:

$$d_i{}^* = d_i \left[\frac{\rho_f \left(\rho_i - \rho_f \right) g}{\mu_f{}^2} \right]^{\frac{1}{3}} \qquad\qquad (3-14)$$

Where:

$\rho_i=$ is the density of the sediment species i

$\rho_f=$ is the fluid density

$d_i =$is the sediment diameter

$\mu_f=$ is the dynamic viscosity of fluid

$g =$is the magnitude of the acceleration of gravity g.

From this, the dimensionless critical Shields parameter is computed using the Soulsby-Whitehouse, (1997) equation:

$$\theta_{cr,i} = \frac{0.3}{1 + 1.2d_i{}^*} + 0.055[1 - exp(-0.02d_i{}^*)] \qquad\qquad (3-15)$$

The local Shields parameter is computed based on the local bed shear stress, τ :

$$\theta i = \frac{\tau}{g \, d_i(\rho_i - \rho_f)} \qquad\qquad (3-16)$$

Where: τ is calculated using the law of the wall and the quadratic law of bottom shear stress for 3D turbulent flow and shallow water turbulent flow, respectively,

with consideration of bed surface roughness. It is assumed that the Nikuradse roughness of the bed surface R_s is proportional to the local median grain diameter in packed sediment $d_{50,packed}$

$$R_s = c_{rough} \, d_{50,packed} \qquad (3-17)$$

where c_{rough} is a user-defined coefficient with default value 1.0 (FLOW-3D manual, 2014). The entrainment lift velocity of sediment is then computed as Mastbergen and Van Den Berg, (2003) :

$$u_{\text{lift},i} = \alpha_i n_s d_*^{0.3} (\theta_i - \theta'_{cr,i})^{1.5} \sqrt{\frac{g \, d_i (\rho_i - \rho_f)}{\rho_f}} \qquad (3-18)$$

Where α_i is the entrainment parameter, whose recommended value is 0.018 (Mastbergen and Van Den Berg, 2003) and n_s is the outward pointing normal to the packed bed interface. $u_{\text{lift},i}$ is then used to compute the amount of packed sediment that is converted into suspension which is effectively acting as a mass source of suspended sediment at the packed bed interface. After that, the sediment is transported with fluid flow.

Bed-load transport is the mode of sediment transportation due to rolling or bouncing over the surface of the packed bed of sediment. The model currently used is formed Meyer-Peter and Müller, (1948) . This model predicts the volumetric flow of sediment per unit width over the surface of the packed bed.

$$\Phi_i = \beta_i (\theta_i - \theta'_{cr,i})^{1.5} \, c_{b,i} \qquad (3-19)$$

Φ_i is the dimensionless bed-load transport rate which is related to the volumetric bed-load transport rate, $q_{b,i}$ by:

$$q_{b,i} = \Phi_i \left[g \frac{(\rho_i - \rho_f)}{\rho_f} \, d_i^3 \right]^{\frac{1}{2}} \qquad (3-20)$$

Where: β_i is the bedload coefficient. It is generally ranged from 5.0 to 5.7 for low transport, around 8.0 for intermediate transport, and up to 13.0 for very high transport. The default value used in Flow-3D is 8.0, which is the most commonly used value in the literature. $c_{b,i}$ is the volume fraction of species i in the bed material (FLOW-3D manual, 2014).

$$c_{b,i} = \frac{net\ volume\ of\ species\ i}{net\ volume\ of\ all\ species} \tag{3-21}$$

and satisfies

$$\sum_{i=1}^{I} c_{b,i} = 1 \tag{3-22}$$

Where i is the total number of species. As $c_{b,i}$ does not exist in the original Meyer-Peter and Müller, (1948) equation, it was added in Equation (3-19) to account for the effect of multiple species. Another piece of information needed is an estimation of the bed-load layer thickness, i.e., the thickness of the saltating sediment, δ_i. The relationship chosen to estimate this thickness is Van Rijn, (1984).

$$\frac{\delta_i}{d_i} = 0.3 d_*^{0.7} \left(\frac{\theta_i}{\theta'_{cr,i}} - 1 \right)^{0.5} \tag{3-23}$$

To compute the motion of the sediment in each computational cell, the value of $q_{b,i}$ is converted into the bed-load velocity by Van Rijn, (1984):

$$u_{bedload,i} = \frac{q_{b,i}}{\delta_i\ c_{b,i}\ f_b} \tag{3-24}$$

Where: f_b is the critical packing fraction of the sediment.

 The bed-load velocity is assumed to be in the same direction as that of the fluid flow adjacent to the packed bed interface. In this study, the parameters selection in sediment scour to build the numerical model after calibration of many runs are critical Shields number = 0.05, entrainment coefficient =0.018 and bed load coefficient = 12 and the maximum packing fraction = 0.64.

3.5 Procedure of FLOW-3D Simulation

In order to simulate the scour depth around a bridge pier and achieve accurate results, multiple steps were carried out. Figure 3.3 is a flow diagram displaying the basic procedure steps of Flow-3D simulation.
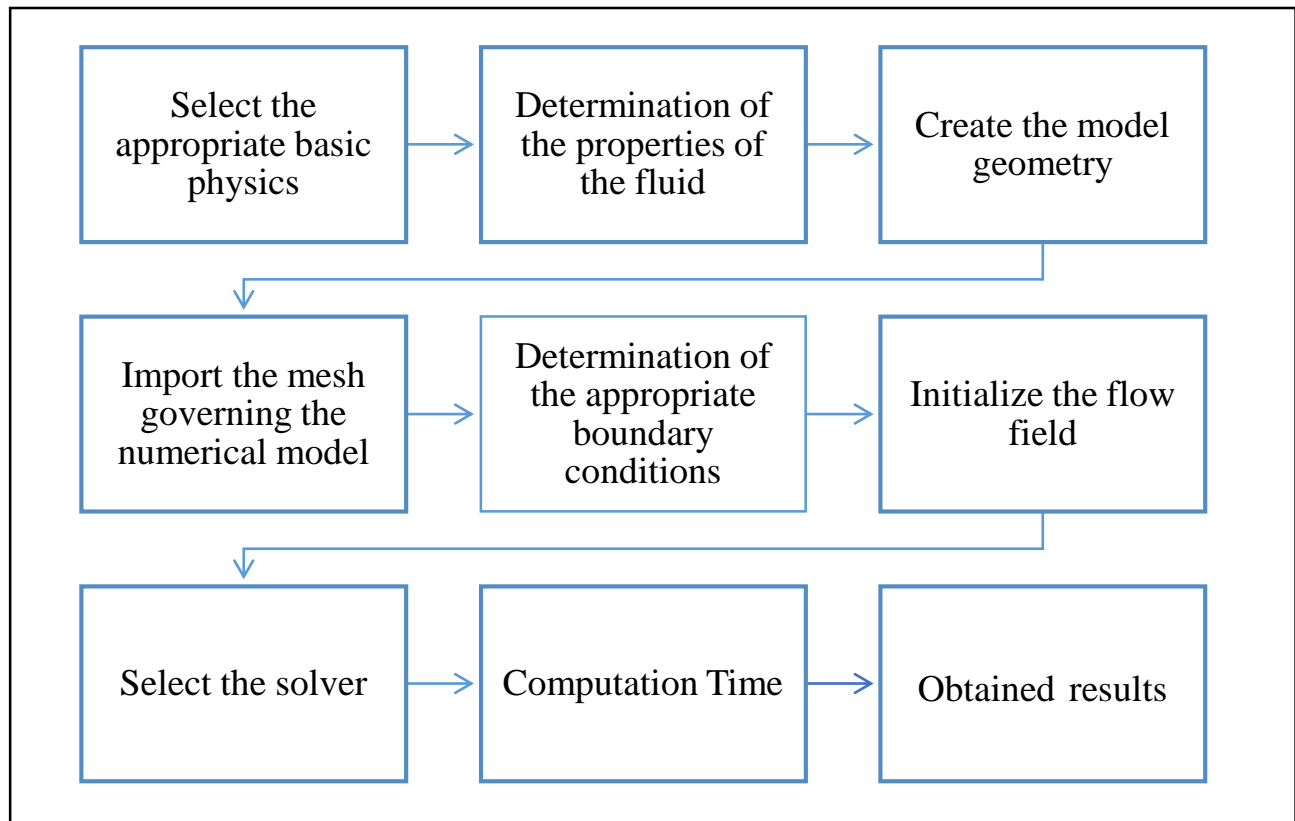
Figure (3-3): Procedure of the numerical simulation by the Flow-3D

3.5.1 Flow-3D physics

There are many different physics options available, only four physics activation are required to obtain accurate simulations of the data that are desired in this study. The gravity option is activated with gravitational acceleration of the vertical or z-direction being set to negative 9.81 m/sec^2. The sediment scour model activated and set to median diameter of 0.385 mm with density of 2650 kg/m^3 and critical shield number of 0.05, bed-load coefficient = 12 while the other sediment

parameters remained of the same default values. These parameters were selected after calibration with physical models. The viscosity and turbulence option is also activated with Newtonian viscosity being applied to the flow along with the selection of an appropriate turbulence model. Once the Flow-3D model is completely prepared, one turbulence model applied in this study as long as the renormalized group (RNG) model is selected.

3.5.2 Material properties

The properties of the fluid such as viscosity, temperature and density should be determined as an input in the numerical model. Fluid is selected using fluid database tab and fluid properties are specified on the fluids tab. In Flow-3D, there is a set of popular materials to help the user. In this study, the temperature of the water is set to 20 °C with density 1000 kg/m^3.

3.5.3 Model geometry

Rectangular flume with different pier shapes (circular, rectangular, square, octagonal, elliptic, oblong, hexagonal, ogival and lenticular) are used to study the effect of piers shape on scour depth and fluid behavior around the bridge pier. For the computational domain in the numerical simulation, inlet locate at a distance of 6b, where b is the pier diameter upstream of the pier with a diameter equal to 5.08 cm. The outlet located at a distance of 14b downstream of the pier. In the inlet of the flume, one solid component was settled to prepare an inflow bottom at the top edge of the sediment at elevation of 12.7 cm in order to prevent against upward movement of sediments in the beginning of simulations.

Width of the flume was set to 45.6 cm, where Raudkivi and Etema, (1983) suggested that the ratio of flume width to pier diameter should be minimum 6.25 to ensure that the flume wall has no effect on scouring. Packed sediment component

was placed on the flume at a depth equal to 12.7 cm and the water depth was 15 cm above the sediment level. The geometric representation the numerical model is shown in Figure 3.4.
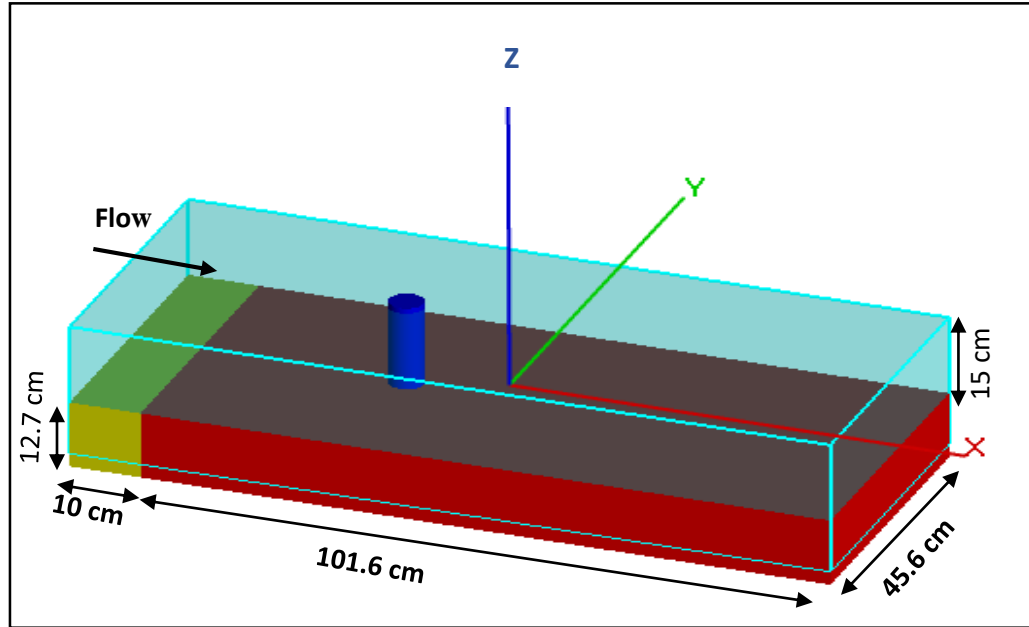
Figure (3-4): Geometry of the numerical model configured by the Flow-3D

Three-dimensional solid geometry of bridge piers was drawn by using SKETCH-UP modeling tool. The pier model used in the simulations is exported as a stereo lithographic (.stl) file format which could be read by Flow-3D from SKETCH-UP. The stl. files are then directly imported into Flow-3D where the appropriate mesh can be generated.

The pier models used in the numerical simulation have a constant length to width ratio with l/b = 2, except circular and square pier, where l/b ratio =1. The geometric representation of pier model is shown in Figure 3.5.
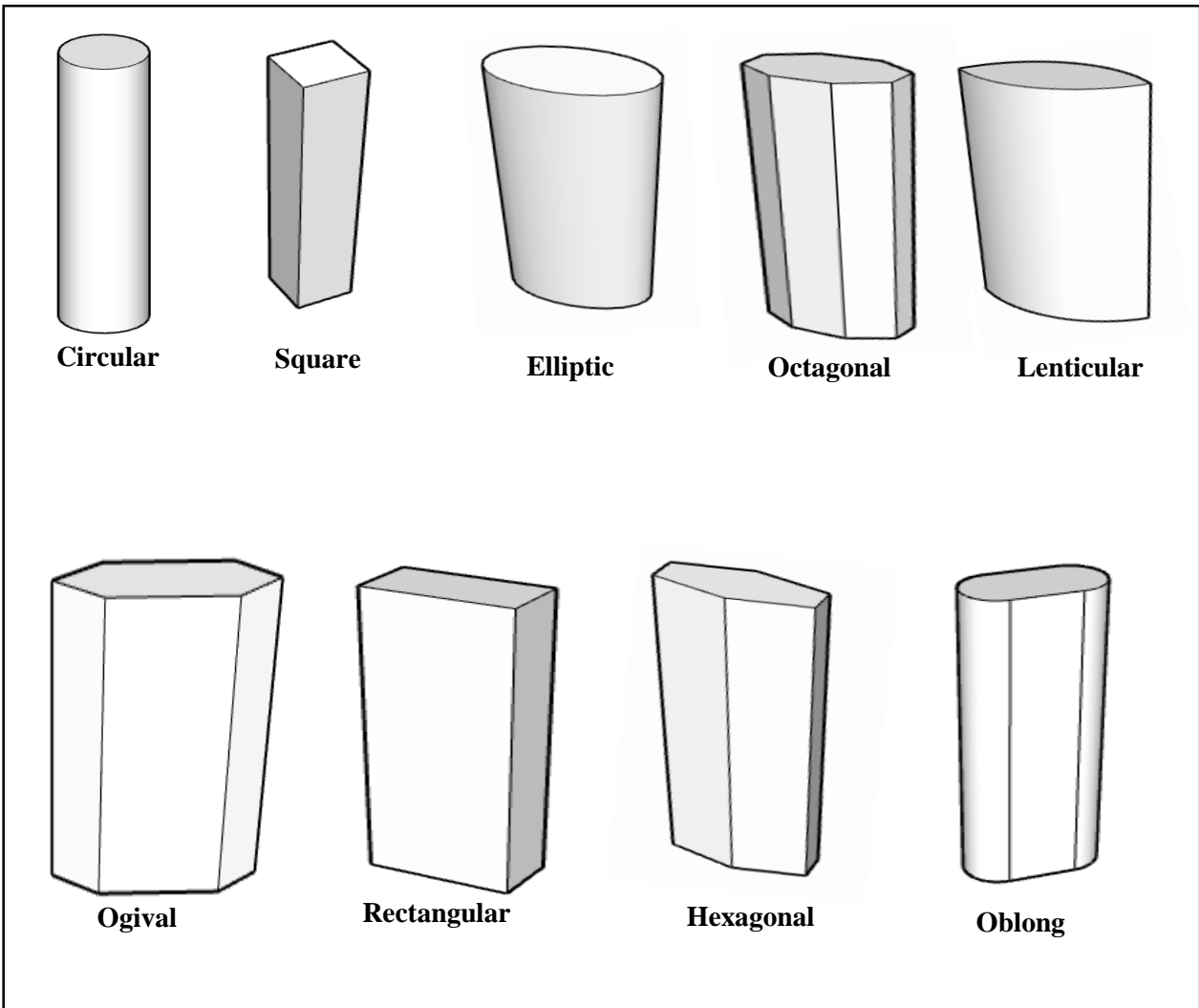
Figure (3-5): Pier models used in simulation with l/b=2.

3.5.4 Meshing

In Flow-3D, mesh generation is the most important issue for accurate solution. If good quality of mesh is generated, one can obtain realistic results from the numerical model. Determining the appropriate grid domain along with a suitable mesh cell size is a critical part of any numerical model simulation.

Grid and cell size can affect both the accuracy of the results and the simulation time. These constraints are often interdependent as the increase or decrease in one

52

could have a positive or negative effect on another. Using finer mesh to increasing accuracy of the result could, possibly, negatively impact the amount of computation time required to reach steady-state despite the use of the more powerful computer because calculations are done for every cell, so the increasing number of cells will increase time of simulation. In addition, decreasing the size of mesh cells would require a decrease in time step size and decrease the resolution to capture the important features of the geometry. The simulation time may either decrease or increase due to the combined effects of computer processor and a coarser mesh.

So, it is important to minimize the size of the cells while including enough resolution to capture the important features of the geometry as well as sufficient flow detail. An effective way to determine the optimal cell size is to start with a relatively large mesh size and then progressively reduce the mesh size until the output no longer changes significantly with any further reductions. Thereby, optimum number of cells should be assigned.

In the beginning, optimum number of cells can be obtained by Fractional Area/Volume Obstacle Representation (FAVOR). FAVOR option is a very powerful method for incorporating geometry effects into the governing equations. Since the cells are orthogonal, it must obtain optimum size of cells to generate system to be nearly the same with the real case. If the cell sizes are not optimum, geometry problems will be occurred as shown in Figure 3.6. To avoid those problems, FAVOR option help users to obtain accurate geometric shapes.

a. **Coarse mesh pre-rendering**   b. **Fine mesh pre-rendering**

c. **Coarse mesh post-rendering**   d. **Fine mesh post-rendering**
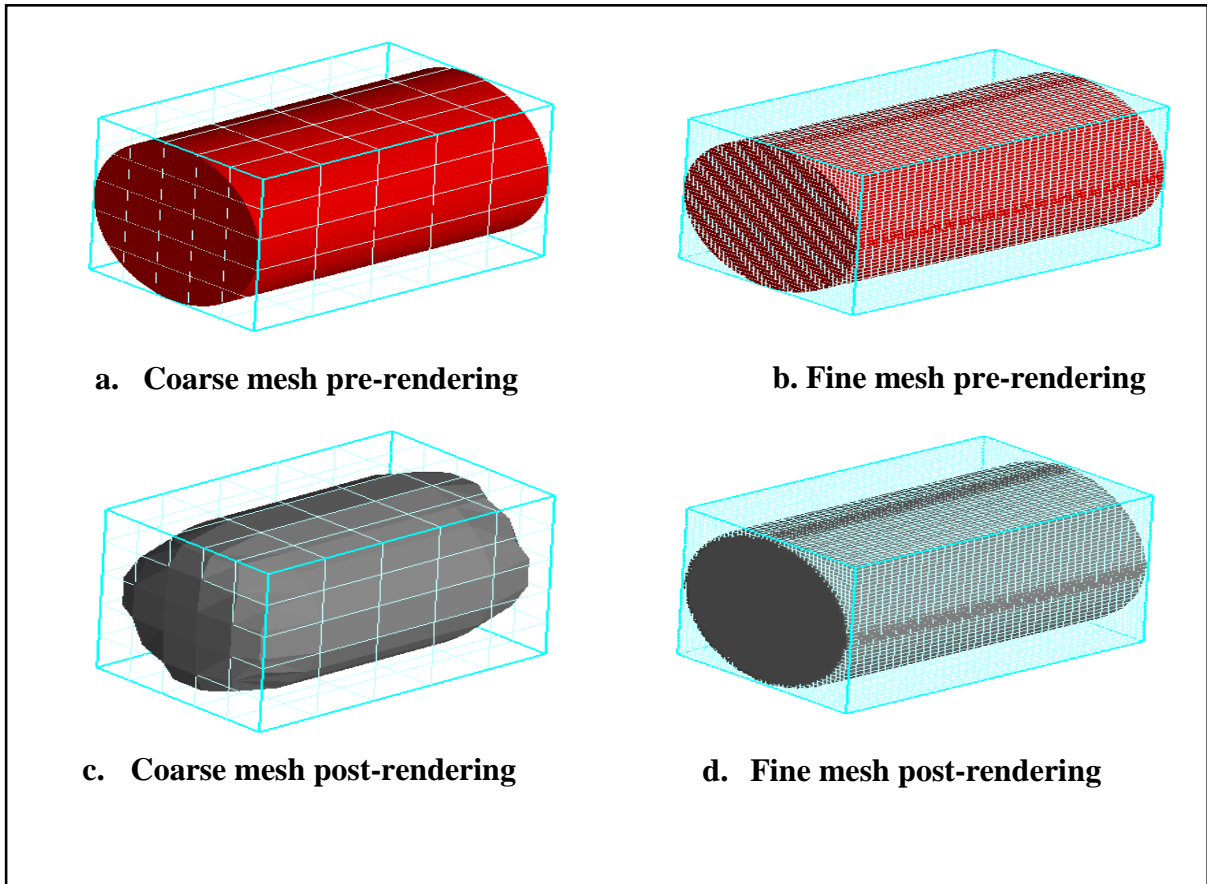
Figure (3-6): FAVOR option with different cell size.

Flow-3D mesh generator uses the Factional Area Volume Obstacle Representation (FAVOR) method to handle the complicated geometries in an orthogonal mesh defined in Cartesian or cylindrical coordinates. Only the orthogonal mesh is allowed to simplify the process of meshing domain in Flow-3D as shown in Figure 3.7. The obstacles are embedded in the orthogonal mesh, which allows separate definition of the mesh and geometry so the modification of geometry has not any influence on the mesh.

| (a)Coarse Mesh | (b)Fine Mesh |
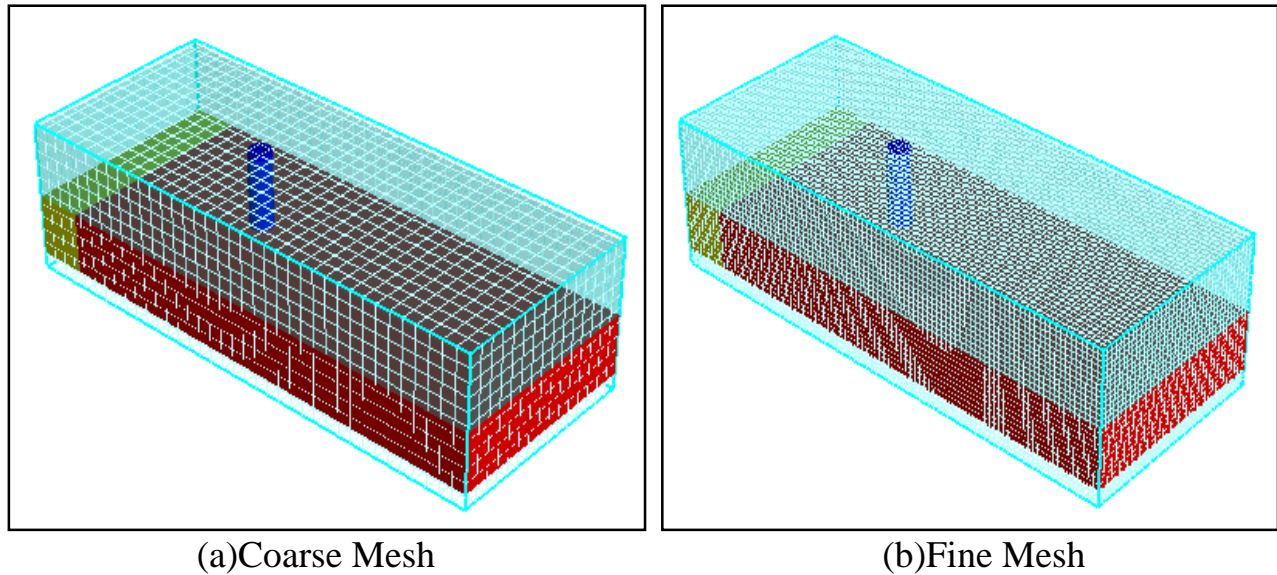
Figure (3-7): Mesh generation by FAVOR

The mesh of Flow-3D software has a cell of cubic shape and considering as one of the affecting factors on the simulation process. In an effort to decrease the computational time required for a simulation to reach steady-state, simulations were first run on a coarse mesh and the approximate solution was then used as input data for the exact same simulated conditions with a finer mesh. Different types of mesh resolution have been tested as this offers best precision/computation time results. The mesh resolution is finally determined as an optimum of computation time and the proper reproduction of the relevant hydraulic phenomenon.

Therefore, different cell sizes are selected as (30, 25, 20, 15,10 ,5 and 1) mm to identify the optimum cell size that satisfy the phenomenon conditions. A number of tests were carried out as shown in Figure 3.8 to determine the best cell size that the depth of scour doesn't change significantly.
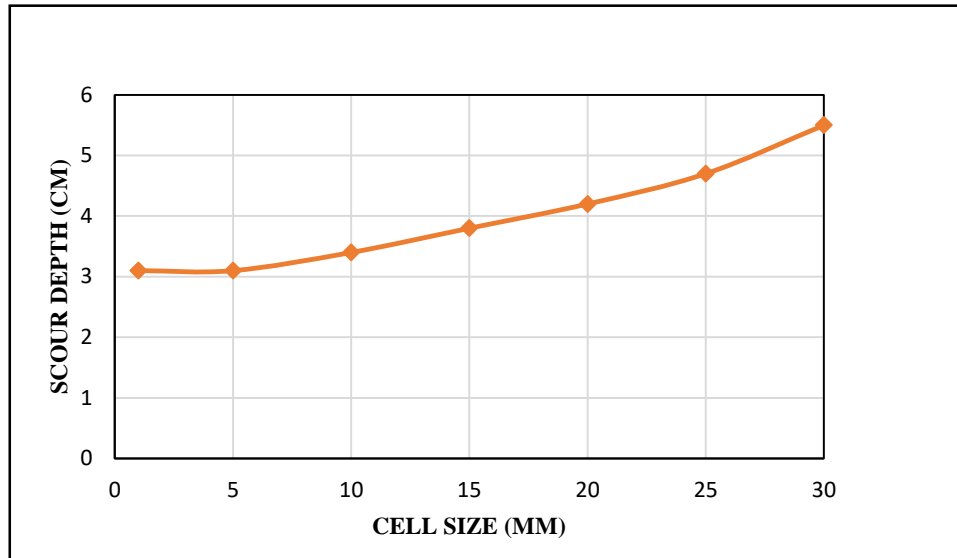
Figure (3-8): Effect of cell size on scour depth

According to the Figure 3.8, when the cell size reaches 5 mm, the scour depth around pier become constant and shows independency from cell size. Larger cell size up to 30 mm caused many problems in simulation and some of the problems that the scour may be occurred in the beginning of the flume (inlet of the model) and another problem is that the cell size doesn't give accurate result. The selection of 5 mm as the optimum cell size depends on the accuracy of results and the high clearness scour depth around pier.

For better estimation of scour development around a pier, two mesh planes with finer resolutions were defined for both sides of the pier in x and y directions. Minimum cell size near the pier is about 5 mm and the maximum cell size is limited as 10 mm to reduce in computation time. Totally, 252,000 cells are generated for the working section which is shown in Figure 3.9.
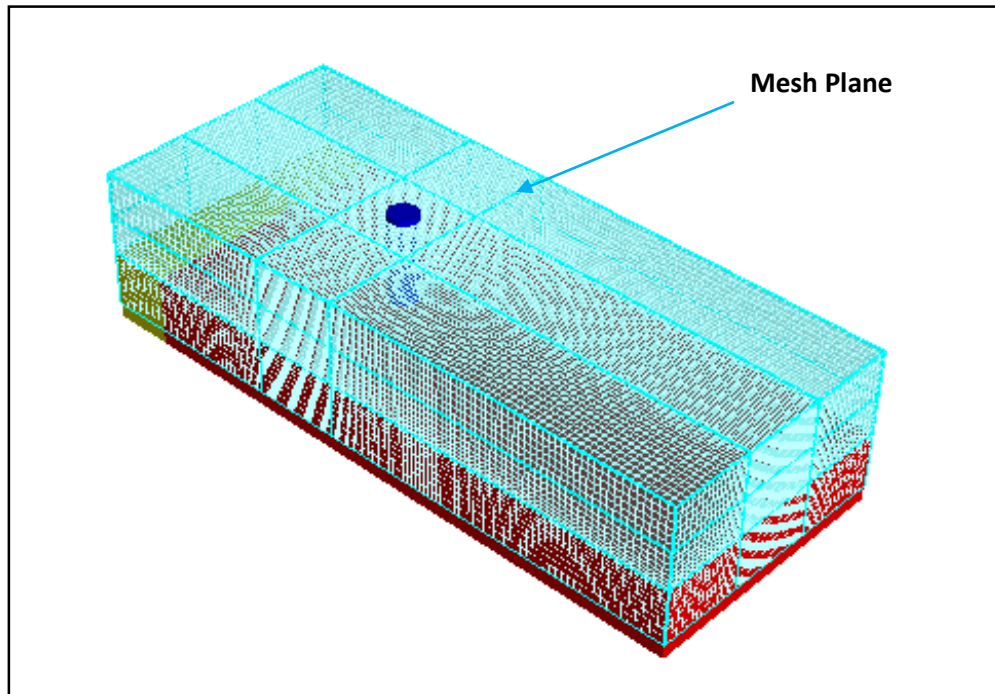
Figure (3-9): Meshing plane structure around a pier

3.5.5 Boundary and initial conditions

An important part of the numerical simulation is the determination of the representative boundary conditions for the hydraulic analysis. The boundary conditions must be matched with the physical conditions of the problem properly. Flow-3D uses the orthogonal hexahedral meshes in the Cartesian coordinates in order to define the three-dimensional flow domain. Thus, there are six different boundaries defined on rectangular mesh prism. The boundary conditions used in this study are shown in Figure 3.10.

1- **Inlet boundary (X-min.):** was set as a specific velocity condition (V), different rang of velocity used in the simulation and used various fluid heights beginning at a stagnation pressure state.

2- **Outlet Boundary (X-max.):** outflow condition (O).

At the outflow boundary, zero-gradient boundary conditions are used and velocities are set equal to the values in the elements closest to the outflow.

3- **Top Boundary (Z-max):** symmetry condition (S).

4- **Bottom boundary (Z-min.):** wall condition (W).

The upper boundary is located above the water surface and the lower boundary is located under the packed sediment. Therefore, as the boundaries are either in the air phase or just below the entire structure, the symmetry condition does not affect the flow and is selected arbitrarily mainly because Flow-3D defaults to this condition at start up.

5- **Side boundary (Y-min., Y-max.):** symmetry condition (S).
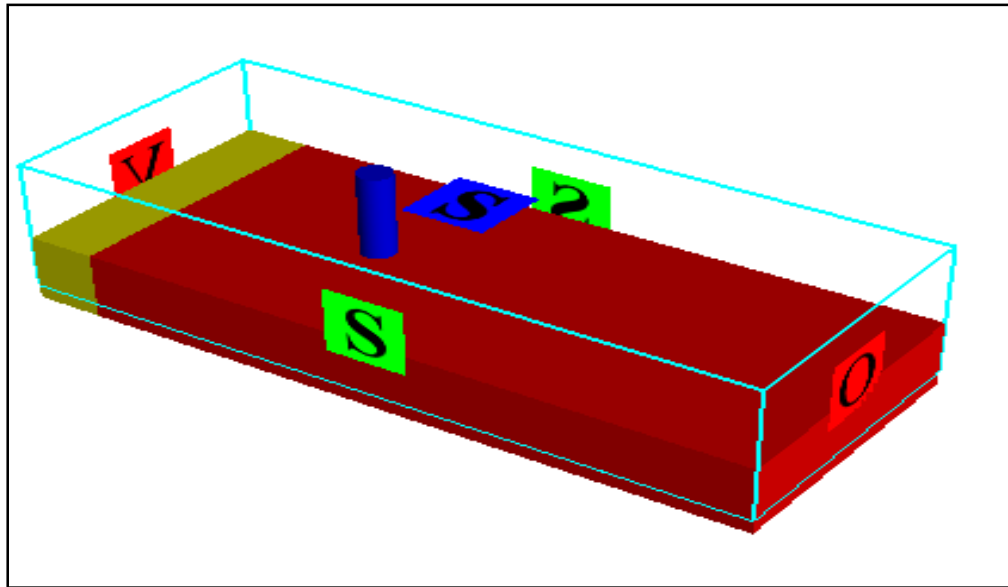
Figure (3-10): Boundary conditions of the numerical model

For initial conditions, the fluid area within the work section is determined and its location starts from the upstream to the end of the downstream as illustrated in Figure 3.11.
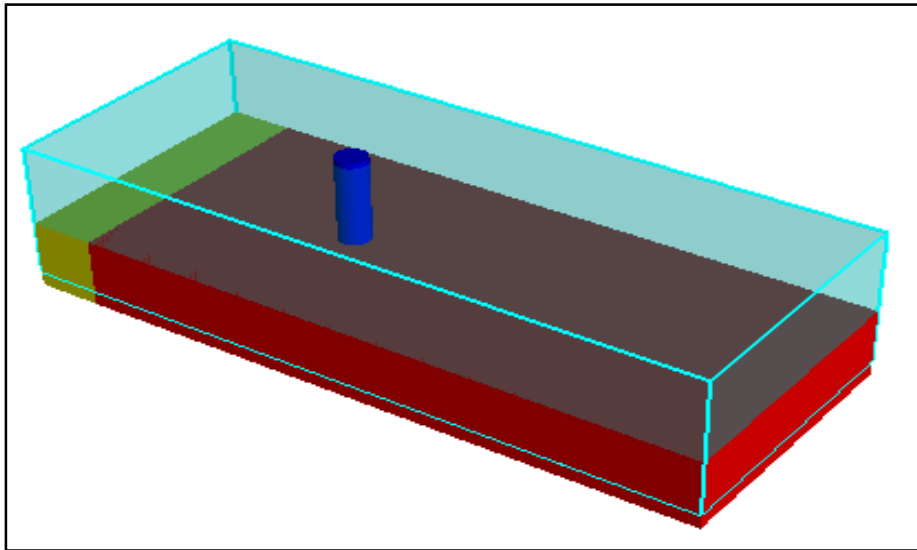
Figure (3-11): Initial condition of the flow region for simulation.

3.5.6 Solution options

Many parameters can affect the simulation results and time where the solution method (implicit or explicit), time step size, convergence settings, and numerical approximations are some of them. Balancing runtime and simulation resolution is an important point. To provide optimum and effective simulation solutions, choosing the right numerical options is very important. Numerical options are specified in the Numeric tab. In this study, the water is used in all simulations. It is assumed to be incompressible and only one fluid is solved in all simulations. The pressure solver is identified as implicit because pressure forces in the momentum equation are always implicitly approximated for incompressible fluids as a means of maintaining the incompressibility of the fluid and stability of the solution. In the numeric option, the GMRES algorithm is the default iteration method and this method can be used for a wide range of problems. To compute the viscous stresses, the explicit viscous algorithm is used. There are many options in Flow-3D to track fluid interfaces. The automatic option is used as the volume of fluid advection model to track fluid

interface. For a sharp interface with a fluid-free surface flow, the most efficient and accurate model in Flow-3D is the automatic option.

3.5.7 Computational time

According to the limitations in data storage capacity and computing power, the end of the time is selected in terms of hydraulic stability, where this is achieved when the phrase "run is steady state". It shows in this state that scour depth continued to increase but very slowly. For numerical simulation, running time was performed for 30-minute because sediment transportation reaches balance state of scour developing and the maximum depth of scour did not exceed 2% from the total scour depth at this time after testing it. Some of the Flow-3D constraints is that the running time for a simulation process, sometimes, exceeds 168 hours for 30-min scour simulation at different cases during this study.

3.6 Dimensional Analysis

Dimensional analysis is an effective tool in formulating problems and representing relationships between different physical quantities by determining their dimensions. Physical mechanism of the local scour around bridge pier can be understood better if appropriate dimensionless parameters describing the phenomenon are defined. The parameters that affect the depth of scour are flow variables, fluid variables, bed sediment variables, pier variables, flume geometry and time. These parameters are categorized in the expression of mass (M), length (L) and time (T), as shown in Table 3.1.

Table (3-1): Parameters that affect the local scour mechanism in (MLT).

1) Parameters characterizing the fluid		Units	Dimensions
ρ	Density of the fluid	kg/m3	ML-3
ν	Kinematic viscosity of the fluid	m^2/s	L^2T^{-1}
g	Gravitational acceleration	m/s^2	LT^{-2}
2) Parameters characterizing the flow		Units	Dimensions
y	Approach flow depth	m	L
V	Approach flow velocity	m/s	LT^{-1}
V_c	Critical mean approach flow (threshold velocity for sediment movement)	m/s	LT^{-1}
3) Parameters characterizing the bed material		Units	Dimensions
ρ_s	Density of the sediment	kg/m^3	ML^{-3}
d_{50}	Median sediment size	mm	L
σ_g	Geometric Standard deviation of particle size distribution	-	-
4) Parameters characterizing the flume		Units	Dimensions
S_o	Channel bed slope	m/m	-
B	Channel width	m	L
5) Parameters characterizing the pier		Units	Dimensions
l	Pier length	m	L
b	Pier diameter or pier width for pier projection	m	L

61

K_s	Pier shape factor	-	-
θ	Angle of approach flow to the axis	-	-
6)	**Time**	**Units**	**Dimensions**
t	Duration of flow	min	T

The depth of the local scouring around the bridge pier is a function of the following parameters and can be presented in the following relations, where d_s represents the maximum depth of scour and f is a general function:

$$ds = f\left(\rho, \nu, V, y, g, \rho_s, d_{50}, \sigma_g, V_c, S_o, B, b, L, K_s, \theta, t\right) \qquad (3-25)$$

$$f_1 = \left(ds, \rho, \nu, V, y, g, \rho_s, d_{50}, \sigma_g, V_c, S_o, B, b, L, K_s, \theta, t\right) \qquad (3-26)$$

Since, there are seventeen variables (n=17) and the number of repetitive variables is (3), and according to the Buckingham π-theorem used in the analysis the dimensionless groups obtained are (17-3) =14.

Each term must contain (m+1) = (3+1) = 4 variable, and the repeated parameters are specified as ρ, V, and b. The equation can be written as Buckingham π-theorem:

$$f_2(\pi_1, \pi_2, \pi_3, \pi_4, \pi_5, \pi_6, \pi_7, \pi_8, \pi_9, \pi_{10}, \pi_{11}, \pi_{12}, \pi_{13}, \pi_{14}) \qquad (3-27)$$

Where: $\pi_1 = \rho^{a1} V^{b1} b^{c1} \, d_s$

           $\pi_2 = \rho^{a2} V^{b2} b^{c2} \, d_{50}$

           $\pi_3 = \rho^{a3} V^{b3} b^{c3} \, S_o$

And the same way for all other parameter.

Taking each term and evaluating:

$$\pi 1 = \rho^{a1} V^{b1} b^{c1} \, d_s$$

Expression these in dimension terms we have:

$$M^0 L^0 T^0 = (M\,L^{-3})^{a_1}(LT^{-1})^{b_1}(L)^{c_1}L$$

For M: $a_1 = 0$

For L: $-3a_1 + b_1 + c_1 + 1 = 0$

Or $b_1 + c_1 = -1$

For T: $-b_1 = 0$

$$c_1 = -1$$

$$\pi_1 = \frac{d_s}{b}$$

By the same way:

$$\pi_2 = \frac{d_{50}}{b} \qquad \pi_3 = \theta \qquad \pi_4 = \frac{L}{b} \qquad \pi_5 = \frac{y}{b} \qquad \pi_6 = K_s \qquad \pi_7 = \frac{B}{b} \qquad \pi_8 = \frac{\rho_s}{\rho}$$

$$\pi_9 = \frac{V_c}{V} \qquad \pi_{10} = \frac{gb}{V^2} \qquad \pi_{11} = \frac{v}{Vb} \qquad \pi_{12} = \sigma_g \qquad \pi_{13} = S_o \qquad \pi_{14} = \frac{tV}{b}$$

Most of these parameters' effects on local scour depth are previously discussed in chapter two. According to the conditions in this study, the overall effects of these parameters can be simplified by the following hypothesis:

1. Only one bed sediment layer is used in this study with uniform gradient and time of scour depth is being considered for all test, so the terms of σ_g and $\frac{tV}{b}$ can be ignored (Obeid, 2016) and (Abbas, 2017).

2. The pier diameters b=50.8, 68.5, 92 mm and the median particle size d_{50}=0.385 mm were used. As $b / d_{50} > 25$ (Melville and Sutherland, 1989), the effect of this term is neglected.

63

3- All the models used have a constant length to width ratio except circular and square piers, so the parameter l/b has ignored.

4- The slope is constant for all runs, since the flume slope is fixed at horizontal (i.e. $S_o = 0$). Thus, the S_o has no effect on scour process.

5- Sediment and fluid densities are constant throughout this study. In this way, the term relative density ρ_s/ρ is excluded.

6- Also the term v/Vb, usually is insignificant parameter and can be neglected from equation (3 - 27) if the flow is fully turbulent around the pier (Ettema, 1998).

7- The term of pier Froude number $\frac{V}{\sqrt{gb}}$ has not been used because of the multicollinearity since it gives a strong correlation with flow intensity V/V_C by a factor 0.75, which means that it has the same influence as the flow intensity.

After the simplification of the equations above and eliminating the parameters with constant and negligible values that has no effect on scour process and applying the assumption, the following equations are obtained:

$$f_3(\pi_1, \pi_3, \pi_5, \pi_6, \pi_7, \pi_9)$$

$$f_3\left(\frac{d_s}{b}, \theta, \frac{y}{b}, K_s, \frac{B}{b}, \frac{V_c}{V}\right) \qquad\qquad (3-28)$$

The function that describes the influence of this parameters on scour depth around pier can be written as:

$$\frac{d_s}{b} = f_4\left(\theta, \frac{y}{b}, K_s, \frac{B}{b}, \frac{V_c}{V}\right) \qquad\qquad (3-29)$$

Chapter Four

Statistical Analysis by GEP and SPSS

4.1 Introduction

A statistical analysis is a formalization of relationships between dependent variables and independent variables in the form of mathematical equations. In this chapter, two techniques of modeling were used to obtain a best prediction of scour depth around bridge pier. These techniques are: Gene expression programming (GEP) and statistic non-linear regression using Statistical Package for Social Sciences (SPSS) software (Version 25). Identifying the best techniques to predict the scour depth by three common error measures i.e., coefficient of determination (R^2), root mean square error (RMSE) and mean absolute error (MAE). In this study, five parameters (pier shape, flow intensity, flow depth, pier width and angle of alignment) were selected as input (independent) variables, while scour depth obtained from numerical simulation by Flow-3D is selected as output (dependent) variables for all models.

The purpose of this statistical analysis is to understand how the aforementioned parameters affects the depended variable and models' development for predicting scour depth. This prediction process could provide an efficient clarification of the role of these parameters in general, so the main objective of this work is to further enhance the available inductive modelling tools to predict bridge scour by using GEP-based models for pier scour prediction using data optioned from numerical simulation and comparing their performance with SPSS.

4.2 Regression Analysis by GEP and SPSS

Regression analysis is a highly useful statistical method for quantifying a relationship between one or more independent variables and a dependent variable to

predict the values of the dependent variables (Ghalati, 2012). The dependent variable commonly referred to as Y while independent variable stands for Xs. In engineering, regression may be applied to correlate data in a wide variety of problems ranging from simple to complex physical and industrial systems. The relationship is expressed through a statistical model equation that predicts a response variable from a function of regression variables. It is used when a continuous dependent variable is to be predicted from a number of independent variables. Regression helps to estimate the value of one variable or the dependent variable from the other variables or the independent variables. The parameters are estimated so that a measure of fit is optimized.

4.3 Gene Expression Programming (GEP)

GEP is a new evolutionary artificial intelligence (AI)-based technique developed by Candida Ferreira in 1999. GEP is an extension of genetic programming (GP) developed by Koza, (1992) and incorporates both the simple, linear chromosomes of fixed length similar to the ones used in GAs called genome and the ramified structures of different sizes and shapes expressed as a phenotype in the form of expression trees (ETs) similar to the parse trees of GP.

Genetic algorithms are a type of optimization algorithm that used to find the optimal solutions to a given computational problem that maximizes or minimizes a particular function. GAs introduced by John Holland in the early 1970s and they apply biological evolution theory to computer systems (Holland, 1975). Like all evolutionary computer systems, GAs are an oversimplification of biological evolution. In this case, solutions to a problem are usually encoded in fixed length strings called chromosomes and each chromosome consists of a number of genes. Each gene is represented by 0 or 1, and the populations of such strings (individuals or candidate solutions) are manipulated in order to evolve a good solution to a

particular problem. In each generation, individuals are reproduced with modification and selected according to fitness function as shown in Figure 4.1. Modification in the original genetic algorithm was introduced by the search operators of mutation, crossover, and inversion, but more recent applications started favoring mutation and crossover, dropping inversion in the process (Ferreira, 2006).
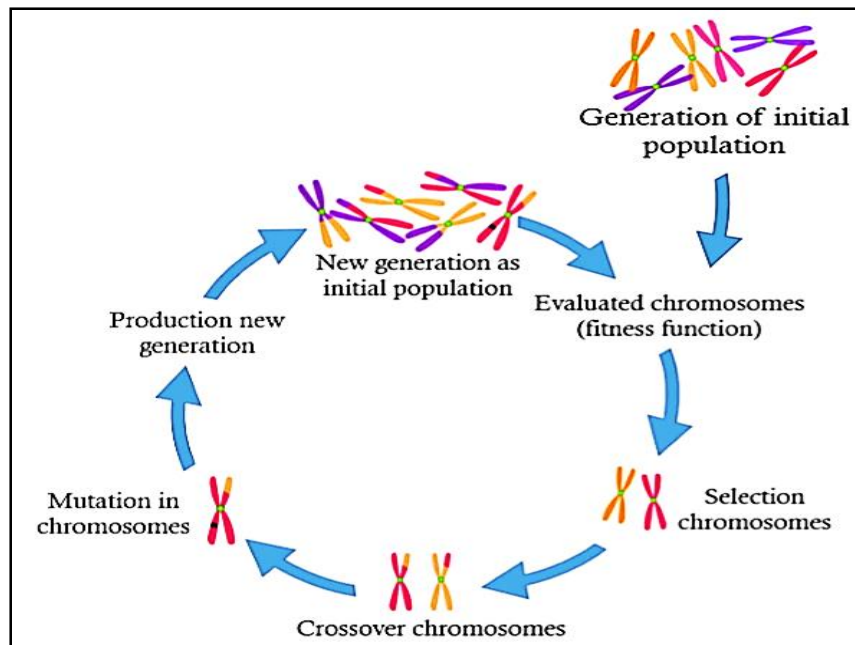
Figure (4-1): Description of genetic algorithms operation (Hassan, 2017).

While genetic programming (or GP) is a branch of the genetic algorithm (Holland, 1975). It is a powerful method used to predict, classify and function findings. GP is a method for learning the most "fit" computer programs by means of artificial evolution (Johari et al., 2006). GP creates equal or unequal length computer programs that consist of variables (terminal) and several mathematical operations sets as solutions. The function set of the system can be composed of arithmetic operations ($+$, $-$, $*$, $/$) and logical functions, mathematical functions ($\sqrt{x}$, tan x, sin h x, x^2, …). GP is considered as an alternative to fixed length solutions through the introduction of parse trees with different sizes and shapes. The alphabet used to create these structures is also more varied than the 0's and 1's of GAs' individuals,

creating a richer, more versa- tile system of representation. However, GP individuals also lack a simple, autonomous genome: like the linear chromosomes of GAs, the nonlinear structures of GP are also naked replicators cursed with the dual role of genotype/phenotype.

The genome is encoded as linear chromosomes of fixed length (just like GAs) that are expressed as phenotype in the form of expression trees by GEP. GEP combines the advantages of both its predecessors, GA and GP, while eliminating some of the limitations of these two techniques (Ferreira, 2006). The GEP system is a full-fledged genotype/phenotype system with expression trees of different sizes and shapes encoded in linear chromosomes of fixed length. Also important is that GEP chromosomes are multi genic, encoding multiple expression trees or sub-programs that can be organized into a much more complex program. For that, Ferreira, (2001) created a new language (called Karva language) to read and express the information of GEP chromosomes. The genes are structurally organized in a head and a tail, and it is this structural and functional organization of GEP genes that always guarantees the production of valid programs, no matter how much or how profoundly we modify the chromosomes. The advantages of GEP are:

- GEP approach is that the creation of genetic diversity is very simplified as genetic operators work at the chromosome level.

- GEP consists of its unique and multigenic nature, which allows the evolution of more complex programs composed of several subprograms. As a result, GEP surpasses the old GP system in 100–10,000 times (Ferreira, 2001; Ferreira, 2002).

- Chromosomes are simple entities that are linear, compact, relatively small and genetically manageable (repetition, mutation, reintegration, transposition, etc.).

68

- The ETs are exclusively the expression of their respective chromosomes; they are the entities upon which selection acts. According to fitness, they are selected to reproduce with modification. During reproduction, it is the chromosomes of the individuals, not the ETs, which are reproduced with modification and move on to the next generation (Ferreira, 2001).

The main goal of GEP is to create a mathematical function, which can be adapted to a set of data provided for the GEP model. For the mathematical equation, the GEP process carried out the symbolic regression by means of the most of the genetic operators of GA.

In the flowchart of GEP represented in Figure 4.2, the process begins with the random generation of the chromosomes of a certain number of individuals (the initial population). Each individual chromosome of the initial population is then evaluated by using a fitness function against a set of fitness cases. Then, these chromosomes are then selected based on the fitness value, the chromosomes with fitter value having a higher chance of selection into the next generation. when the chromosomes are selected, they are reproduced with some modifications carried out by genetic operators (mutation, inversion, trans- position and recombination, etc.). Mutation is the most efficient genetic operator which is sometime used as the only modification method. The process is then repeated for a certain number of generations or until a good solution has been found. In the GEP system, several of these genetic operators used for genetic modification of chromosomes are explained as follows (Ferreira, 2006):

- Mutation is the most efficient and influential of all the genetic operators. In GEP, mutation allowed to be occurred at any position in chromosome. However, the structural organization of chromosomes should be stayed

the same. Thus, in the heads of genes, function can change into another function or terminal, but in the tails, terminals can only change into terminals (the head includes some mathematical operators, variables and constant (+, -, *, /,1, a, b, c…), while terminal symbols which are variables and constants (1, a, b, c…) are included in the tail). In this way, the structural organization of chromosomes is maintained and all new individuals produced by mutation are structurally corrected programs.

- Inversion: In this operator, a sequence within the head of a gene might be randomly selected and inverted. In GEP, the inversion operator randomly chooses the chromosome, the gene to be modified and the start and terminal points of the portion of head to be inverted. Small inversion rate pi of 0.1 is used as this operator is rarely used as the only source of genetic variation.

- Insertion sequence (IS) transposition: IS elements are short parts of the genome that have a function or terminal in the first position. This operator selects the chromosome randomly, the gene to be modified and the beginning and the end of the IS element and moves it to the beginning of the gene immediately after the root.

- Root insertion sequence (RIS) transposition: This is a short part of the genome like the IS element with the only one difference is that the starting point here is always a function. RIS selects the chromosome randomly, the gene to be modified and the starting and the ending points of the RIS element and moves it to the starting point of the gene.

- Gene transposition: In gene transposition, whole gene acts as a transposon and transposes itself to the beginning of the chromosome. Unlike other forms of transposition, in this operation the transposon (the gene) is omitted at the place of origin.

- Single or double cross-over/recombination: In single recombination, the parent chromosomes are paired and split at exactly the same point. The material downstream of the recombination point is afterwards exchanged between the two chromosomes. In double cross-over, two parent chromosomes are paired and two points are randomly chosen as cross-over points. The material between the recombination points is then exchanged between the parent chromosomes, forming two new daughter chromosomes.

- Gene recombination: Entire genes are exchanged between two parent chromosomes, forming two offspring chromosomes containing genes from both parents. The operator of gene recombination randomly chooses the two parent chromosomes and the gene to be exchanged.

Since a random numerical constant (RNC) is an essential part of any mathematical model, it must be taken into account when extracting an empirical expression of the response function being modelled. GEP has the ability to handle RNCs efficiently while giving a defined range of minimum and maximum values (Khan et al., 2012).

GEP consists two important players, chromosomes and expression trees (ETs). The expression of the genetic information is encoded in the chromosome. As in nature, the process of information decoding is named translation and this translation implies a code and a set of rules. The genetic code in GEP is very simple; a one-to-one relation between the symbols of the chromosome and the nodes are represented in the trees. The rules determine the spatial organization of nodes in the expression trees and the type of interaction between sub- ETs.
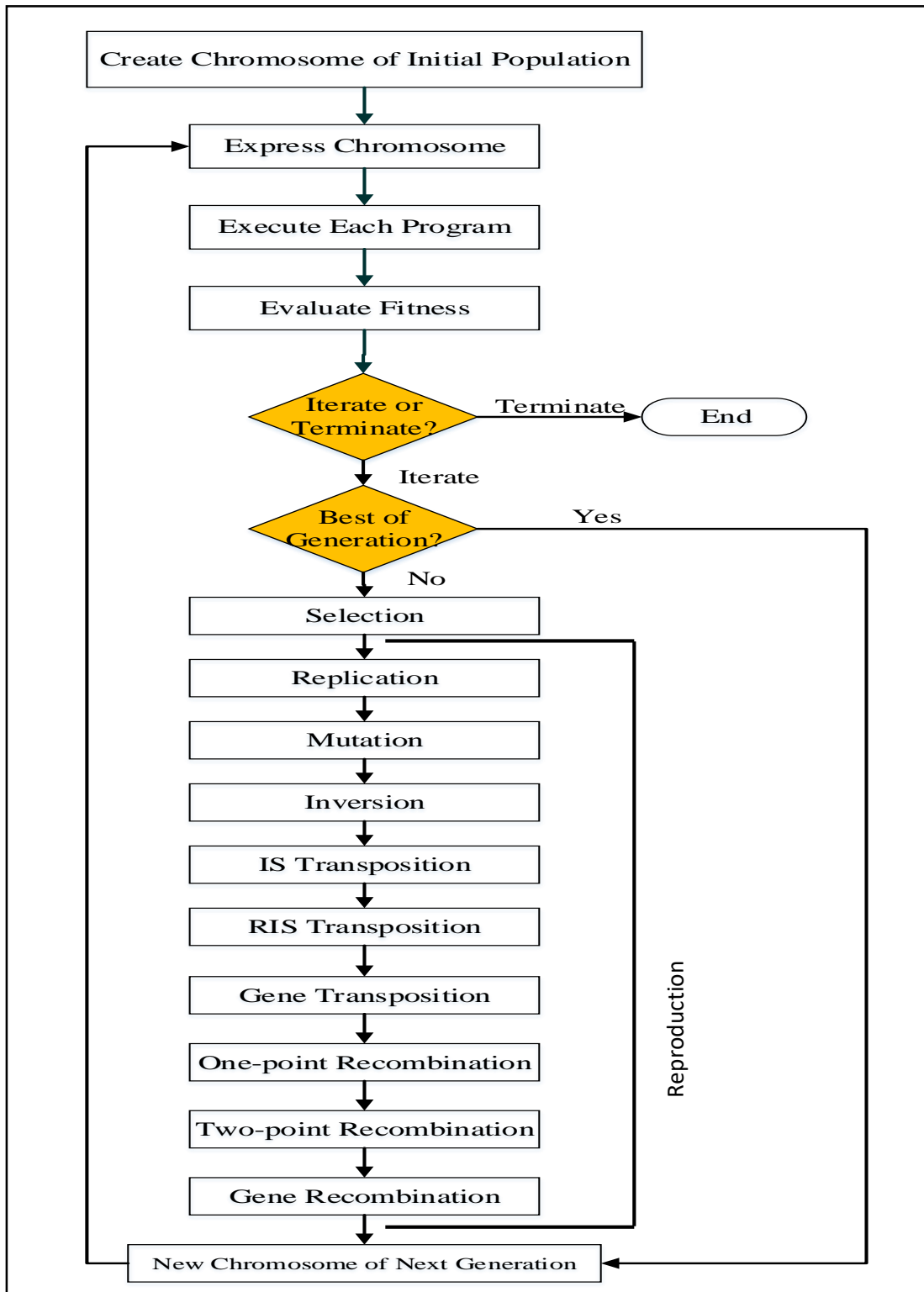
Figure (4-2): Flow chart of gene expression algorithm (Ferreira, 2006)

4.4 GEP Modeling for Bridge Pier Scour Depth

The powerful software package named GeneXproTools 5.0 is use in this work to develop GEP-based models for bridge pier scour depth prediction. This program provides a compact and explicit mathematical expression for the bridge scour model. The problem that are going to solve with gene expression programming, is a symbolic regression (function finding), where used to find an expression that satisfactorily explains the dependent.

Initially, the available datasets (total of 729) of bridge pier scour depth are obtained from numerical simulation of bridge pier at different cases. This data represented in Equation (3-29), these parameters in equation θ , $\frac{y}{b}$, K_s , $\frac{B}{b}$, $\frac{V_c}{V}$ assigned to columns as independent input variable while the local scour depth $\frac{ds}{b}$ is used as dependent output variable then a model of output variable $\frac{ds}{b}$ is developed by using GEP . These datasets are divided into training and validation/testing datasets. The training set consists of 583 observations (about 80%); this training data set was randomly chosen and used to build GEP model. The validation/testing set consisting of 146 data (about 20%) was used for testing or validating GEP model. After data division, different parameters for the model construction were decided which are demonstrated in the following six-step procedure:

- First step: GEP starts with an initial population of individuals. The population of individuals consists of chromosomes of fixed length. The chromosome may be single gene or multi-genic. Population can be used at any size in the initial population but the population range from 30 to100 chromosomes gave good results in the past (Ferreira, 2001). After many trials to determine optimum population size to give good results, the optimum size of population selected in this model is 50 chromosomes.

- Second step: after initializing the population, each individual is evaluated and its fitness function was computed using the mean square error (RMSE) as the fitness function.

- Third step: after selecting the fitness function, the next step is to select the set of functions F and the set of terminals T for each gene of the chromosome. The basic arithmetic operators and powers used in this study to design this model, thus giving F = {+, -, *, /, power }; and the terminal set including the independent variable and random numerical constant, giving $T = \{ \theta , \frac{y}{b} , K_s , \frac{B}{b} , \frac{V_c}{V}, ?\}$ where '?' represented random numerical constant (RNC) .

- Fourth step: this step is to represent structural organization of the chromosomes. This means to determine the number of gens and the length of their head. First starts with single gene and then gradually increase it. According to Ferreira, (2001), growing the number of gene in chromosome from one to three increases the success rate; therefore, after many trails, three gene is used in each chromosome and the chromosome is called (multigenic) and the head is equal to eight (h=8). To represent the random numerical constants D_C, five floating- type random numerical constants per gene is selected in the range {-10, 10}.

- Fifth step: selection the linking function in this step. Since there are three genes, the result can be generated from three different sub-ETs. To get the final solution, these sub-ETs (Expression trees) are linked by addition operator (+).

- Sixth step: finally, choosing the set of genetic operators that cause variation and their rates. A combination of all genetic operators like mutation, inversion, transposition (IS, RIS and gene transposition),

recombination (one-point, two- point and gene recombination), and D_c-specific genetic were used in this study to cause the variation and their rates. Two one-point mutations with a rate of 0.044 were used. The rates of the other genetic operators are given in Table 4.1.

The model is simulated by GeneXproTools after all the model parameters were determined. This program is run for a number of generation and stopped when no improvement in the value of fitness function and coefficient of determination is observed.

Table (4-1): Parameters of GEP model for pier scour depth problem

parameters	values
Population size	50
Function set	+, -, *, /, power
Terminal set	$\theta , \dfrac{y}{b} , K_s , \dfrac{B}{b} , \dfrac{V_c}{V}, ?$
Random numerical constant (RNC)	05
RNC type	Floating point
RNC range	[-10, 10]
Head length	08
Number of genes	03
Linking function	+
Fitness function	RMSE
Mutation rate	0.044
Inversion rate	0.1
IS transposition rate	0.1
RIS transposition rate	0.1
Gene transposition rate	0.1
One-point recombination rate	0.1
Two-point recombination rate	0.3

parameters	values
Gene recombination rate	0.3
Dc-specific mutation rate	0.044
Dc-specific inversion rate	0.1
Dc-specific IS transposition rate	0.1
Random constant mutation rate	0.01

4.5 SPSS Modeling to Predict Scour Depth Around Bridge Pier

SPSS is a Windows-based program that can be used to perform data entry and analysis, and to create tables and graphs. SPSS is capable of handling large amounts of data and can perform a wide range of analyzes. More details about SPSS prediction model is displayed below.

4.5.1 Model preparation

One of the main works of this study is to develop a model from the results obtained from numerical simulation. Empirical modeling is done using SPSS software. The variables introduced to the empirical modeling are flow intensity, flow depth, pier width, shape factors and angle of alignment; these variables represent independent variable while local scour depth (ds/b) represent dependent variable. The gathered results are 729 from numerical simulation of bridge pier scour depth; this dataset is divided randomly into 80% to generate the model and the other 20% to validate it. The first step to construct a model is to define the correlation between the variables by using SPSS Pearson's correlation. Many combinations of variables are used starting from only constant to quadratic form of both variables with the incorporation of multiple terms of both variables discussed above.

4.5.2 Identification of dependent and independent variable for empirical modeling

Program testing needs to identify dependent and independent variables of the developed models to achieve the requirements to build the models. The variables adopted for calculation are listed in Table (4-2).

Table (4-2): Dependent and independent variables considered in regression analysis

Independent Variables	
Abbreviation	**Description**
V/V$_C$	Flow Intensity
Y/b	Flow depth
b/B	Pier width
Ks	Pier shape factor
Kθ	Flow alignment factor
Dependent Variables	
ds/b	Local scour depth

4.5.3 Correlation between variables

Correlation is a statistical method that explains how strongly two variables are related to each other. Correlation between variables are measured by the correlation coefficient. The value of correlation coefficient ranges between -1 and 1. The correlation degree is classified as follow:

- Perfect correlation exists when the first variable changes with the same ratio as the second variable.

- Correlation with high degree is existed when the correlation coefficient value is higher than 0.75.

- Correlation with moderate degree is existed when the value of correlation coefficient is between (0.5 - 0.75).

- There is low degree of correlation when the value of correlation coefficient is between (0.25-0.5).

- There is no linear correlation when the correlation coefficient value rang is between (0-0.25

The correlation used in this study represented in Table (4-3) which explains the bivariate Pearsons' correlation between variables.

Table (4-3): Correlation between variables.

		ds/b	y/b	V/V$_C$	b/B	Ks	Kθ
ds/b	**Pearson Correlation**	1	.618*	.336*	.273*	.097*	.126*
	Sig. (2-tailed)		.000	.000	.000	.009	.001
	N	729	729	729	729	729	729
y/b	**Pearson Correlation**	.618*	1	.000	.000	.000	-.004
	Sig. (2-tailed)	.000		1.000	1.000	1.000	.924
	N	729	729	729	729	729	729
V/V$_C$	**Pearson Correlation**	.336*	.000	1	.000	.000	.001
	Sig. (2-tailed)	.000	1.000		1.000	1.000	.988
	N	729	729	729	729	729	729
b/B	**Pearson Correlation**	.273*	.000	.000	1	.000	.000

		ds/b	y/b	V/V$_C$	b/B	Ks	Kθ
	Sig. (2-tailed)	.000	1.000	1.000		1.000	.992
	N	729	729	729	729	729	729
Ks	Pearson Correlation	.097*	.000	.000	.000	1	.025
	Sig. (2-tailed)	.009	1.000	1.000	1.000		.495
	N	729	729	729	729	729	729
Kθ	Pearson Correlation	.126*	-.004	.001	.000	.025	1
	Sig. (2-tailed)	.001	.924	.988	.992	.495	
	N	729	729	729	729	729	729

*. Correlation is significant at the 0.01 level (2-tailed) significant level.

This table shows:

1. The independent variables have very low to absent of correlation between each other, which is good for model accuracy.
2. The correlation between ds/b and V/V$_C$ are good when compared with pier width b/B but the correlation with V/V$_C$ is more significant.
3. The scour depth ds/b have the most significant correlation to flow depth y/b.
4. There is no correlation between scour depth ds/b and both Ks and Kθ.

Chapter Five

Analysis and Discussion of Results

5.1 Introduction

The results in this chapter were analyzed and discussed at four different parts. The first part includes the validation of the numerical simulation using the laboratory model of Melville, (1975) by comparing results of the laboratory experiments with the numerical simulation results of CFD code. The second part includes numerical simulation results by Flow-3D at different pier shapes of (circular, elliptic, oblong, rectangular, square, hexagonal, octagonal, ogival and lenticular).

The selected variables for numerical simulation were (flow depth, flow intensity, pier width, and flow angle of alignment for each pier shape) with each of them having three different values. The third part presents the results of optimum pier shape that give minimum scour depth by using different shape having constant area exposed to different value of flow intensity. In the last part, the data obtained from the numerical simulation were used to develop scour depth formula by using two techniques namely gene expression programming (GEP) and statistic non-linear regression using SPSS.

5.2 Model Validation

As the process of local scouring around bridge piers is complex and difficult to measure, it is primarily studied in numerical work. This validation aims to compare the results of the Melville, (1975) laboratory experiments of local scour around bridge piers with numerical simulation results of CFD code. To test the effectiveness of the numerical model, this numerical model was simulated in similar conditions to the physical model. The boundary conditions were applied to the numerical model and some important parameters that directly affect the results were

calibrated and after verifying the conformity percentage of numerical results with laboratory results; the calibrated values of parameters were used in the numerical simulation. Figures 5.1 show the three-dimensional output of numerical model for the maximum scour depth development over 1800 sec with the physical model.
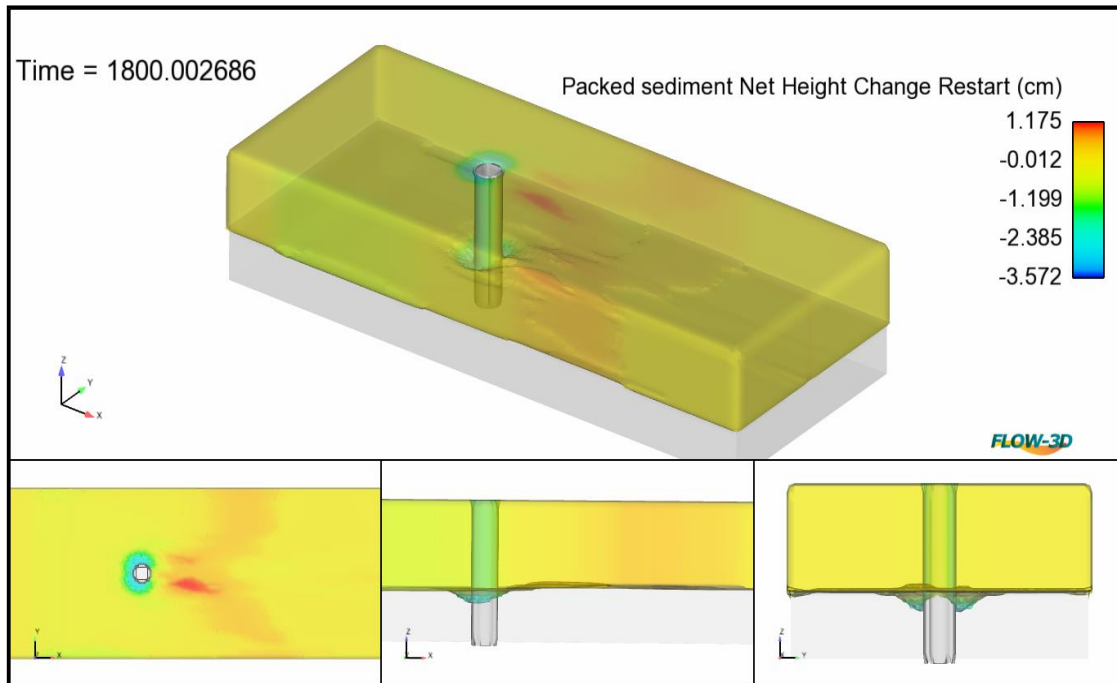
Figure (5-1): Scour depth (in negative value) at different views around pier.

Figures (5-2) shows the results of scour depth around cylindrical bridge pier for the physical model Melville, (1975), While Figure (5-3) presents the scour depth of the numerical model.
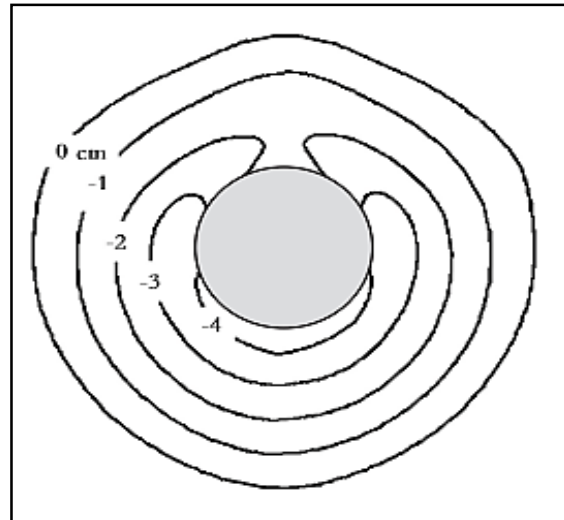
Figure (5-2): Contour lines represented the scour depth around the pier for
Melville, (1975) model
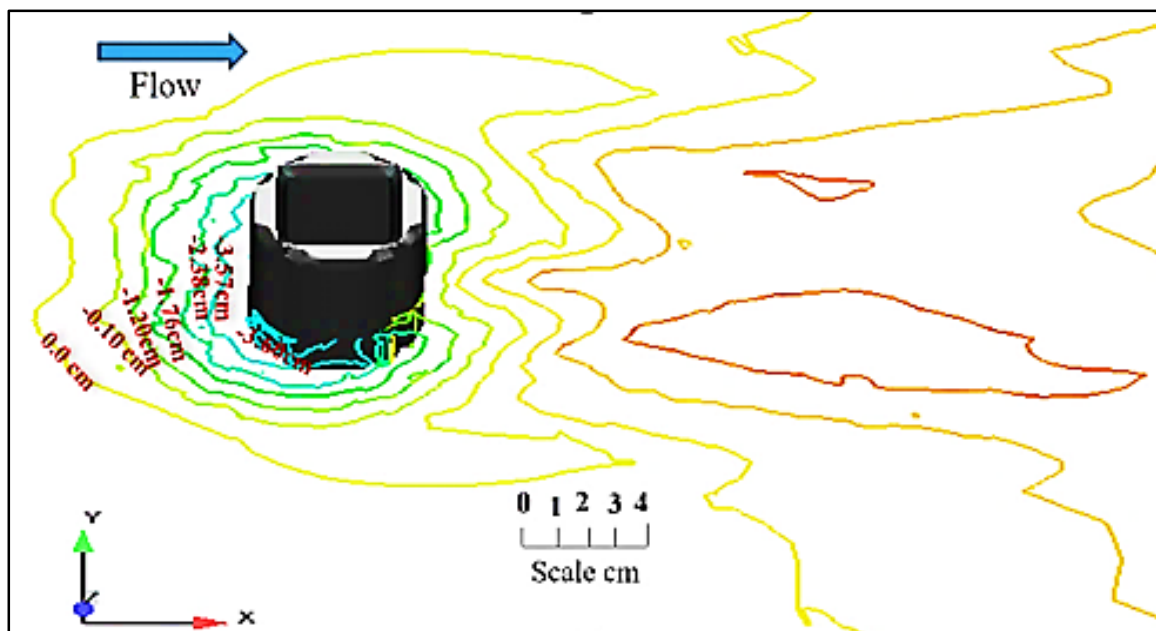
Figure (5-3): Contour lines represented the scour depth around the pier for the
numerical model.

Figure (5-4) presents the development of scour depth with time and compares
final results with the experimental value. The maximum scour depth obtained from
numerical model is 3.6 cm, while the maximum scour depth for experimental model
is 4 cm. The results showed a good agreement with experimental results with error
ratio close to 10%.
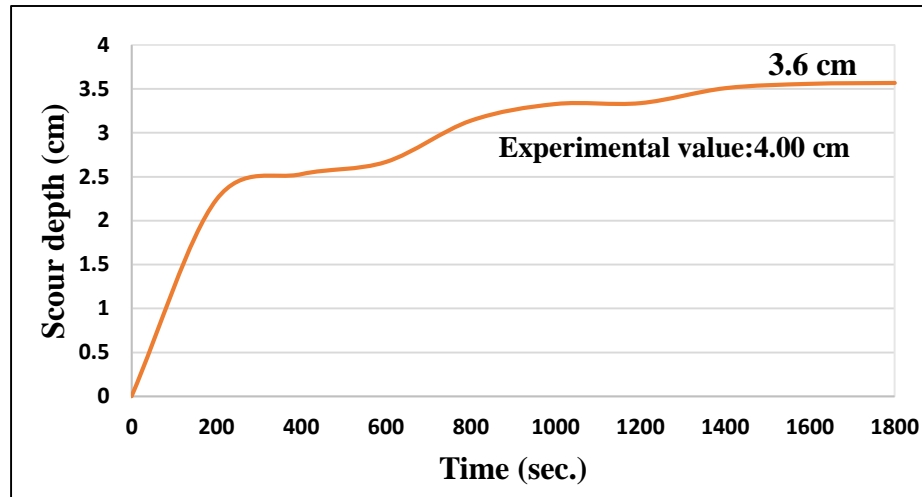
Figure (5-4): Scour depth against time around circular pier.

Figures 5.5 and 5.6 show comparisons of the distribution of the flow velocity on the slice of y=0 between the experiment measurements Melville, (1975) and the numerical simulations at 1800 second simulation time. The speed is normalized same as the experiment by the mean approached flow velocity which is 0.25m/sec. In both the simulation and the experiment, it can be found that a strong downward flow is developed along the pier face produced rather large velocity components near the bed, which distorted the profiles in the vicinity of the cylindrical pier. Flow is separated at the nose of the scour hole and reattached at the front of the pier, forming a horseshoe vortex, which can be clearly identified from both the simulation and the experiment.
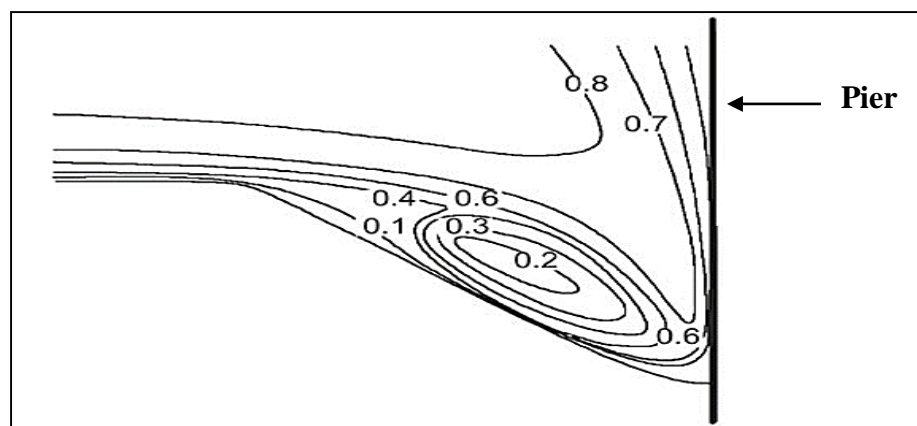
Figure (5-5): Side view of contour map of flow velocity around a pier at 1800 sec resulted by Melville experiment (Melville, 1975).
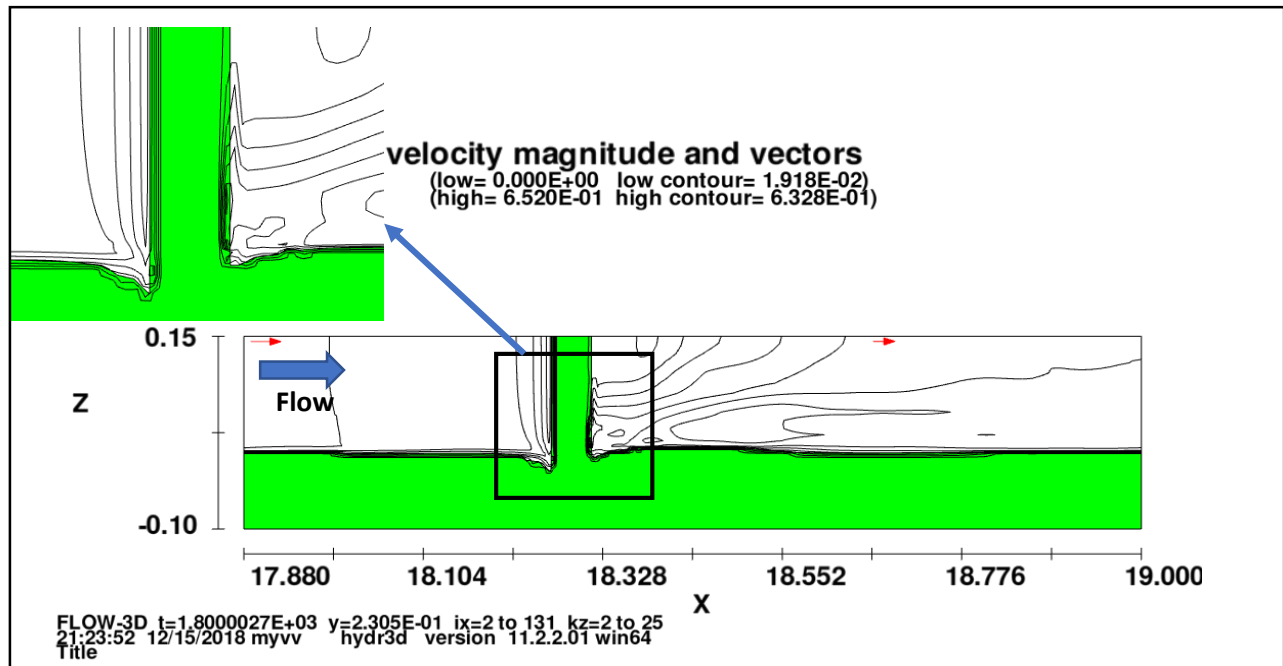
Figure (5-6): Contour map of flow velocity distribution around a pier at
1800 sec resulted by numerical simulation.

5.3 Influence of Main Parameters on Scour Around Different Pier Shapes

As mentioned in chapter two and in dimensional analysis technique in chapter three (section 3.6), there are several parameters that can control the depth of scour and the features of bed elevations upstream and downstream of a pier. In this section, the effects of the main controlling parameters clearly defined by viewing the bed profiles at the end of the run time. It should be noted that by focusing the effect of any parameter, the same simulation conditions are held fixed, leaving only the effect of this parameter selected.

The effect of these parameters presented on series of runs have been conducted around different pier shapes at different conditions to study variation of scour at each pier shape. In these series of runs, the time development of scour as well as the efficiency of shape is studied. All runs are conducted under clear-water conditions at flow intensity (V/V_C) equal to 0.55, 0.76 and 1. The critical threshold velocity occurs at $V=V_C$, at which just starts the sediment movement. Accordingly,

to overcome this situation (the beginning stops of live bed scour) the flow velocity was taken equal to V_C. Critical velocity calculated by FHWA-HIF, (2012) equation, as follows

$$V_c = 6.19 \, y^{\frac{1}{6}} \, d_{50}^{\frac{1}{3}} \qquad\qquad (5-1)$$

Where:

V_C: Critical velocity above which bed material of size d_{50} and smaller will be transported (m/s)

y: Average depth of flow (m)

d_{50}: Median particle size (m)

After that series of runs at different conditions, first started with different flow depth, three runs takes for each pier shape at flow depth (y/b) equal to 0.20, 0.98 and 2.95. Then, a second series of three runs was conducted for each pier at pier width (b/B) (b represent upstream width of a pier) equal to 0.11, 0.15 and 0.2 with different flow angle of alignments ($\theta°$) of 0, 30° and 45°. These angles are represented by Kθ (correlation coefficient of flow alignment) in scour depth development formula, which Kθ calculated by the equation of FHWA-HIF, (2012).

$$K\boldsymbol{\theta} = (cos \, \boldsymbol{\theta} + \frac{l}{b} sin \, \boldsymbol{\theta})^{0.65} \qquad\qquad (5-2)$$

Where:

l/b: is length to width ratio.

All piers' shapes used in this study have constant length to width ratio l/b of 2, except circular and square shapes which have l/b of 1. For all runs, running time was 1800 seconds because sediment transportation reach balance state at this time after testing it, as shown in Figure 5-7. The runs conditions for each shape of bridge piers are summarized in Table 5.1.
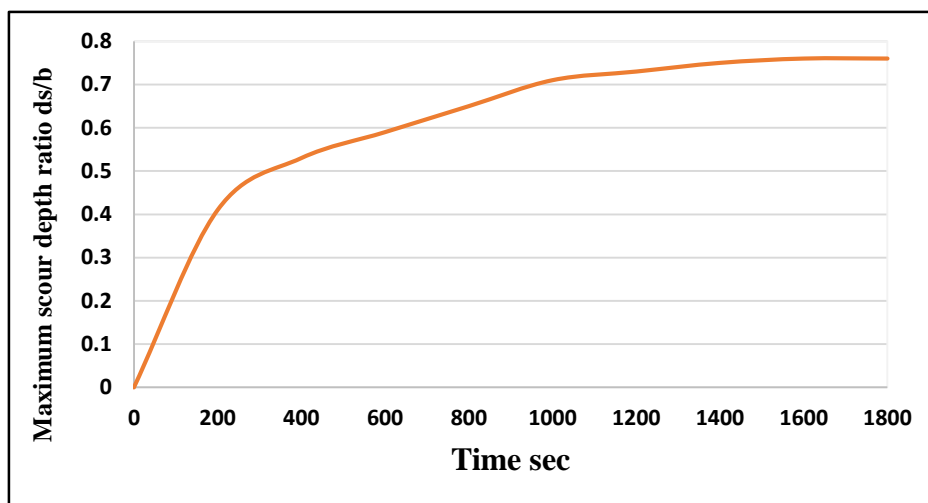
Figure (5-7): Scour depth versus time of numerical model for rectangular pier shape

Table (5-1): Run conditions for each pier shapes

No.	Pier shapes	Flow Intensity V/V_C	Flow depth y/b (m)	Angle of alignment θ°	Pier Width b/B
1		0.55	0.20	0	0.11
2	All shapes	0.76	0.98	30	0.15
3		1.0	2.95	45	0.20

5.3.1 Influence of flow intensity V/V_C

The intensity of flow has a direct influence on the scour depth. To show the impact of the flow intensity on the depth of scour, 27 runs were made around piers that have different shapes (circular, elliptic, oblong, rectangular, square, hexagonal, octagonal, ogival and lenticular) at different values of flow intensities (V/V_C) of 0.55, 0.76, and 1 at constant flow depth and pier width. It is observed that scour starts at upstream face of the pier and the deposition takes place at the downstream of the

pier. Figures 5.8, 5.9 and 5.10 (for runs number 10,13 and 12, respectively as illustrated in Appendix A) show scour depth and deposition of sand around three typical piers that have different shape for $V/V_C = 0.76$ at the end of run time of 1800 second.

It is clear from these figures, that the position of the maximum scour depth is located at front side of the pier and scour depth increases approximately linearly with flow intensity for all pier shapes. Maximum scour depth represents the blue color label of scour depth, while red color represents the sediment deposition.
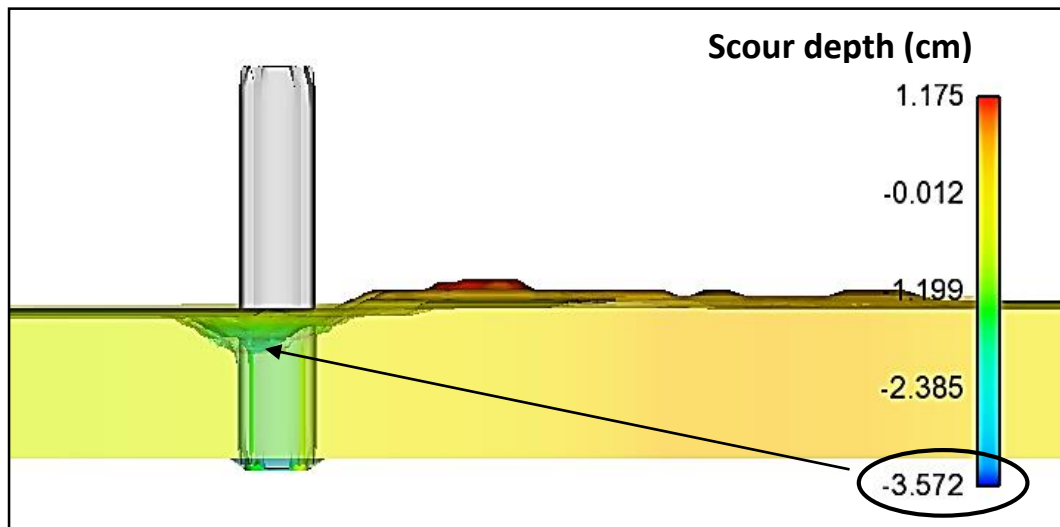
Figure (5-8): Side view of scour depth and sand deposition around circular pier at V/V_C =0.76, y/b=2.95, b/B=0.11, Ks=1.00, Kθ=1.00.
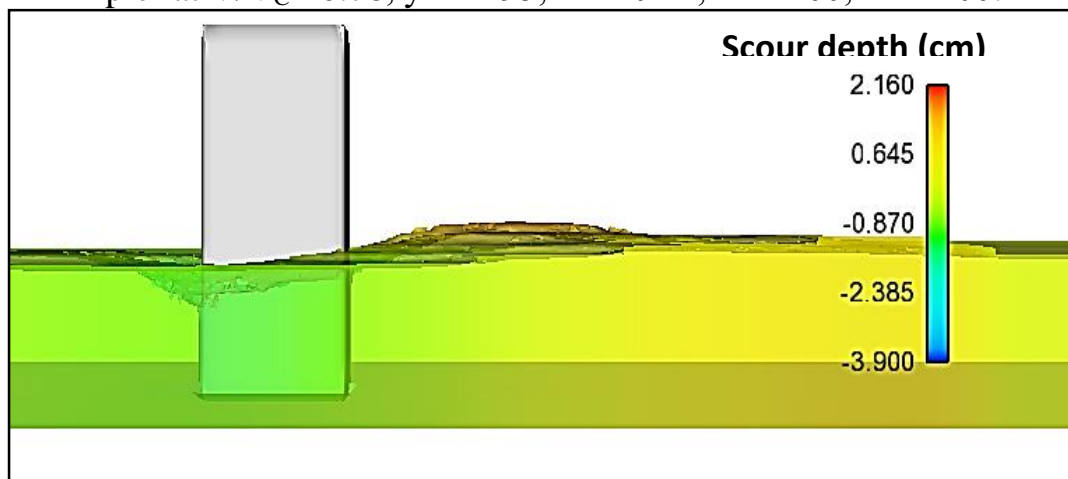
Figure (5-9): Side view of scour depth and sand deposition around rectangular pier at V/V_C =0.76, y/b=2.95, b/B=0.11, Ks=1.26, Kθ=1.00.
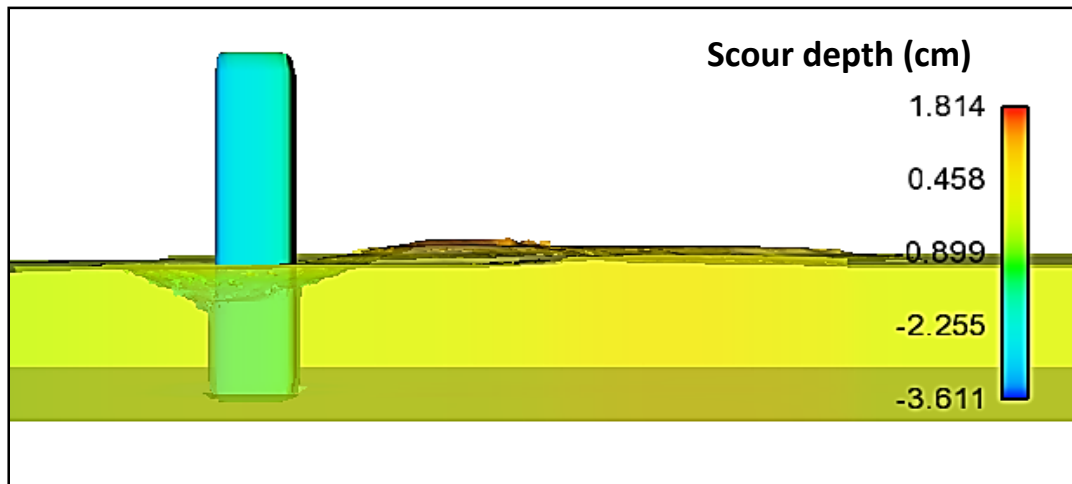
Figure (5-10): Side view of scour depth and sand deposition around square pier at V/V$_C$ =0.76, y/b=2.95, b/B=0.11, Ks=1.16, Kθ=1.00.

Figure 5.11 illustrate the variation of scour depth with flow intensity at constant flow depth. As it can be seen from this figure, scour depth is increasing almost linearly with flow intensity. High rate of scour depth can be noticed at flow intensity (V/V$_C$) of 1 and scour depth reach a peak value at this intensity. This finding is in agreement with these of previous investigation for clear water condition. This attributing to the increase in separation zone by increasing flow intensity; this separation will produce more eddies. Hence, the vorticity of the horseshoe, if this vorticity interferes with the surface roller its action will vanish. Maximum scour depth ratio (ds/b) can be observed for rectangular shape of ds/b=1.279 at V/V$_C$ =1, while minimum depth of scour is observed at lenticular pier of ds/b=0.85 at V/V$_C$ =1. These results are summarized in Table 5.2.
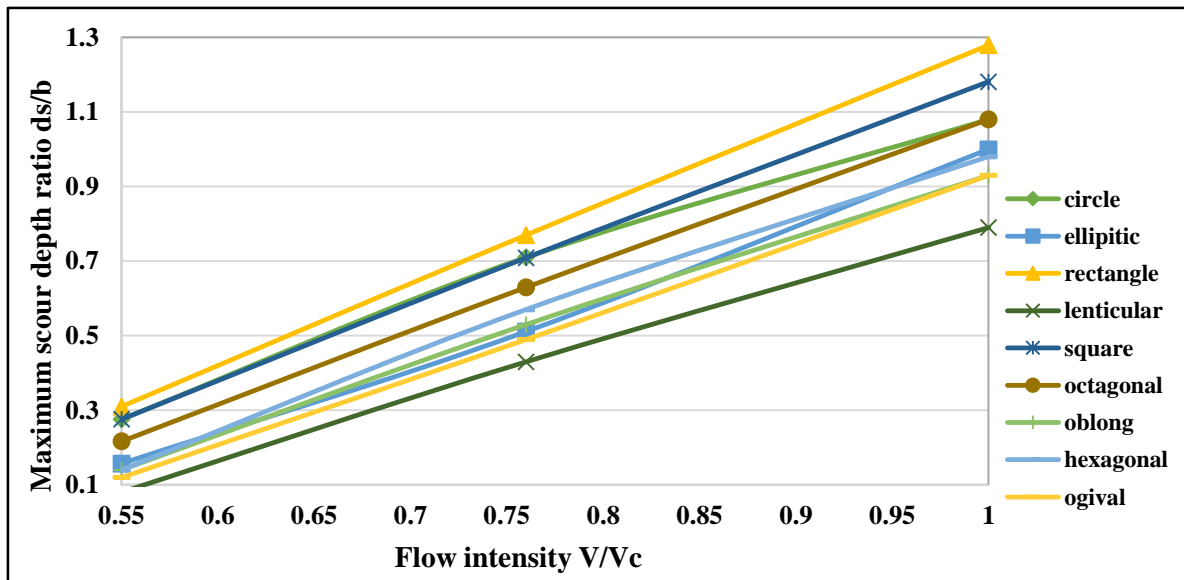
Figure (5-11): Influence of flow intensity on scour depth at different pier shapes.

Table (5-2): Results of the influence of flow intensity on scour depth for each pier shape at y/b=2.95, b/B=0.11, Kθ=1.00.

Pier Shape	Maximum Scour depth ratio ds/b		
	V/V$_C$ =0.55	V/V$_C$ =0.76	V/V$_C$ =1.0
Circular	0.28	0.71	1.08
Rectangular	0.31	0.77	1.28
Square	0.28	0.71	1.18
Elliptic	0.16	0.51	1.00
Ogival	0.12	0.49	0.93
Hexagonal	0.14	0.57	0.98
Oblong	0.14	0.53	0.93
Octagonal	0.22	0.63	1.08
Lenticular	0.08	0.43	0.79

5.3.2 Influence of flow depth ratio y/b

The scouring process is directly proportional to flow depth. To represent the influence of flow depth on scour, a series of run of 81 runs operated at three different value of flow depth ratio y/b of 0.2, 0.98 and 2.95 were conducted and each value of flow depth ratio runs at three different value of flow intensity V/V_C 0.55,0.76 and 1 at constant pier width around different pier shapes to state the behavior of scour with the variation of flow depth. Many researchers have shown that the propagation of scour occurs as the flow depth increases and the rate of this propagation is slowing to a limiting value of flow depth at which its effect is absent. This situation is represented in representative model of the circular pier shape at flow depth ratio (y/b) of 0.2, 0.98 and 2.95 for V/V_C =1 in Figures 5.12, 5.13 and 5.14 (for runs 19, 46 and 73 represented in Appendix A). From these figures, scour depth reach a maximum value at y/b =2.95 and V/V_C = 1, and the maximum depth of scour occurred in the front and in the side of the pier. There is a little deposition of sediment behind the pier at this flow depth ratio, while at minimum flow depth ratio of y/b= 0.20, scour depth developed slowly with time and reach maximum value at the beginning of the run with little scour depth.
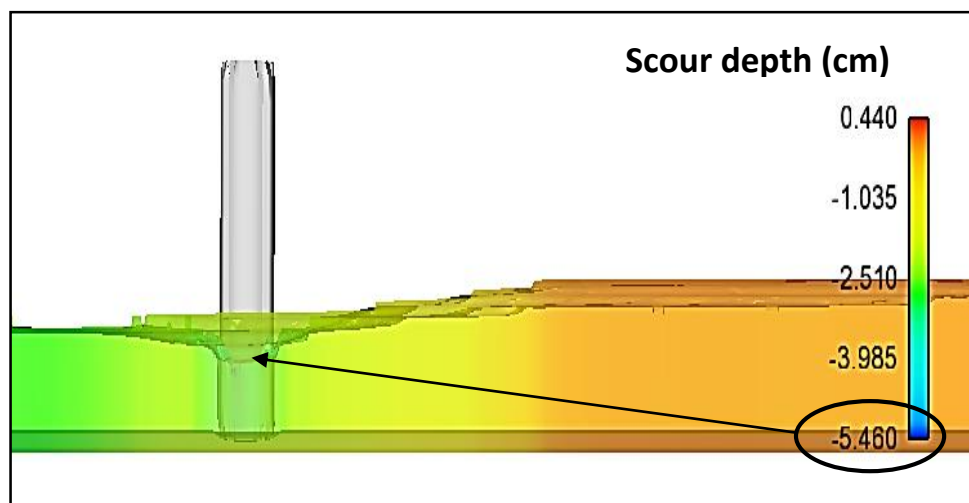
Figure (5-12): Side view of scour depth around circular pier at y/b=2.95, V/Vc=1.00, b/B=0.11, Ks=1.00, Kθ=1.00.
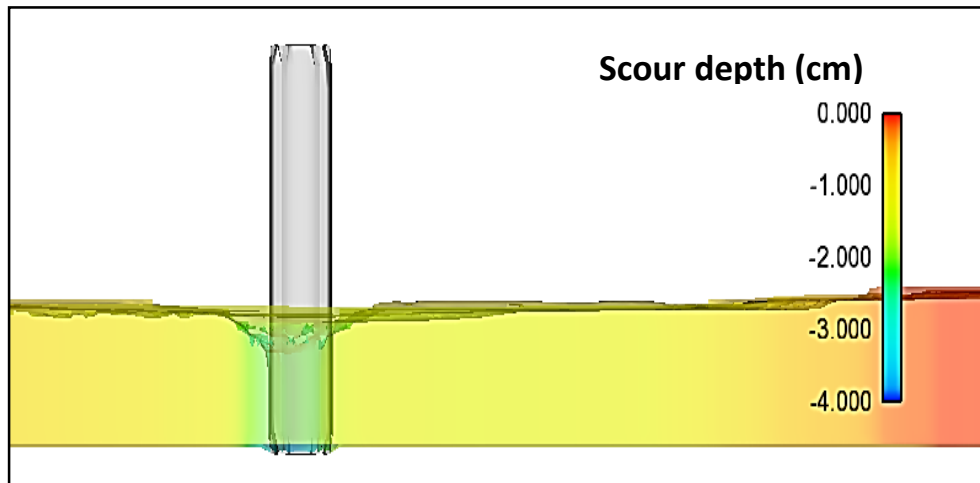
Figure (5-13): Side view of scour depth around circular pier at y/b=0.98, V/V$_C$ =1.00, b/B=0.11, Ks=1.00, Kθ=1.00.
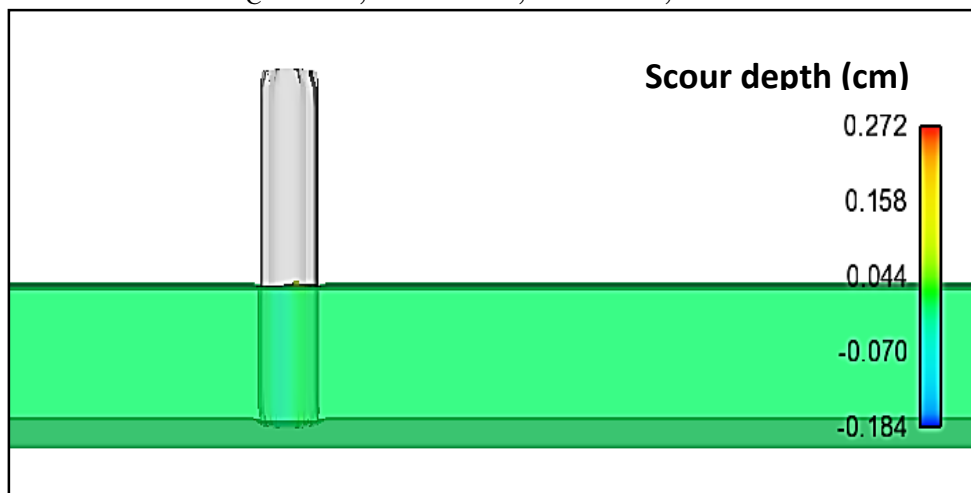
Figure (5-14): Side view of scour depth around circular pier at y/b=0.2, V/V$_C$ =1.00, b/B=0.11, Ks=1.00, Kθ=1.00.

To show the impact of the flow depth on the scour depth around different pier shapes, different values of flow depth are plotted against the maximum depth of scour for all values of flow intensity and for all pier shapes as shown in Figures 5.15 to 5.23.

As it can be seen in these figures, the scour depth increases with the increase in flow depth for different velocities. As the flow depth decreases, the surface roller becomes relatively more dominant and causes the horseshoe vortex to be less capable of entraining sediment. Therefore, for shallower flows, the local scour depth

is reduced. Generally, these figures showed that the greatest value of scour depth occurs when the value of the flow depth ratio y/b is 2.95 and this maximum value of scour depth occurred around rectangular pier at $V/V_C =1$ while minimum depth of scour observed around in lenticular pier at $V/V_C =1$. All results are represented in Table A.1 in Appendix A.
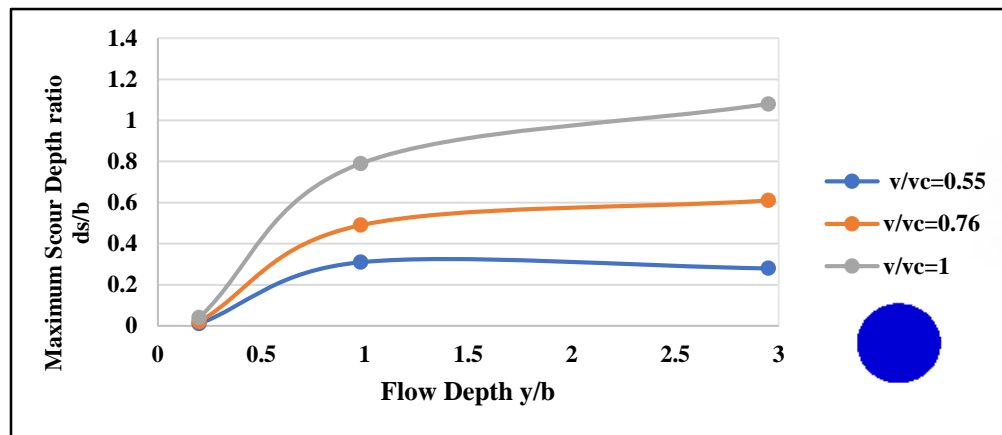
Figure (5-15): Development of scour depth with flow depth around circular pier shape at different value of flow intensity, b/B=0.11, Ks=1.00, Kθ=1.00.
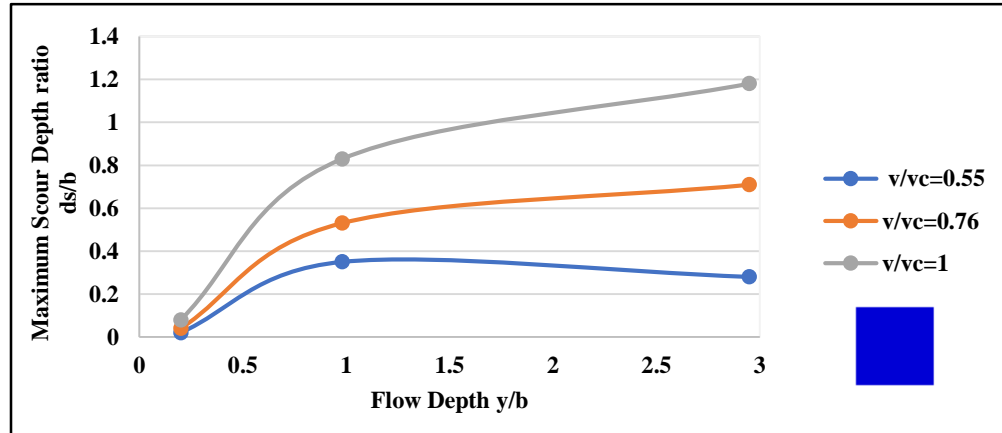
Figure (5-16): Development of scour depth with flow depth around square pier shape at different value of flow intensity, b/B=0.11, Ks=1.16, Kθ=1.00.
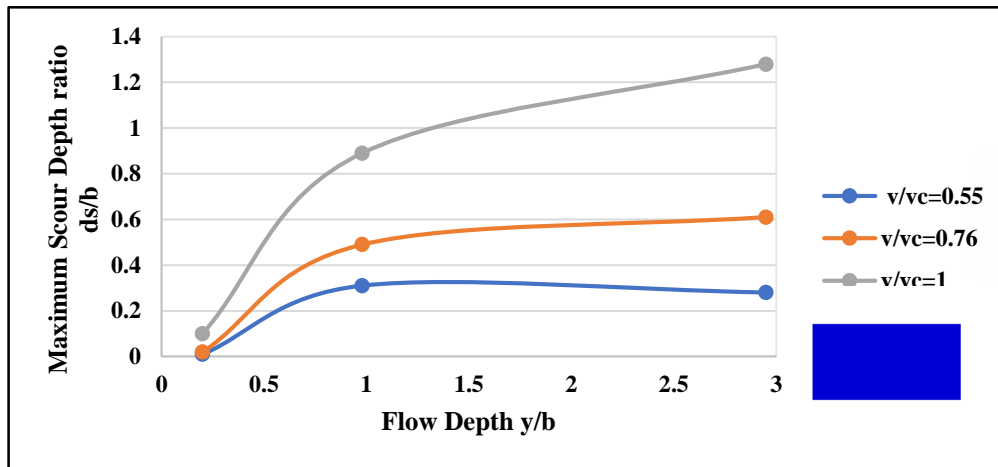
Figure (5-17): Development of scour depth with flow depth around rectangular pier shape at different value of flow intensity, b/B=0.11, Ks=1.26, Kθ=1.00.
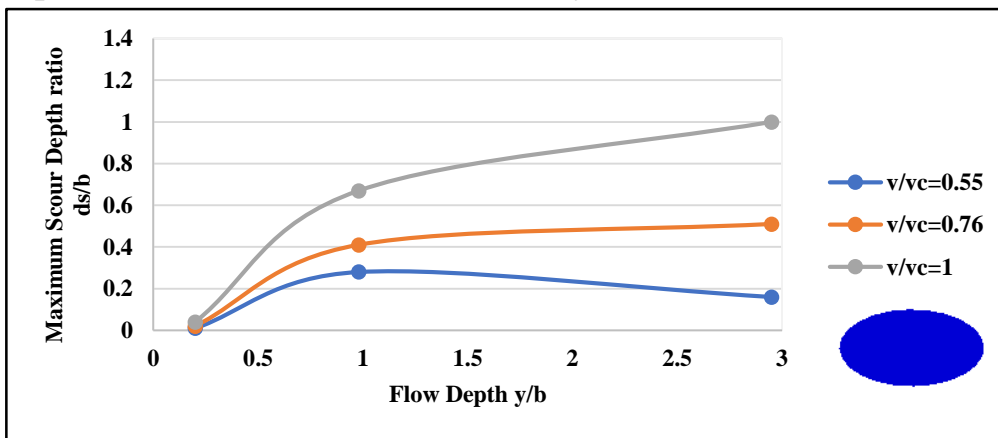
Figure (5-18): Development of scour depth with flow depth around elliptic pier shape at different value of flow intensity, b/B=0.11, Ks=0.84, Kθ=1.00.
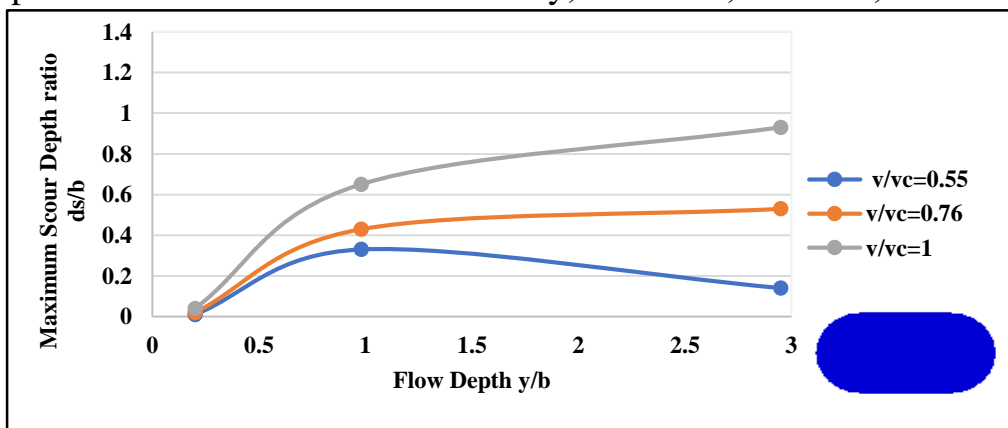
Figure (5-19): Development of scour depth with flow depth around oblong pier shape at different value of flow intensity, b/B=0.11, Ks=0.87, Kθ=1.00.

93
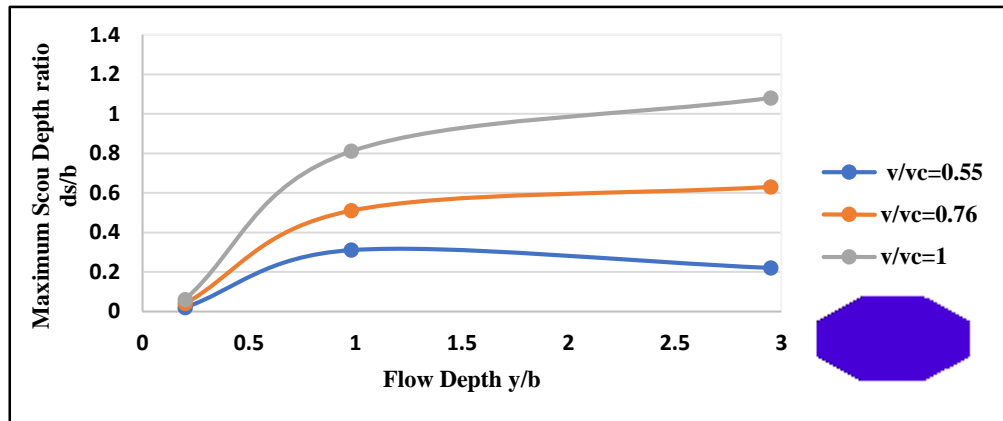
Figure (5-20): Development of scour depth with flow depth around octagonal pier shape at different value of flow intensity, b/B=0.11, Ks=1.03, Kθ=1.00.
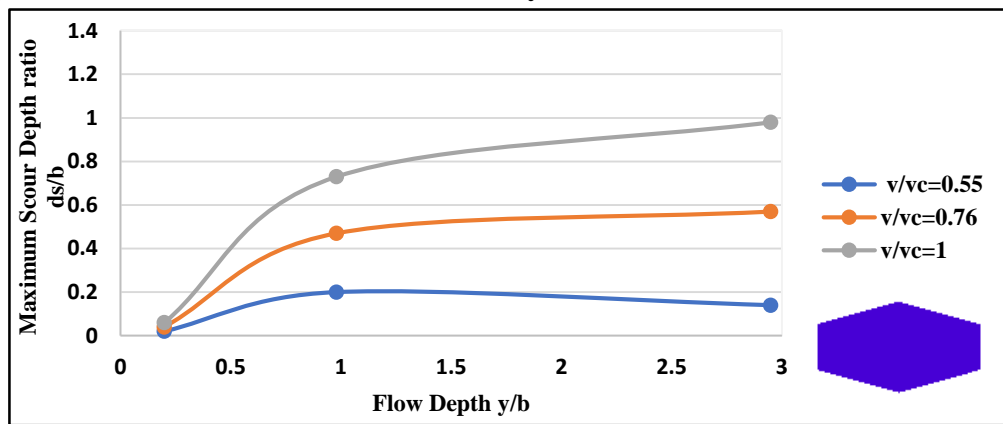
Figure (5-21): Development of scour depth with flow depth around hexagonal pier shape at different value of flow intensity, b/B=0.11, Ks=0.94, Kθ=1.00.
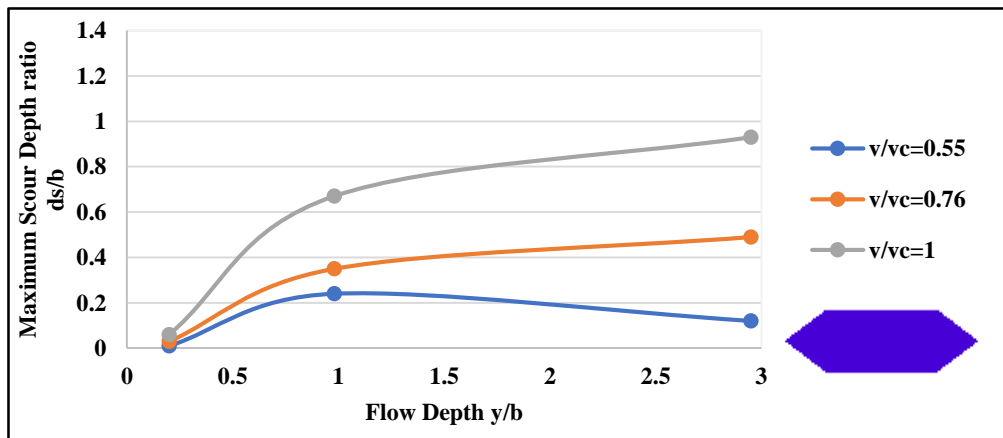
Figure (5-22): Development of scour depth with flow depth around ogival pier shape at different value of flow intensity, b/B=0.11, Ks=0.81, Kθ=1.00.
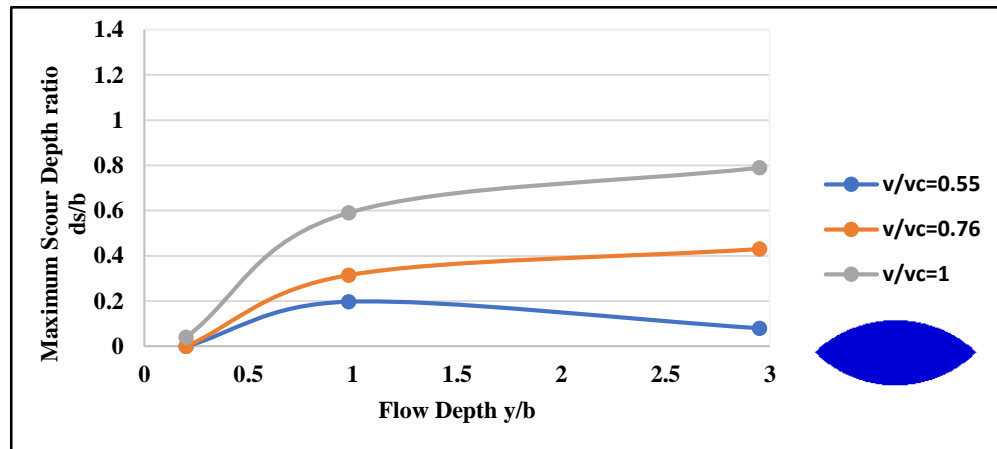
Figure (5-23): Development of scour depth with flow depth around lenticular pier shape at different value of flow intensity, b/B=0.11, Ks=0.71, Kθ=1.00.

5.3.3 Influence of pier width ratio b/B

To study the effect of the variation of pier width on scour at different pier shapes, a total of 243 runs are operated at different level of flow depth and flow intensity as illustrated in Figure 5.24. This figure presents a summary of pier width value taken at different cases to investigate the optimum effectiveness of pier width at these parameters on the maximum depth of scour.

Figures 5.25, 5.26 and 5.27 (for runs 37, 118 and 199 illustrated in Appendix A), represent side view of scour development around typical pier (circular shape). From these figures, scour depth become larger with the increase in pier width. On the other hand, these figures indicate that more scour can be occur at upstream half of the pier, whereas little scour found at downstream and more sediment deposition at downstream of the pier. This observation can be explained by the fact that scouring is due to the horseshoe vortex system whose dimension is a function of the diameter of the pier.
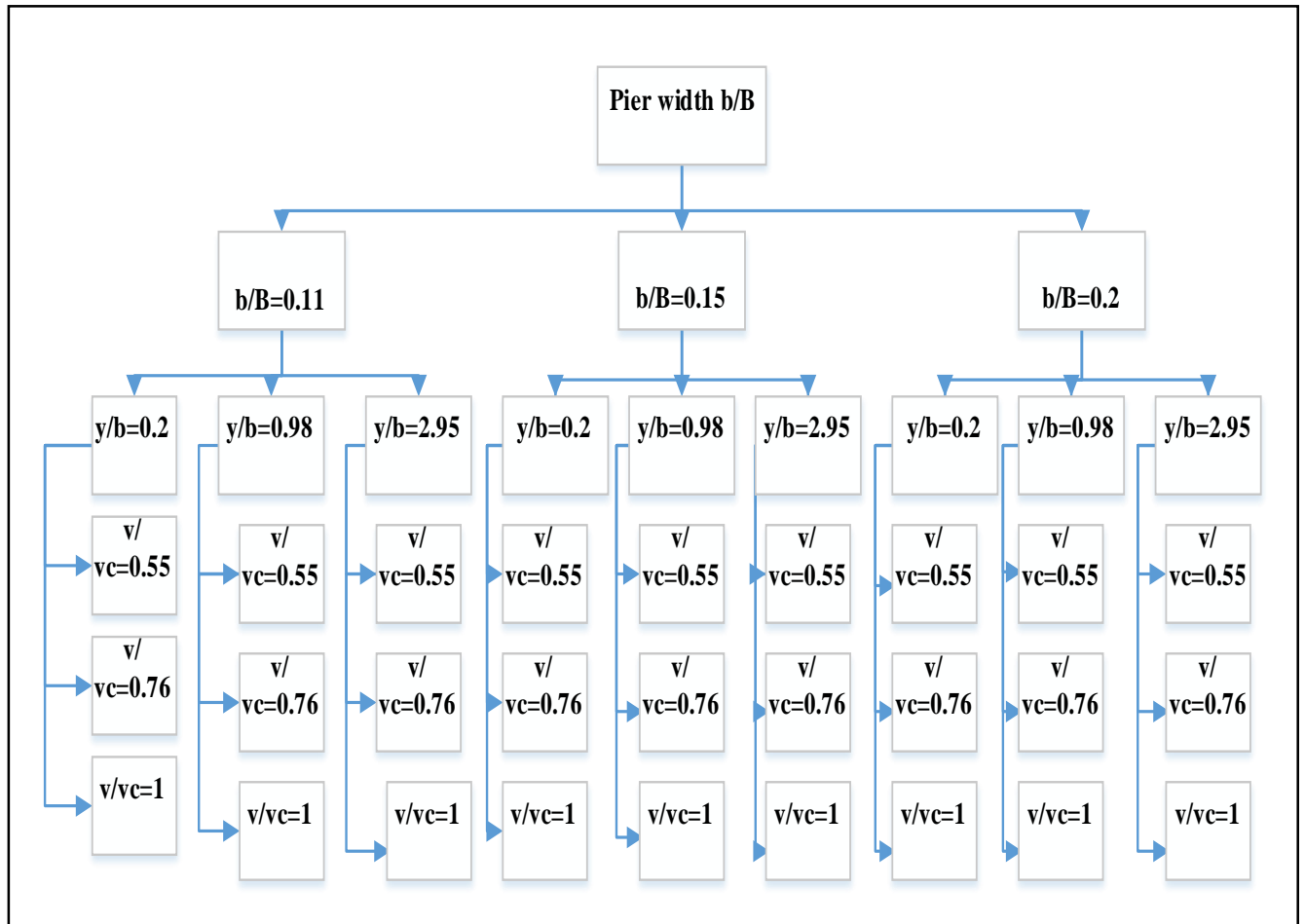
Figure (5-24): Summary of pier width value at different cases
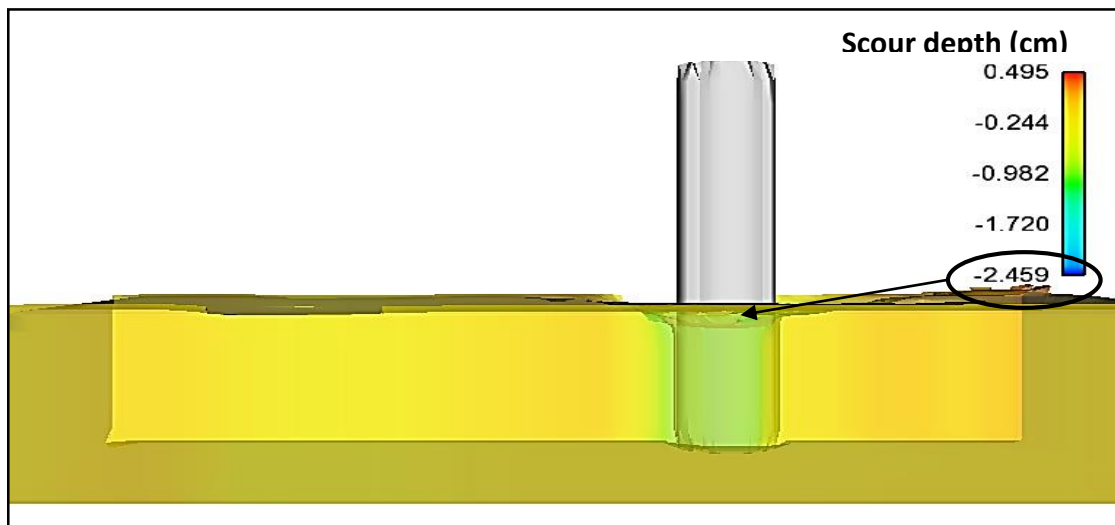
Figure (5-25): Side view of scour depth around circular pier at b/B=0.11, y/b=0.98, V/V$_C$ =0.76, Ks=1.00, Kθ=1.00.
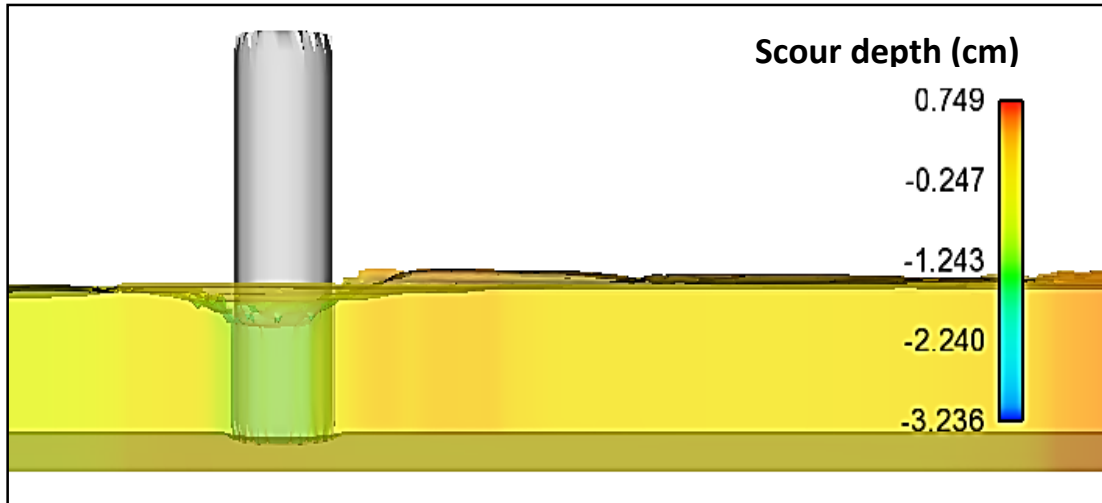
Figure (5-26): Side view of scour depth around circular pier at b/B=0.15, y/b=0.98, V/V$_C$ =0.76, Ks=1.00, Kθ=1.00.
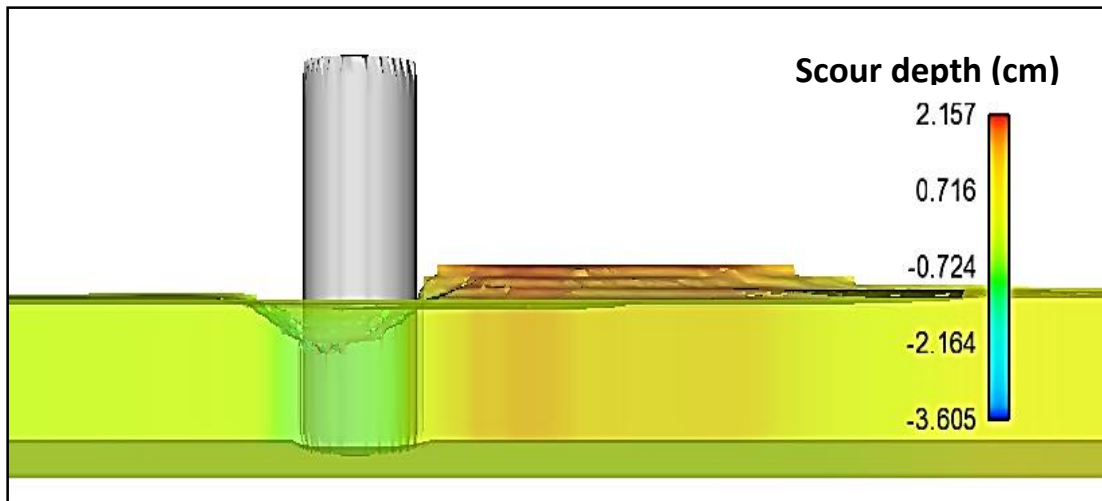
Figure (5-27): Side view of scour depth around circular pier at b/B=0.20, y/b =0.98, V/V$_C$ =0.76, Ks=1.00, Kθ=1.00.

To demonstrate the impact of pier width on pier shapes, curves were plotted between the scour depth and pier width for all pier shapes, and between flow depth and flow intensity. Figures 5.28 to 5.36 represent a variation pier width at constant y/b =2.95. In general, it is clear from these figures that width of the pier has a direct effect on the depth of scour. Scour depth is steadily growing with the increase of pier width ratio to reach maximum scour depth at ratio of 0.20. It can be seen from aforementioned figures that maximum scour is also observed in rectangular pier with

scour rate ds/b= 1.56, while minimum scour is observed in lenticular with scour rate ds/b =1.1. This value is measured at maximum value of flow intensity and flow depth, y/b=2.95 and V/V_C =1, respectively.
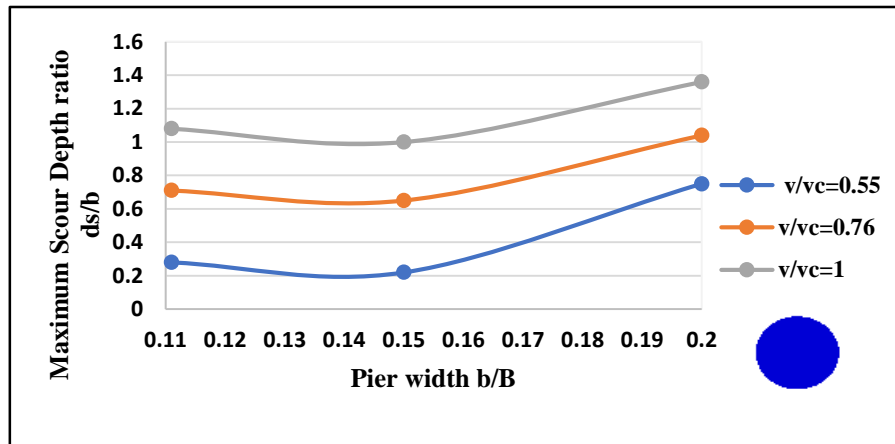
Figure (5-28): Scour depth versus pier width around circular pier at different value of flow intensity for y/b=2.95, Ks=1.00, Kθ=1.00.
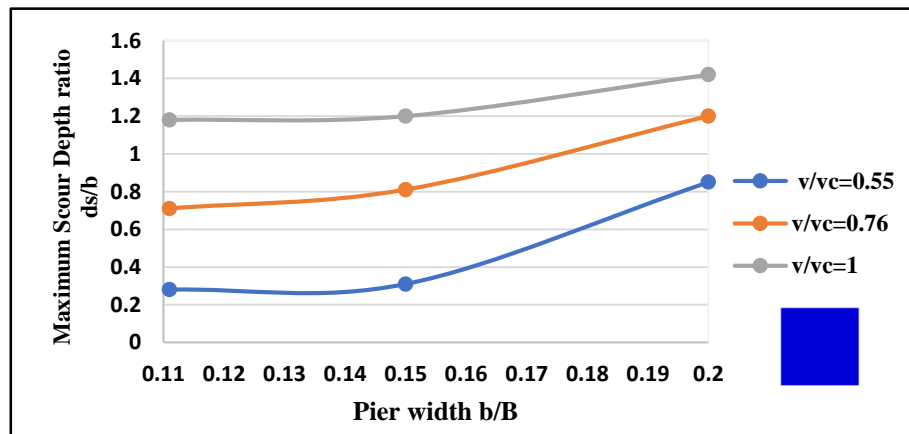
Figure (5-29): Scour depth versus pier width around square pier at different value of flow intensity for y/b=2.95, Ks=1.16, Kθ=1.00.
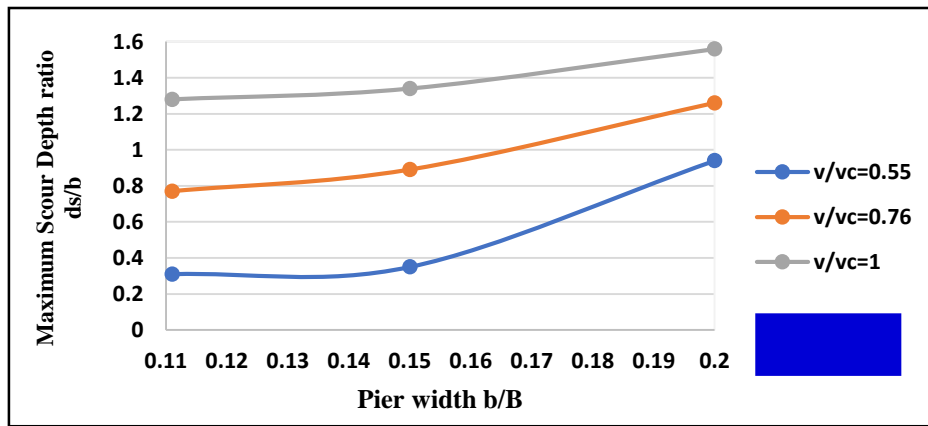
Figure (5-30): Scour depth versus pier width around rectangular pier at different value of flow intensity for y/b=2.95, Ks=1.26, Kθ=1.00.
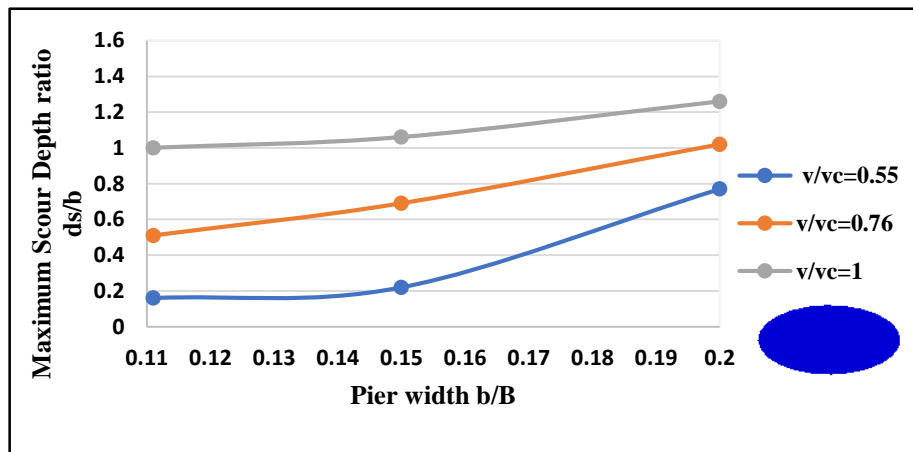
Figure (5-31): Scour depth versus pier width around elliptic pier at different value of flow intensity for y/b=2.95, Ks=0.84, Kθ=1.00.
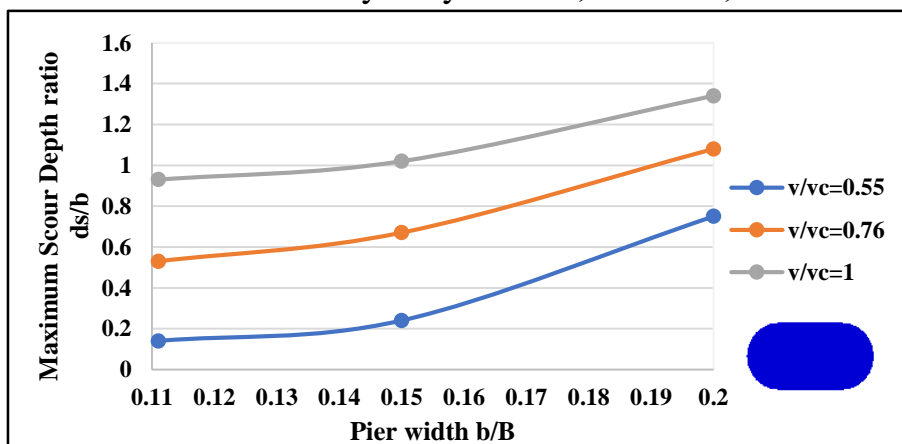
Figure (5-32): Scour depth versus pier width around oblong pier at different value of flow intensity for y/b=2.95, Ks=0.87, Kθ=1.00.
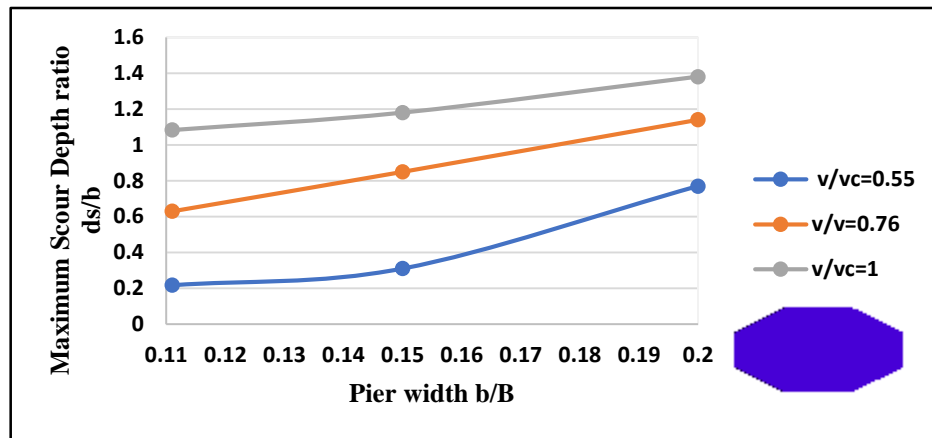
Figure (5-33): Scour depth versus pier width around octagonal pier at different value of flow intensity for y/b=2.95, Ks=1.03, Kθ=1.00.
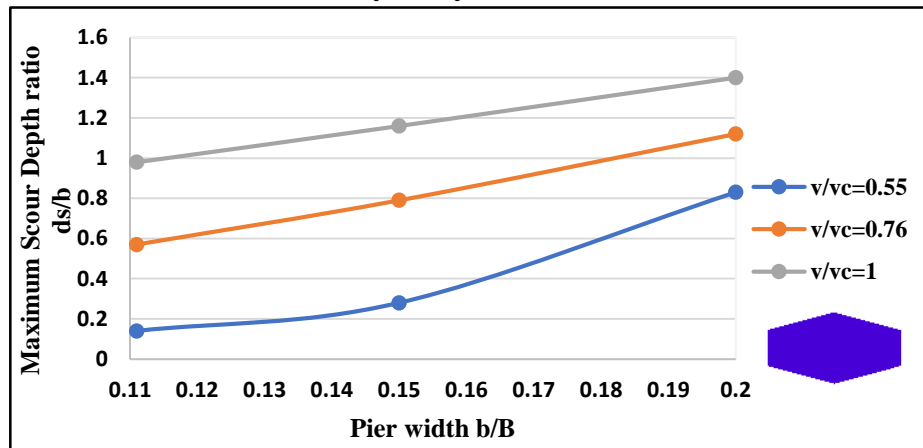
Figure (5-34): Scour depth versus pier width around hexagonal pier at different value of flow intensity for y/b=2.95, Ks=0.94, Kθ=1.00.
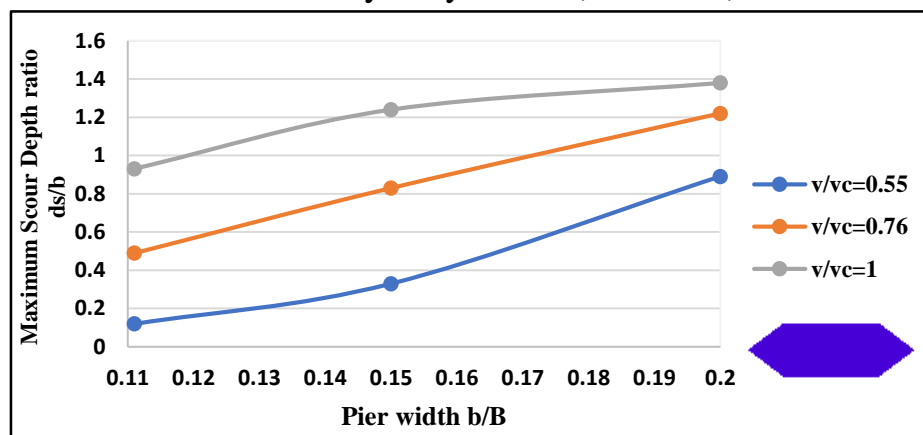
Figure (5-35): Scour depth versus pier width around ogival pier at different value of flow intensity for y/b=2.95, Ks=0.81, Kθ=1.00.
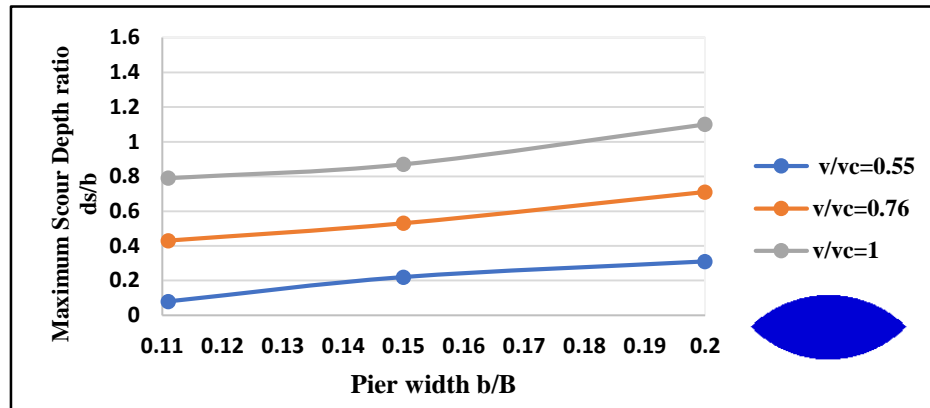
Figure (5-36): Scour depth versus pier width around lenticular pier at different value of flow intensity for y/b=2.95, Ks=0.71, Kθ=1.00.

5.3.4 Influence of flow alignment or angle of attack θ°.

Angle of attack is the angle between the direction of the bridge pier and the direction of the flow. The effect of the angle of attack on the maximum depth of scour was studied by using three angels 0, 30° and 45°. To show the impact of these angles on scour around different pier shapes, 729 runs were conducted on all previous cases of flow intensity, flow depth and pier width for all pier shapes. All pier shapes are exposed to different angles by rotating the upstream face as represent in Figure 5.37.
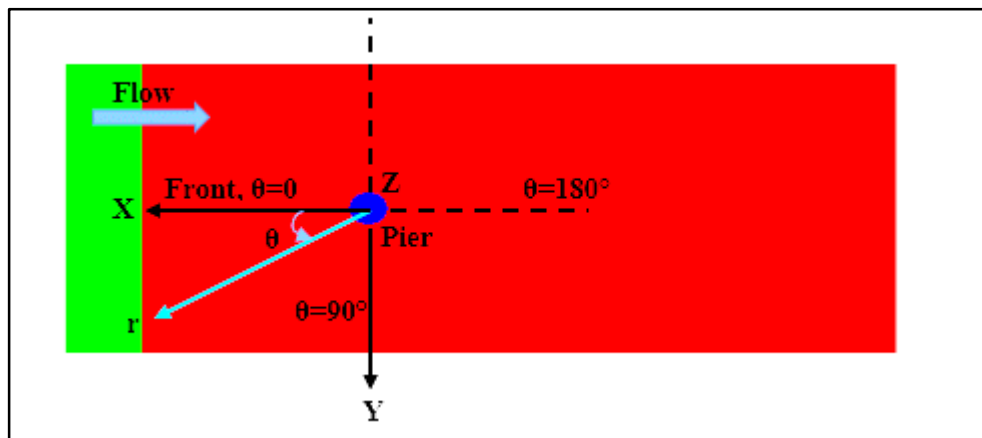
Figure (5-37): Coordinates systems for angle of attacks

The scour depth variation around typical pier (lenticular shape) is illustrated in Figures 5.38, 5.39 and 5.40 (for runs 113, 599 and 356, respectively illustrated in

Appendix A). As it can be seen from these figures, scour depth increase with the increase in the angle of attack and the point of maximum scour depth moves along the exposed side of the pier towards the rear. The scour depth at the rear becomes greater than that happens at the front face of the pier.
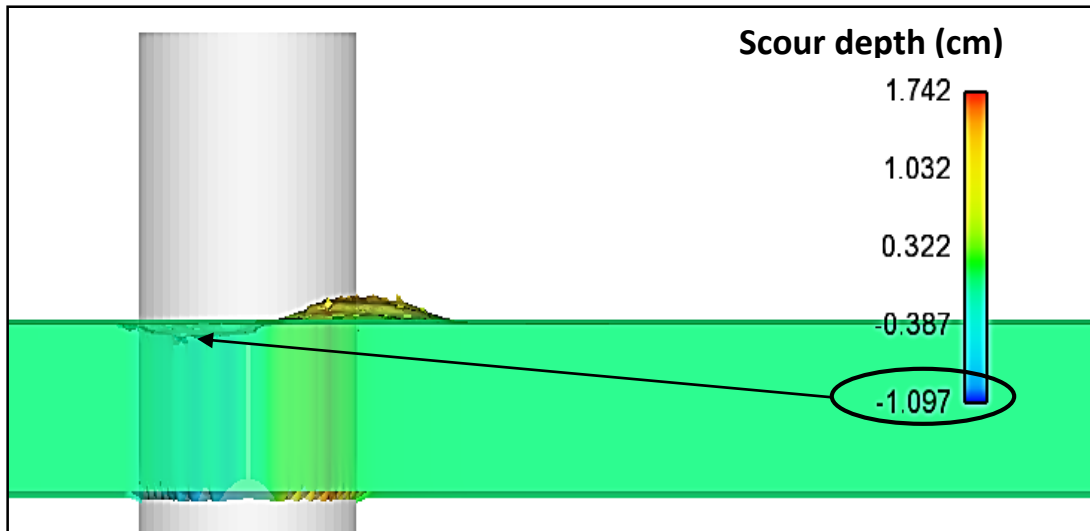
Figure (5-38): Side view of scour depth around lenticular pier at angle of attack 0⁰, V/V$_C$ =0.55, y/b=0.98, b/B=0.15, Ks=0.71.
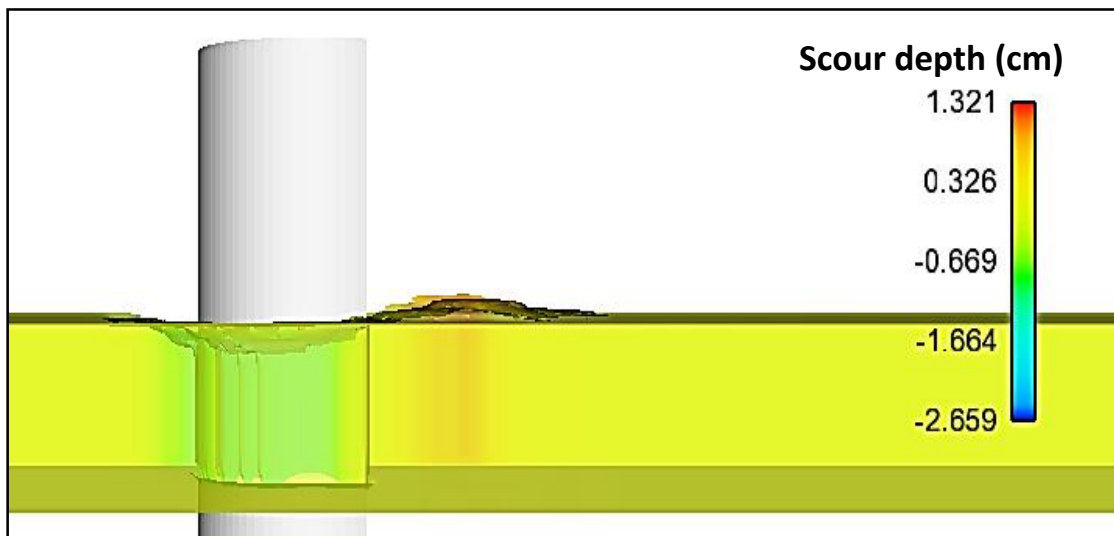
Figure (5-39): Side view of scour depth around lenticular pier at angle of attack 30º, V/V$_C$ =0.55, y/b=0.98, b/B=0.15, Ks=0.71.
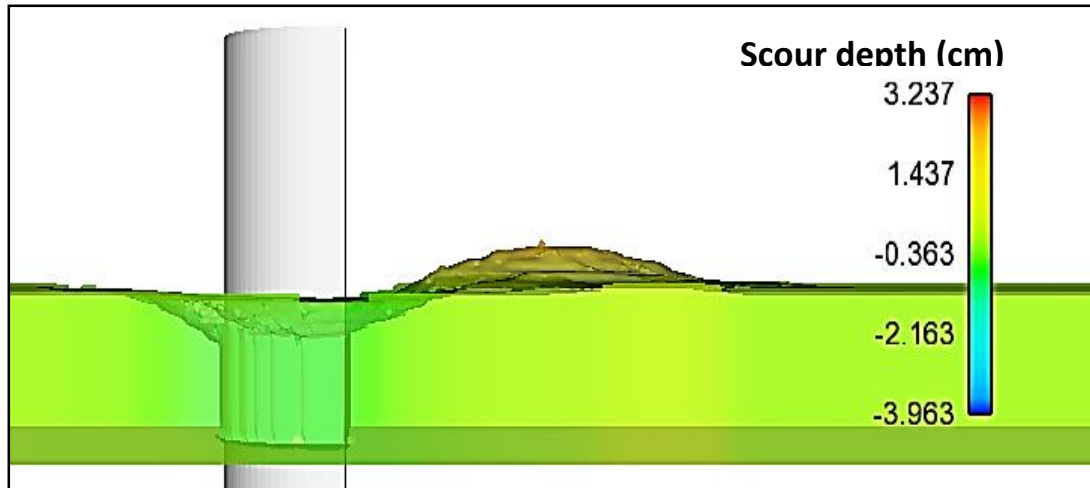
Figure (5-40): Side view of scour depth around lenticular pier at angle of attack 45°, V/V$_C$ =0.55, y/b=2.95, b/B=0.15, Ks=0.71.

To study the behavior of pier shapes scour under changing angle of attack, part of the results is represented in Figures 5.41 to 5.48 and the other part of the results is represented in Appendix A. These figures represent the relationship between maximum scour depth and angle of attack with variation of flow intensity V/V$_C$ at constant pier width b/B and flow depth y/b.

The depth of local scour for all shapes of pier is highly dependent on the alignment or orientation of the pier to the flow. However, the circular pier is exception which it remains unaffected despite the change in angles of attack due to its symmetrical and even shape, unlike the other shapes.

So, maximum scour depth occurred at angle 45° while minimum scour depth occurred when pier is aligned to flow (angle of attack 0°). Maximum scour is occurred in octagonal shape with scour depth ds/b =1.63 and minimum scour is observed at elliptic pier ds/b=1.04 at angle 45°. This change in scour value for each shape is the result of increase in the effective frontal width of the pier.
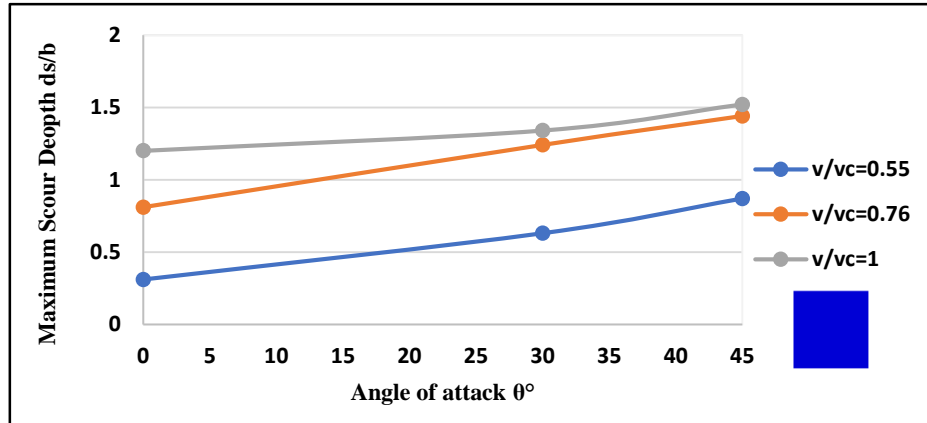
Figure (5-41): Scour depth versus angle of attack around square pier at different value of flow intensity for y/b=2.95, b/B=0.15, Ks=1.16.
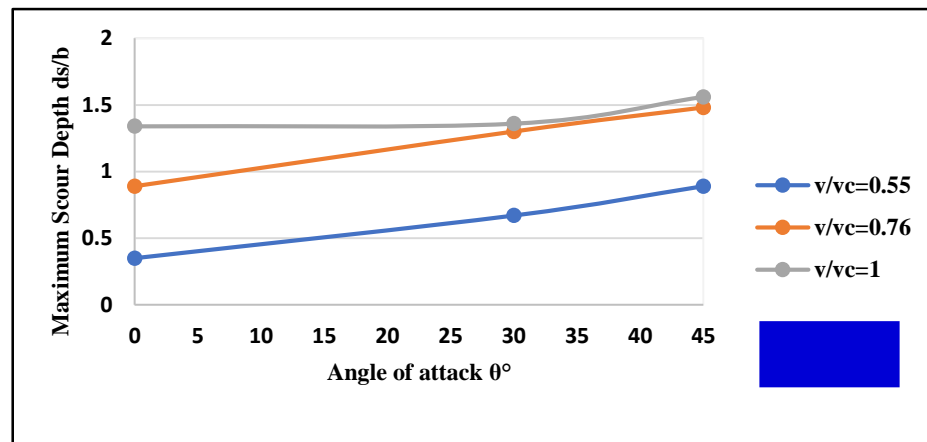
Figure (5-42): Scour depth versus angle of attack around rectangular pier at different value of flow intensity for y/b=2.95, b/B=0.15, Ks=1.26.
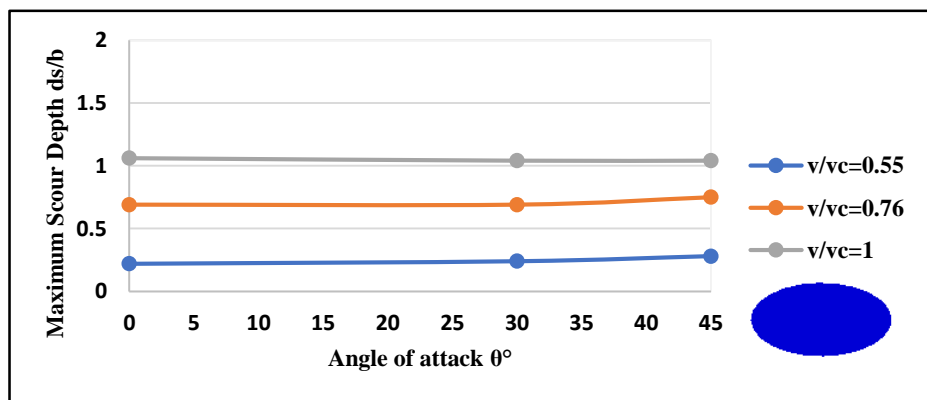
Figure (5-43): Scour depth versus angle of attack around elliptic pier at different value of flow intensity for y/b=2.95, b/B=0.15, Ks=0.84.
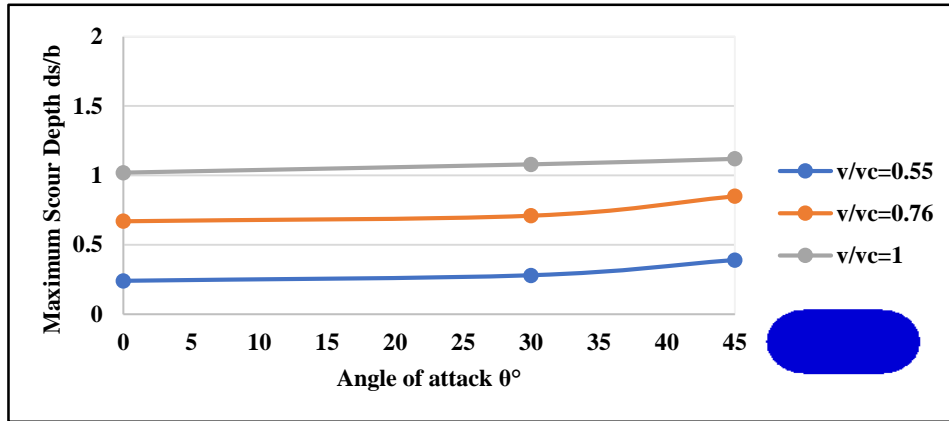
Figure (5-44): Scour depth versus angle of attack around oblong pier at different value of flow intensity for y/b=2.95, b/B=0.15, Ks=0.87.
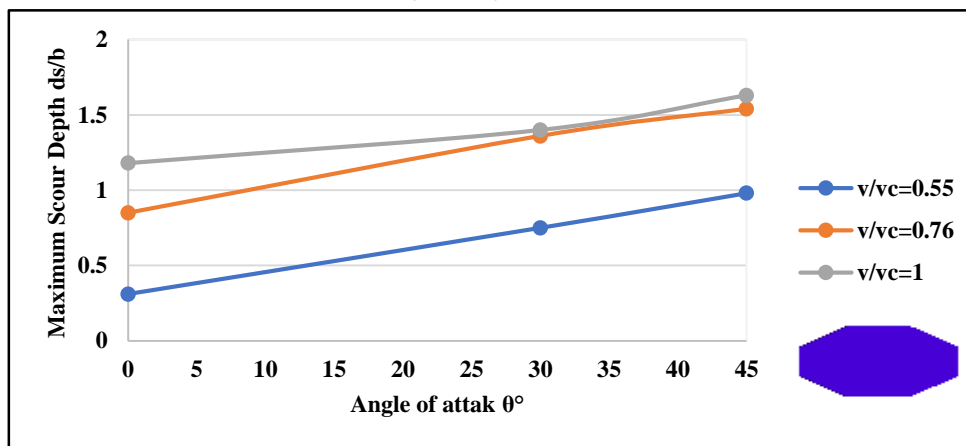
Figure (5-45): Scour depth versus angle of attack around octagonal pier at different value of flow intensity for y/b=2.95, b/B=0.15, Ks=1.03.
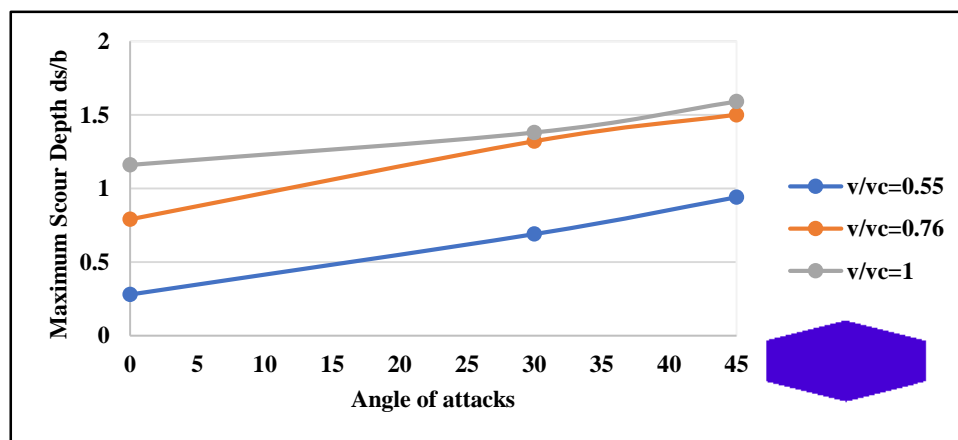
Figure (5-46): Scour depth versus angle of attack around hexagonal pier at different value of flow intensity for y/b=2.95, b/B=0.15, Ks=0.94.
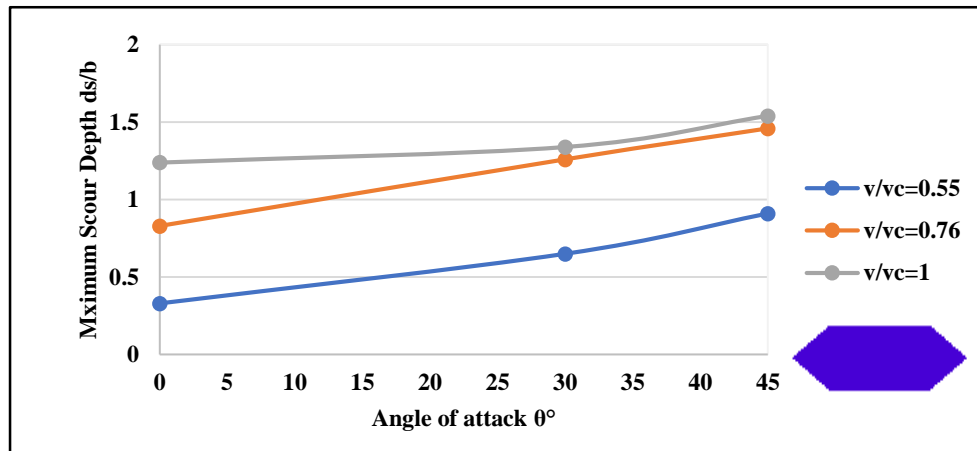
Figure (5-47): Scour depth versus angle of attack around ogival pier at different value of flow intensity for y/b=2.95, b/B=0.15, Ks=0.81.
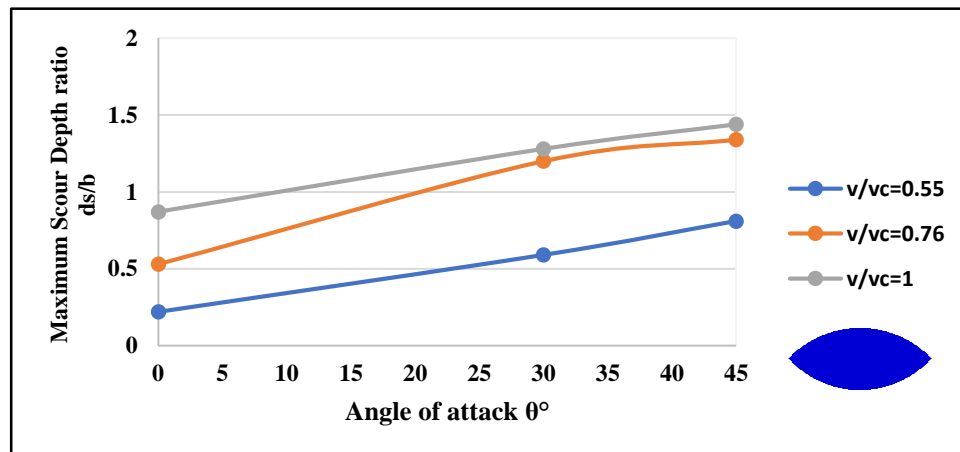
Figure (5-48): Scour depth versus angle of attack around lenticular pier at different value of flow intensity for y/b=2.95, b/B=0.15, Ks=0.71.

5.3.5 Shape factor Ks

Shape factor is defined as the ratio of scour depth recorded for a particular shape to the scour depth for a standard pier shape. The circular pier shape was chosen to be standard pier shape when the most spread scour predictors have been conducted for this pier shape. Shape factors for uniform piers, that is piers having constant section throughout their depth, have been proposed by several investigators. Values of shape factor in Table 5.3 are obtained by simulating nine pier shapes alignment with flow under the same condition, likewise flow depth, flow intensity and pier width are calculated scour depth for each pier shape. The shape factor is calculated using

equation 5-3 (Melville and Coleman, 2000) when the pier aligned with flow for l/b=2. The effect of the pier shape factor with the variation of pier alignment to flow has been studied by a few researchers Hamill, (2004) and Bridge Scour Manual, (2013), who stated that when the angle of alignment is greater than 5°, the shape factor Ks should be taken equal to 1 and the correlation factor for the angle of alignment (Kθ) is dominated.

$$K_s = \frac{ds_{(non-circular)}}{ds_{(circular)}} \qquad\qquad (5-3)$$

Where : $ds_{(non-circular)}$ is scour depth for non-circular piers and $ds_{(circular)}$ is the scour depth for circular pier.

Table (5-3): calculated value of shape factor.

No.	Geometry	l/b	Ks
1	Circular	1	1.00
2	Elliptic	2	0.84
3	Square	1	1.16
4	Rectangular	2	1.26
5	Oblong	2	0.87
6	Ogival	2	0.81
7	Hexagonal	2	0.94
8	Octagonal	2	1.03
9	Lenticular	2	0.71

5.4 Effect of Geometry

A total of 729 runs is operated at different condition to determine behavior of each pier shape under these conditions. The results of all runs are represented in Table A.1 and in Appendix A. After completing the results of the influence of different factor on scour, it was observed that the nose of pier is best scour protection measure as discussed below.

The formation of horseshoe and wake vortices depends on geometry of pier. Therefore, the current study focuses the investigation of the effect of pier's geometry (pier's shape) on scour. Through a series of runs on different shapes, under different flow conditions and pier geometry, it is observed that lenticular pier is best protecting measure against local scour instead of other conventional shapes. Theoretical explanation for it is that the piers is an obstruction creates stagnation zone. Therefore, when high velocity flow impacts on upstream side of the pier, it creates velocity jet that moves downward direction and creates scour hole. Intensity of velocity jet is a function of approach velocity and exposed area of the pier. Although hexagonal and ogival pier also looks alike lenticular with minimum upstream nose area, presence of corner causes higher scour at corner itself. It is observed that ogival pier and hexagonal pier's corner are the starting point of local scour which propagate around the pier as explained in Figures 5.49 and 5.50. For lenticular pier, it is observed that scour starts merely from upstream face and ends at midsection, as illustrated in Figure 5.51. History of bridge failure indicates that bridge failure takes place because of tilting of the pier from one side, so lenticular pier considered perfectly safe from both upstream and downstream sides.
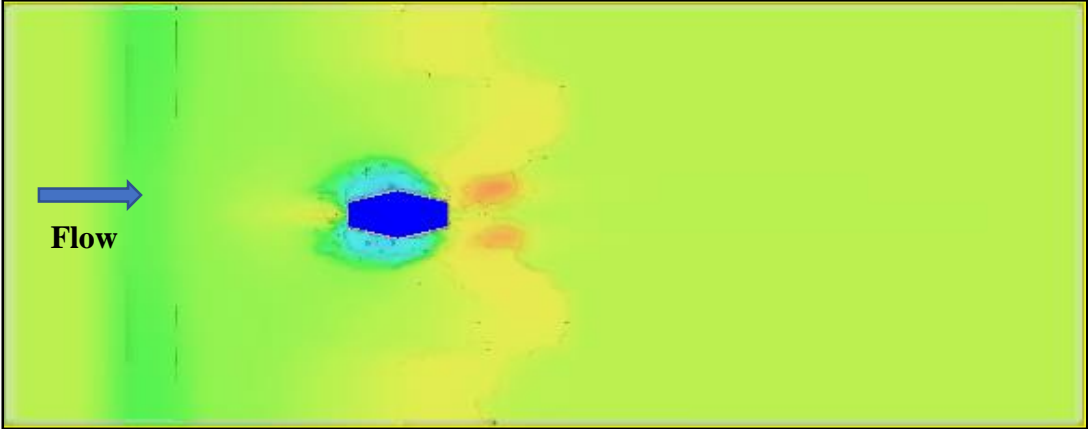
Figure (5-49): Top view of scour depth around hexagonal pier shape.
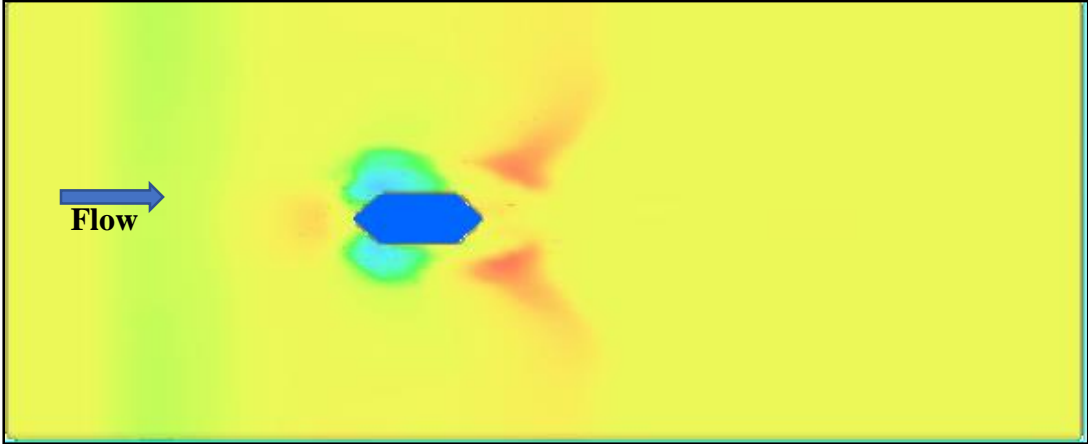
Figure (5-50): Top view of scour depth around ogival pier shape.
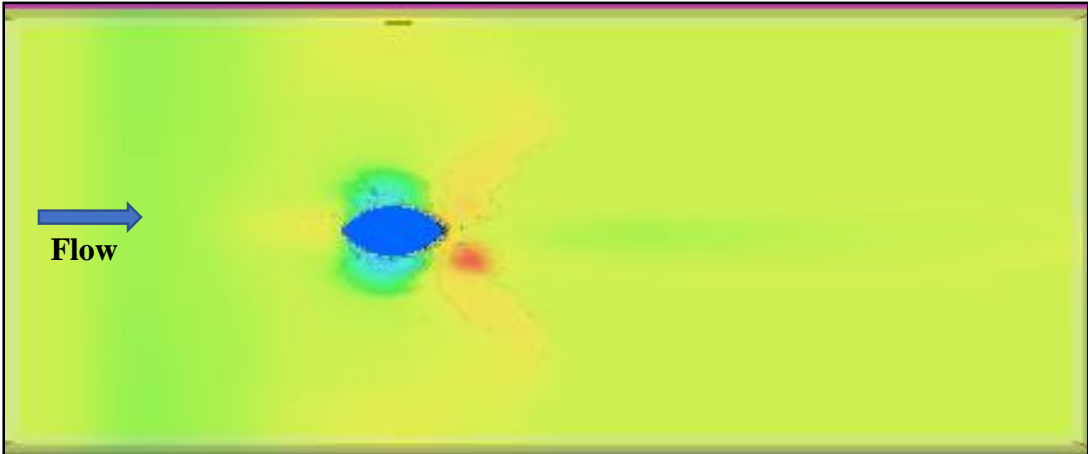
Figure (5-51): Top view of scour depth around lenticular pier shape.

An additional to the previous test, four simulations were carried out on four pier shapes of the most widespread pier shapes (circle, square, elliptic and lenticular). To keep the test fair, the volume of concrete used is the same and has the same surface area. This is to ensure that optimum shape gives minimum depth of scour while still maintains the cost. All simulations were done under the same conditions but under varying flow intensity. The curve in Figure 5.52 showed that the lenticular shape gave the lowest scour depth. The previous simulation also gave the same result, leading to make the conclusion that the lenticular shape behaves the same in all conditions, so the lenticular pier is the optimum pier shape.
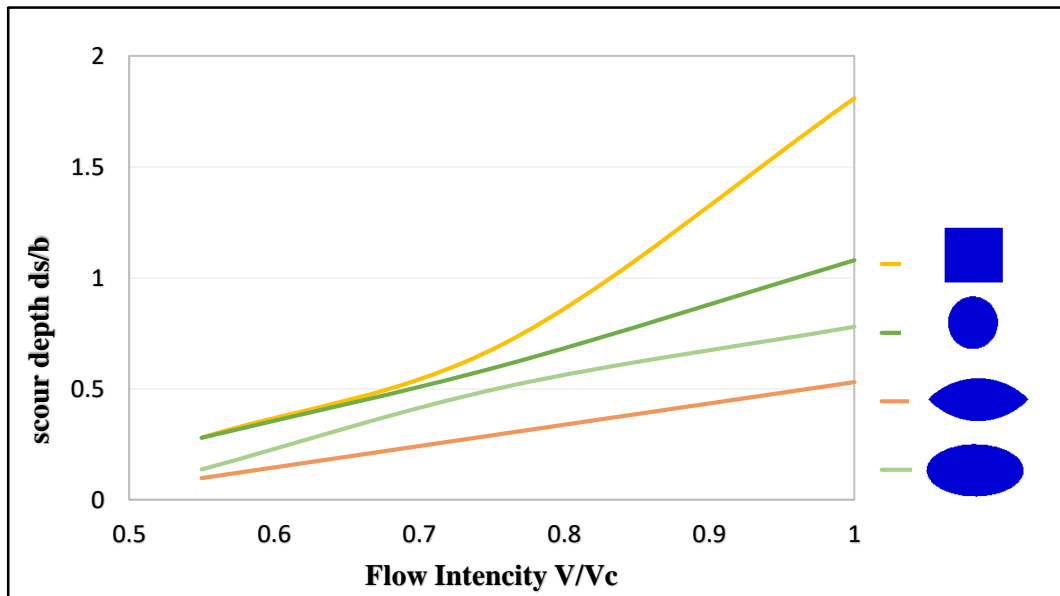
Figure (5-52): Optimum pier shape at V/Vc=0.76, y/b=2.95, b/B=0.11.

Through this numerical observation, it is concluded that square pier has higher scour compared to other geometries because of the maximum exposed area and lenticular geometry has the minimum scour depth.

5.5 Statistical Analysis to Development New Scour Depth Formula

The scour depth is a function of some variables represented in Equation 5.4, which are discussed previously in the section of dimensional analysis. The data set (total of 729) obtained from numerical simulation by Flow-3D were modeled by using two statistical software GEP and SPSS to developed a theoretical model for predicting the relative maximum scour depth (ds/b) at bridge pier and identifying the best techniques to predict the scour depth by three statistical parameters R^2, RMSE and MAE

$$\frac{d_s}{b} = f_4 \left(\theta \, , \frac{y}{b} \, , K_s \, , \frac{B}{b} \, , \frac{V_c}{V} \right) \qquad\qquad (5-4)$$

5.5.1 Genetic Expression Programming GEP model

The available data are randomly divided by the program into training and validation/testing datasets. The training set consists of 583 data (80% of the total) and it used for the development of GEP model, while the testing set consists of the remaining data of 146 data (approximately 20%) and used for the model validation.

The program was run for a number of generations and was stopped when there was no development in fitness function value or coefficient of determination or when the model reaches maximum fitness function (maximum fitness 1000). After some trials it was found that there was no appreciable change after 324365 generations and maximum fitness function (RMSE) for training and validation are 868.82 and 859.33, respectively.

Scour depth (ds/b) equation is a function of expression tree (ET) which state in Equation 5.5 and the corresponding expression trees language are shown in Figure 5.53.

$$\frac{ds}{b} = ET1 + ET2 + ET3 \tag{5-5}$$

Gene 1:

$$\text{Sub } ET1 = d2 * \left[\frac{\frac{d1}{d0} + \frac{d4}{d1}}{d0 + C1 + d1} \right] \tag{5-6}$$

Gene 2:

$$sub\ ET2 = (d0 * d2) * [((C4 * d3) + d1) + (C4 * d4)] \tag{5-7}$$

Gene 3:

$$sub\ ET3 = d2 - \left[\left((d1^{d0} * d2) + \frac{d0}{d1} \right) * d2 \right] \tag{5-8}$$

The corresponding explicit equation obtained from the GEP model for ds/b is given in Equation 5.9:

So, the scour depth (ds/b) formula is:

$$\frac{ds}{b} = d2 * \left(\frac{\frac{d1}{d0} + \frac{d4}{d1}}{d0 + d1 - 7.38} \right) + (d0 * d2)$$
$$* [2.66 * d3 + d1 + 2.66 * d4] + d2$$
$$- \left[\left((d1^{d0} * d2) + \frac{d0}{d1} \right) * d2 \right] \tag{5-9}$$

Where the definition of the parameters used in equation 5.6, 5.7, 5.8 and equation 5.9 are represented in Table 5.4.

Table (5-4): Definition of parameters in (ET)

Parameters	Definition
d0	$\dfrac{V}{V_C}$
d1	$\dfrac{y}{b}$
d2	$\dfrac{b}{B}$
d3	Ks
d4	$K\theta$
C1 (gene1)	-7.38
C4 (gene2)	2.66

The training and testing results of the GEP model are presented in Figures 5.54 to 5.57. The statistical results presented in Table 5.6 were carried out to determine the formula that gives minimum prediction errors. The scatterplot of estimated (training data set and testing dataset) versus measured values is used to investigate the degree of similarity between predictor and measured values.
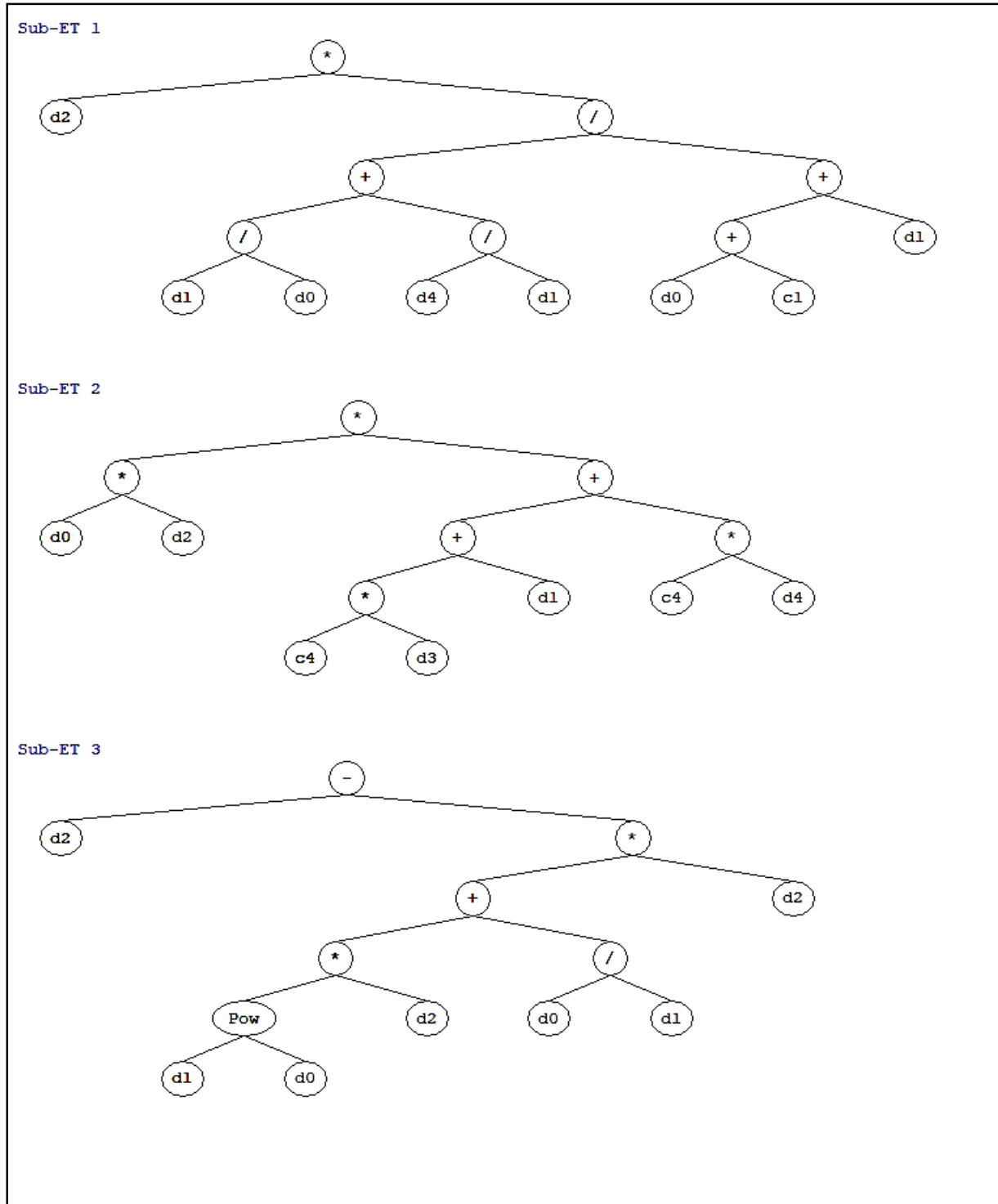
Figure (5-53): Expression Trees (ET) for the GEP formulation for scour depth.

Training results:
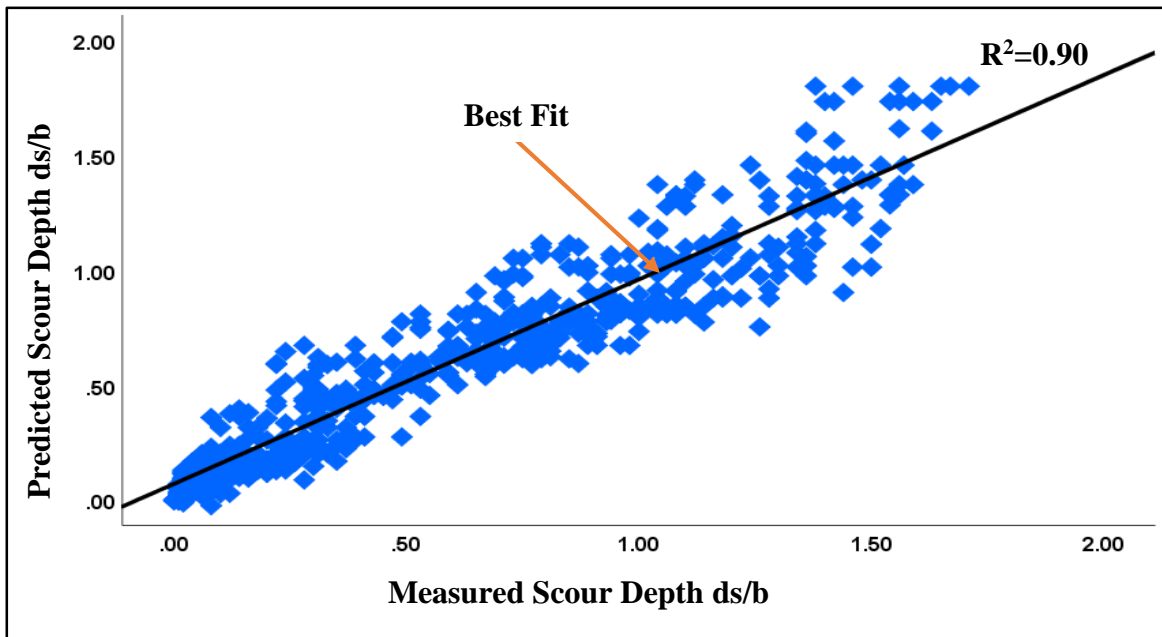
Figure (5-54): Scattered plot of measured ds/b versus predicted ds/b
(Training data)
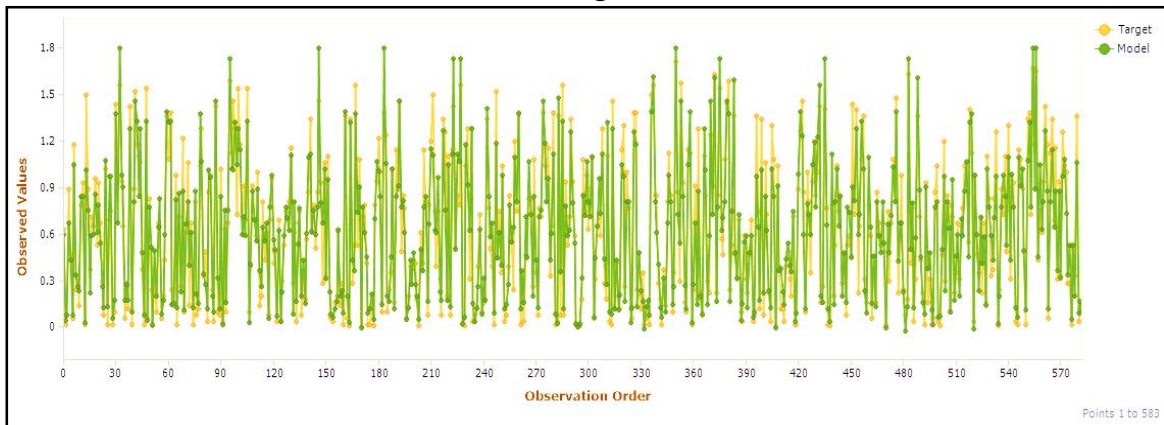
Figure (5-55): Curve fitting between predicted (yellow color) and measured
(green color) scour depth (Training data)

Testing results:
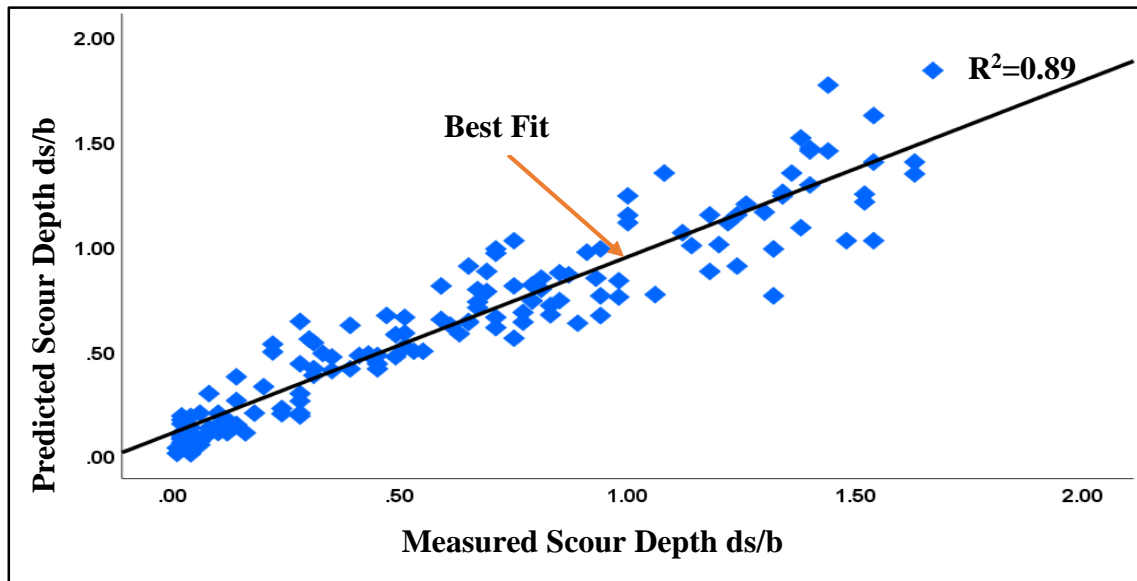
Figure (5-56): Scattered plot of measured ds/b versus predicted ds/b
(Testing data)
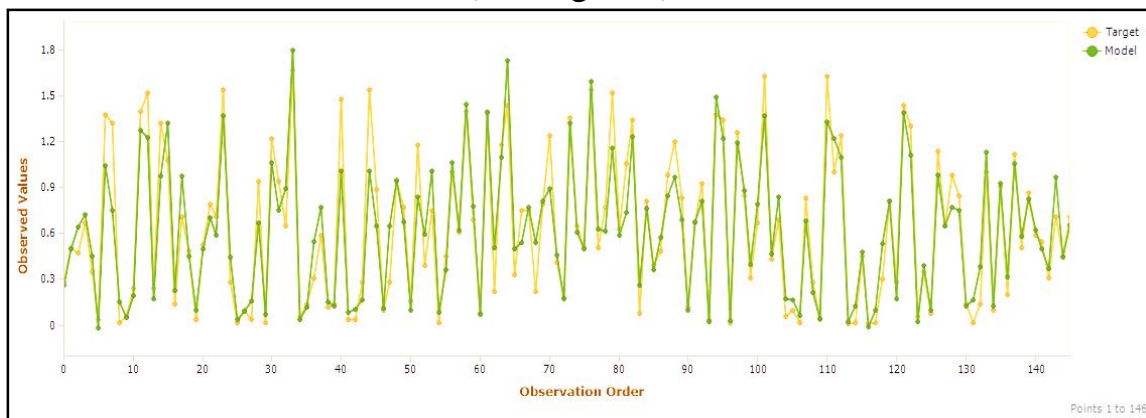
Figure (5-57): Curve fitting between predicted (yellow color) and measured
(green color) scour depth (Testing data).

Table (5-5): Statistical results of GEP model.

No.	Error measure	GEP Model	
		Training data	Testing data
1	R^2	0.90	0.89
2	RMSE	0.151	0.164
3	MAE	0.115	0.119

116

From these results, The GEP approach resulted in highly nonlinear relationship between ds/b and the input parameters. GEP provided a high value of R^2 for the testing data which indicates a perfect prediction to scour depth which indicating very little discrepancy between measured and predicted scour depth and a low value of RMSE and MAE implies a good performance of the applied method.

Figure 5-56 illustrates the check of the adequacy of the model. It indicates that acceptable scatter can recognize between predicted and measured scour depth. Figure 5-57 presents good fitness between predicted and measured scour depth with a little variance between them.

5.5.2 SPSS predicting model

For SPSS prediction model, the same splitting of dataset in GEP is used in SPSS model. SPSS software was run to achieve the required analysis and model building. For simplicity, linear models were tried first and give R^2 of 0.66. Unfortunately, test with linear models failed to represent the observations. However, it was found that all prediction models were non-linear. It is worth mentioning that specifying the thesis size prevents the presentation of the analysis of the tested models, so this section include the final formula of scour depth equation.

<u>**The scour depth formula is:**</u>

$$\frac{ds}{b} = 1.01 + 0.18 * \frac{v}{vc} + 0.474 * \frac{y}{b} + 0.144 * \frac{b}{B} + 0.09 * k\theta - 0.028$$
$$* \left(\frac{v}{vc}\right)^2 - 0.3743 * \left(\frac{y}{b}\right)^2 + 0.017 * \frac{y}{b} * ks \qquad (5-10)$$

The comparison between measured scour depth and predicted scour ds/b is represented in scatterplots for training and validation data in Figures 5.58 and 5.59. Its statistical results are presented in Table 5.6.
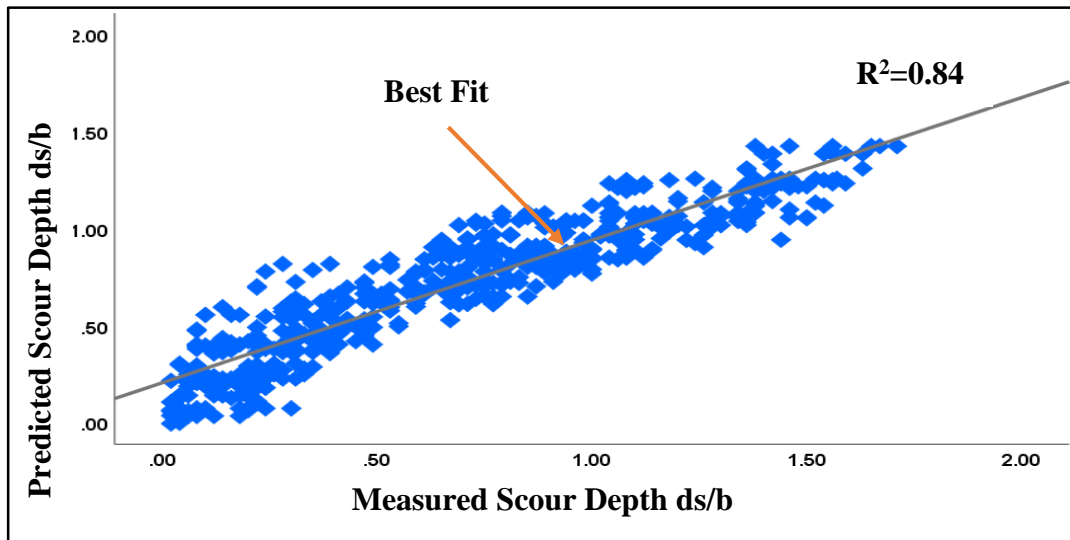
Figure (5-58): Scattered plot of measured ds/b versus predicted ds/b
for training data
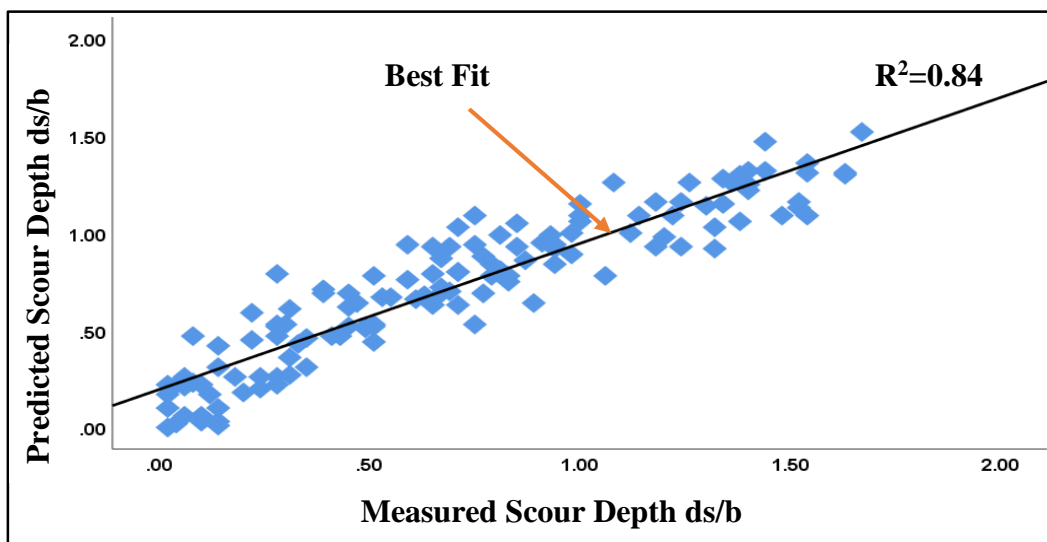
Figure (5-59): Scattered plot of measured ds/b versus predicted ds/b
for testing data

Table (5-6): Statistical results of SPSS.

No.	Error measure	SPSS Model	
		Training data	**Testing data**
1	R^2	0.84	0.84
2	RMSE	0.171	0.171
3	MAE	0.128	0.128

5.6 Sensitivity Analysis

Sensitivity analysis are conducted by using SPSS software to determine the influence of each input parameters on the scour depth predicted from GEP and to identify the most sensitive parameter(s) which will need a spatial attention in the feature studies. There are many factors affect the magnitude of scour depth at piers. These includes pier width, pier shape, flow depth, approach velocity and angle of attacks. The different input combinations as shown in Table 5.7 are studied by removing one input variable in each case and its effect on predicted scour is evaluated in terms of the root mean square error (RMSE) and coefficient of determination (R^2) as main performance criteria. Results in Table 5.7 and Figure 5.60 suggest that the approach depth of flow has major influence in predicting the local scour in comparison to other input parameters and removing any other input parameter have no major influence on the predicting depth of scour.

Table (5-7): Sensitivity analysis.

Input combination	Input parameter removed	R^2	RMSE
v/vc, b/B, y/b, Ks and Kθ	-	0.89	0.152
b/B, y/b, Ks and Kθ	v/vc	0.723	0.257
v/vc, y/b, Ks and Kθ	b/B	0.746	0.205
v/vc, b/B, y/b and Kθ	Ks	0.878	0.17
v/vc, b/B, y/b, Ks	Kθ	0.849	0.189
v/vc, b/B, Ks and Kθ	y/b	0.327	0.399
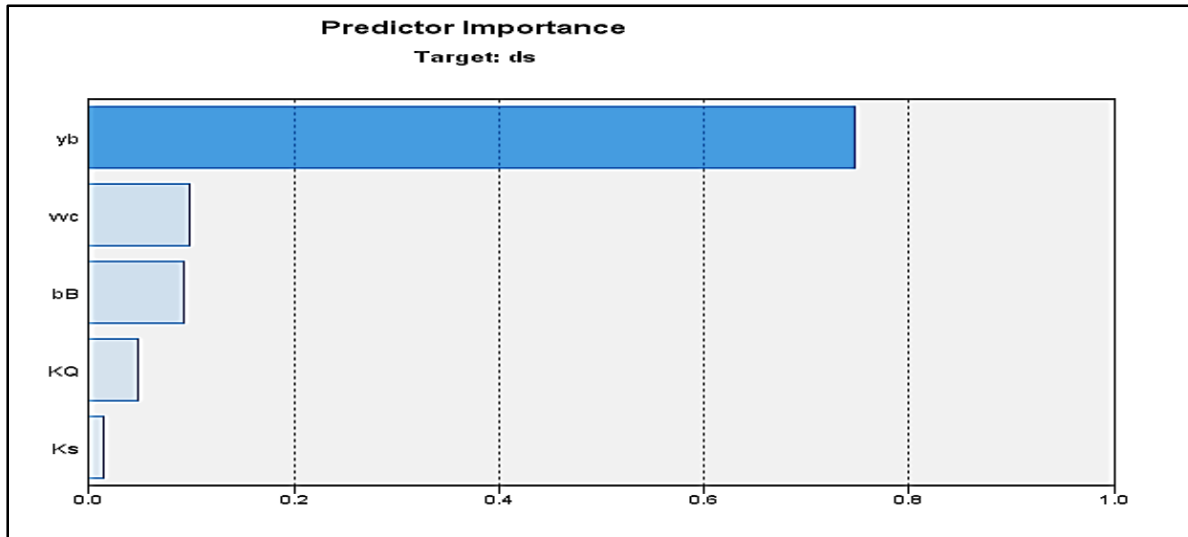
Figure (5-60): Importance of input variables

5.7 Comparison of GEP with SPSS

The performance of GEP model was evaluated by comparing its performance with SPSS model. The predicted scour depth is computed by GEP model and SPSS model and are compared with the measured scour depth. The statistical measures R^2, RMSE and MAE were calculated for the both models and illustrated in Table 5.8; the scatter plot for the comparison between SPSS and GEP models are shown in Figure 5.61.

It is observed that the GEP model performs better than the SPSS model; it produced smaller values for RMSE and MAE and greater value of R^2 as compared to SPSS. According to the scatter plot in Figure 5.61, gene expression programming is least scattered from the line of perfect agreement than that of the SPSS model. SPSS equation is of low performance as compared with GEP, but in general, it performs reasonably good results.

In summary, GEP performs better than SPSS with respect to statistical measures and scatter plots. GEP has the ability to provide an explicit and compact empirical expression that could be useful for designers.

Table (5-8): Statistical performance of GEP and SPSS for testing data.

Model	R^2	RMSE	MAE
GEP	0.89	0.152	0.118
SPSS	0.84	0.171	0.128
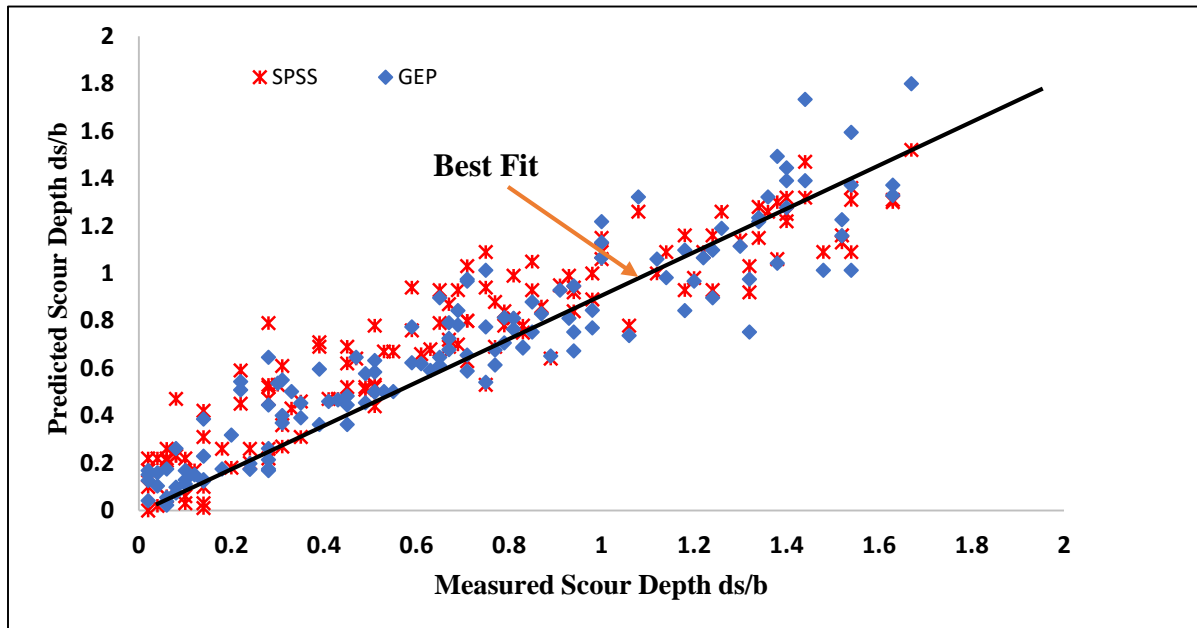
Figure (5-61): Comparison of GEP and SPSS in scour depth predicting (testing data)

Chapter Six

Conclusions and Recommendations

6.1 Introduction

  The problem of local scouring around different bridge piers shape under different conditions has been studied numerically. This has been done by Flow-3D to represent the development of local scour and the maximum depth of the scour hole which is the critical parameter in the design of bridge. This study deal with influence of main parameters on scour around different pier shapes to conclude optimum pier shape that give minimum depth of scour. The main findings of this study are presented in this chapter, followed by the recommendations of the future studies.

6.2 Conclusions

The conclusions of this study are:

1. The comparison of the result between the numerical model with Melville laboratory experiment model indicates that rate of error equal to 10 % on the maximum depth of scour hole. This observation shows a good validation between the numerical and experimental work, so the numerical simulation successfully reproduces the scour depth.

2. The depth of scour increases directly with increase in flow intensity, flow depth, pier width and angle of attack.

3. Maximum increase in scour depth around standard pier shape (circular pier) was is 74%, 96% and 21% for flow intensity, flow depth and pier width, respectively.

4. With the increase in angle of attack, the relative scour depth at an angle of 30° and 45° were about 1.5 times the angle of 0^0. The largest angle of attacks (θ) was equal to 45° yielded the largest pier scour depth. This

increase in scour value happens because of the increase in the effective frontal width of the pier. The minimum depth of scour occurred when the pier aligned to flow. Therefore, angle 0 is the optimum angle of attacks.

5. Maximum depth of scour is observed in rectangular pier while minimum depth of scour occurred around lenticular pier.

6. To ensure the optimum shape of pier gives minimum depth of scour while maintaining the cost, the results of the simulation performed on four pier shapes having the same volume and surface area showed that lenticular pier have less scour depth by 70% as compared with square. So, lenticular is considered an optimum hydraulic design of pier.

7. The location of maximum scour depth is always at the pier face and scour depth decreases towards the downstream side of the pier. One exception happens when the angle of attack changes and the maximum scour depth occurs at the side of the pier and moves towards the rear.

8. Downstream sediment deposition is the greatest for the pier width ratio b/B=0.2.

9. The scour depth formula obtained from GEP model performed better than SPSS model because it produces smaller values for RMSE and MAE and greater value for R^2. The formula helps to evaluate the maximum scour depth for similar conditions to those covered in this study.

10. According to sensitivity analysis, flow depth parameter has the most impact on scour depth prediction compared to other input parameters.

6.3 Recommendations

The following recommendations are proposed for further study:

1. Developing of new empirical formula is recommended, which includes the effects of sediment size, flume slope, uniform and non-uniform sediments on scour depth.

2. It is recommended to take different range of sediment size and study its influence on scour depth.

3. To be in a universal situation, it is recommended to take into consideration the live bed scour, i.e., the intensity of velocity greater than one.

4. Genetic algorithms optimization techniques are recommended to be used to find optimum pier shape that gives minimum depth of scour and minimum cost.

References

- Abdul-Nour, M. . (1990) "**Scouring depth around multiple**", M.Sc. Thesis , Department of Irrigation and Drainage , University of Baghdad.
- Abbas, H. A. (2017) "**An Experimental Study of Scour Resulting from the Plash of Free Water Jet in Stilling Basin Floor**", M.SC. Thesis to the College of Engineering/ University of Babylon.
- Al-Shukur, A.-H. K. and Hadi Obeid, Z. (2016) "**Experimental study of bridge pier shape to minimize local scour**", International Journal of Civil Engineering and Technology (IJCIET), 7(1), pp. 162–171.
- Alabi, P. D. (2006) "**Time development of local scour at a bridge pier fitted with a collar**", M.SC. Thesis.
- Ali, K. H. M., Karim, O. A., and O'Connor, B. A. (1997) "**Flow patterns around bridge piers and offshore structures**", Proceedings, Congress of the International Association of Hydraulic Research, IAHR, San Francisco, CA, USA, 225.
- Ali, K.H.M, and Karim, O. (2002). "Simulation of Flow around Piers", J. Hydraulic. Research, IAHR, 40(2), 161-174.
- Annandale, G. (1995) "**Erodibility**", Journal of Hydraulic Research, pp. 471–494.
- Ansari, S.A., Kothyari, U.C. and Ranga Raju, K. G. (2002)"**Influence of cohesion on scour around bridge piers**", Journal of Hydraulic Research, IAHR, pp. 40(6): 717-729.
- Ashtiani,A.B. and Kordkandi A., (2013) "**Flow field around single and tandem piers**", Flow Turbulence and Combustion, Vol. 90, Issue 3, pp 471–490.
- Bata, C , (1960), Ere/ija eke novesadskeg mastorskog stube **"scour around bridge piers"**, Inst. za Vodoprivedu. Jaroslav Cerni Beograd, Yugoslavia.
- Bozkus, Z. and Osman, Y. (2004) "**Effects of inclination of bridge piers on scouring depth**", Journal of Hydraulic Engineering, ASCE, p. 130(8): 827-832.
- Breusers, H.N.C. and Raudkivi, A. . (1991) "**Scouring, hydraulic structures design manual**", IAHR, A.A. Balkema, Rotterdam,.
- Breusers, Nicollet and Shen (1977) "**Local scour around cylindrical piers**", Journal of Hydraulic Research,IAHR, 15 (3): 211-252 .
- Bridge scour manual (2005) "**Drainage section**". State of Florida department of transportation. Office of design drainage section Tallahassee , Florida.
- Bridge scour manual (2013) " **Manual**", Department of Transport and Main Roads, State of Queensland.
- Carmo, J. S. A. do (2014) "**Experimental study on local scour around bridge piers in rivers**", https://www.researchgate.net/publication/232311062
- Chabert and Engeldinger. (1956) Etude des affouillements autour des piles de points "**Study of scour at bridge piers**", P. Bureau Central d'Etudes les Equipment d'Outre-Mer, Laboratoire National d'Hydraulique, France.
- Chang, H. H. and Wiley, J. (1988) "**Fluvial processes in river engineering**", John Wiley & Sons, 432 p.
- Chang, W.Y, Lai, J.S. and Yen, C.L., (1999), "**Simulation of scour depth evolution at pier nose**." International Water Resources Engineering Conference, August, Session BS-05, Water Resources Publications, LLC, Highlands Ranch, CO.

- Chen, C. J. et al. (2002) "**Finite analytic method in flows and heat transfer**". American Society of Mechanical Engineers Digital Collection.
- Cheremisinoff, N.P. and Cheng, S. L. (1987) "**Hydraulic mechanics 2**", Civil Engineering Practice, Technomic PublishedCompany, , Lancaster, Pennsylvania, U.S.A. 780 p.
- Chiew, Y. M. (1984). "**Local scour at bridge piers**", PhD Thesis. University of Auckland, Auckland, New Zealand.
- Chiew, Y. (1992) "**Scour protection at bridge piers**", Journal of Hydraulic Engineering, 118(9), pp. 1260–1269. doi: 10.1061/(asce)0733-9429(1992)118:9(1260).
- Chiew, Y. M. and Melville, B. M., (1987), "**Local scour around bridge piers**", Journal of Hydraulic Research, IAHR, Vol. 25, No. 1, pp.15- 26.
- Chitale, S. V., (I960), **"Discussion on Laursen (1960)"**; Trans. ASCE, 127. pp. 191/196.
- Colfman, N. L., (1971), **"Analyzing laboratory measurements of scour at cylindrical piers in sand beds"**. Proc. 14th IAHR Congress, Paris, 3, pp. 307/313.
- Das, S., Das, R. and Mazumdar, A. (2012) "**Scour hole characteristics around a vertical pier under clear water scour conditions**",.
- Date, A. W. (2005) "**introduction to computational fluid dynamics** ", Cambridge University Press.
- Drikakis, D. (2003) "**Advances in turbulent flow computations using high-resolution methods**", Progress in Aerospace Sciences, 39(6–7), pp. 405–424. doi: 10.1016/S0376-0421(03)00075-7.
- E. V. RichardsonI Ph.D. and J. R. Richardson Ph.D. (2001) "**Bridge scour**" , Journal civil engineering deparment Colorado State University Ff. Collins ,Colorao.
- Ettema, Melville and Barkdole (1998) "**Scale effect in pier- scour experiments**", Journal of hydraulic engineering 124(Vi), NO. (6) pp. 639–642.
- Ettema, R. (1980) "**Scour at bridge piers**", PhD Thesis, Auckland University, Auckland, New Zealand.
- Fanzetti, S., Larcan, E. and M. (1982) "**Influence of tests duration on the evaluation of ultimate scour around circular piers** ", International Conference on the Hydraulic Modelling of Civil Engineering Structures, Organised and Sponsored by BHRA Fluid Engineering, University of Warwick, Coventry, England, September 22- 24, 16 p.
- Ferreira, C. (2001) "**Gene Expression Programming : A new adaptive algorithm for solving problems**", Departamento de Ciências Agrárias Universidade dos Açores 9701-851 Terra-Chã Angra do Heroísmo, Portugal, Vol. 13, issue 2: 87-129, 2001.
- Ferreira, C. (2002) "**Gene Expression Programming in problem solving**", Soft Computing and Industry, Springer-Verlag London, pp. 635–653. doi: 10.1007/978-1-4471-0123-9_54.
- Ferreira, C. (2006) "**Gene Expression Programming studies in computational intelligence** ", Springer, Studies in Computational Intelligence, Volume 21.
- Ferziger, J. H. and Perić, M. (2002) **"Solution of the Navier-Stokes equations in computational methods for fluid dynamics**". Springer, pp. 157–216.
- FHWA-HIF (2012) "**Evaluating scour at bridges fifth edition**", U.S. Department of Transportation. Federal Highway Administration , Hydraulic Engineering Circular No. 18.
- Flow -3D manual (2014) "**Flow-3D user manual**" version 11, Flow Science Santa Fe, NM.
- Gacek, J. D. (2007) "**Numerical simulation of flow through a spillway and diversion structure**", M.SC. Thesis.

- Ghalati, R. M. (2012) "**Effect of foundation geometry on short abutment scour**", PhD Thesis, Universiti Sains Malaysia.
- Ghasemi, M. (2017) "**The scour bridge simulation around a cylindrical pier using Flow-3D**", Journal of Hydrosciences and Environment, ISSN: 2345-5608.
- Graf, W. H. . (1996) "**Local scour around piers.**" Annual Report, E. P. F. d. Lausanne, ed., Laboratoire de Recherches Hydrauliques, Lausanne, Switzerland, B.33.1-B.33.8.
- Günala M. and Ismael A. (2016) "**Experimental investigation of turbulent flow field at downstream-facing experimental investigation of turbulent flow field at downstream-facing round nosed pier**". doi: 10.12693/APhysPolA.130.126.
- Hamidi, A. and Siadatmousavi, S. M. (2017) "**Numerical simulation of scour and flow field for different arrangements of two piers using SSIIM model**", Ain Shams Engineering Journal. Ain Shams University. doi: 10.1016/j.asej.2017.03.012.
- Hamill, (2004) "**Bridge hydraulics***"*, School of Civil and Structural Engineering University of Plymouth . This edition published in the Taylor & Francis e-Library, vol. 127, no.7.
- Hassan, W. H. (2017) "**Optimal design of sewer networks using genetic algorithm**",. M.SC thesis university of Kerbala civil enginnering.
- Heidarpour M., Khodarahmi, Z. and Mousavi, S.F., (2003), "**Control and reduction of local scour at bridge pier groups using slot**". Proceedings, 30th iahr Congress, Thessaloniki, Greece, August 24 - 29.
- Hirshfield, F. (2015) "**The impact of ice conditions on local scour around bridge**", PhD Thesis, university of Northern British Columbia.
- Hirt, C. W. and Sicilian, J. M. (1985) "**A porosity technique for the definition of obstacles in rectangular cell meshes**", in International Conference on Numerical Ship Hydrodynamics, 4th.
- Hirt, C.W, Nichols, B.D., 1981, "**Volume of fluid (VOF) methods for dynamics of free boundaries**" Journal of Comput. Phys. 39: 201–225.
- Hoffmans, G.J.C.M. and Verheij, H. J. (1997) "**Scour manual**",. Balkema, Rotterdam, Netherlands, p. 205 p.
- Hosny, M. M. (1995) "**Experimental study of local scour around circular bridge piers in cohesive soils**", Colorado State University, Fort Collins.
- Holland, J. H. （1975) "**Adaptation in natural and artificial system"**, University of Michigan Press, Ann Arbor, Mich.
- Jahangirzadeh, A. et al. (2014) "**Experimental and numerical investigation of the effect of different shapes of collars on the reduction of scour around a single bridge pier**", PLoS ONE, 9(6). doi: 10.1371/journal.pone.0098592.
- Jain, S. C. (1981), **"Maximum clear-water scour around cylindrical piers".** Journal of Hydraulic Engineering, ASCE, 107 (5), 611-625.
- Johari, A., Habibagahi, G., and Ghahramani, A. （2006) "**Prediction of soil-water characteristic curve using genetic programming**" J. Geotech. Geoenviron. Eng., 132（5), 661–665.
- Karim, O. A. (2015) "**Simulation of flow around piers Simulation**" écoulements autour de piles de ponts', (March 2002). doi: 10.1080/00221680209499859.
- Khwairakpam, Ray, Das, S., Das, R. and Mazumdar, A. (2012) "**Scour hole**

characteristics around a vertical pier under clear water scour conditions", ARPN Journal of Engineering and Applied Sciences, Vol. 7, No. 6, ISSN 1819-6608.

- Khan, M. et al. (2012) "**Bridge pier scour prediction by gene expression programming**" Journal of Hydroinformatics, doi: 10.2166/hydro.2011.008.
- Khsaf, S. I. (2010) "**A study of scour around Al-Kufa bridge piers**", Kufa Engineering Journal.Vol.1No.1,2010, University of Kufa / College Engineering / Civil Department.
- Lauchlan, C. S. . (1999) "**Pier scour countermeasures**", PhD Thesis, Department of Civil and Resources Engineering, University of Auckland, Auckland, New Zealand.
- Lauchlan, C. S. and Melville, B. W. (2001) "**Riprap protection at bridge piers**", Journal of Hydraulic Engineering. American Society of Civil Engineers, 127(5), pp. 412–418.
- Laursen, E.M. and Toch, A. (1956) "**Scour around bridge piers and abutments**", Iowa Highway Research Board, Bulletin , Bureau of Public Roads, Iowa. Lim,.
- Laursen, E. M. and Toch, A. (1956a) "**Scour around bridge piers and abutments**". Iowa Highway Research Board Ames, IA.
- Laursen, E. M. and Toch, A. (1956b) "**Scour around bridge piers and abutments** ", Iowa Highway Research Board Ames, IA. NO.(4).
- Lee, S. O., and Sturm, T. W. (2009) "**Effect of sediment size on physical modeling of bridge pier scour**", Journal of Hydraulic Engineering, ASCE, 135 (10):
- Lee, S. O. (2006) "**Phihsical modeling of local scour around complex bridge piers**", PhD Thesis, School of Civil and Environmental Engineering.
- Liu, S., Yang, Y. and Wu, X. (2017) "**Simulations of local scour around a cylindrical bridge pier and a semicircular abutment using unsteady k-ε model combined with σ - grid** ", pp. 598–614. doi: 10.2174/1874149501711010598.
- Little, P. R., (1977) "**Scour at bridge pier and abutments**", M.SC Thesis, University of Cape Town
- Maatooq, J. . (1999) "**Evaluation analysis and new concepts of scour process around bridge pier**", Ph.D. Thesis, The university of technology.
- Manual (2013) "**Bridge Scour Manual**", State of Queensland (Department of Transport and Main Roads).
- Mastbergen, D. R. and Van Den Berg, J. H. (2003) "**Breaching in fine sands and the generation of sustained turbidity currents in submarine canyons**", Sedimentology, 50(4), pp. 625–637. doi: 10.1046/j.1365-3091.2003.00554.x.
- Melville, B. (2008) "**The physics of local scour**", Fourth International Conference on Scour and Erosion (1), pp. 28–40.
- Melville and Coleman, S. E. (2000) "**Bridge scour**", University of Auckland, Auckland, New Zealand, Water Resources Publications, LLC, Colorado, U.S.A.
- Melville, B. W. (1975) "**Local scour at bridge sites**", University of Auckland, New Zealand, phd. Thesis, Dept. of Civil eng., Rep. No. 117.
- Melville, B. W. (1997) "**Pier and abutment scour: integrated approach**.", Journal of Hydraulic Engineering, ASCE, (123(2): 125-136).
- Melville, B. W. and Raudkivi, A. J. (1977) "**Flow characteristics in local scour at bridge piers**", Journal of Hydraulic Research. Taylor & Francis Group, 15(4), pp. 373–380.
- Melville, B. w., and Sutherland, A. I. (1988). "**Design method for local scour at bridge piers**." Journal of Hydraulic Engineering, ASCE, Vol.114, No.10, 1210-1226.
- Melville, B.W., Chiew Y.M., (1999) "**Time scale for local scour at bridge piers**", Journal

of Hydraulic Engineering, ASCE, 125(1): 59-65

- Mendoza-Cabrales, C. (1993) "**Computation of flow past a cylinder mounted on a flat plate**", Proceedings - National Conference on Hydraulic Engineering, Venice, Italy.
- Meyer-Peter, E. and Müller, R. (1948) "**Formulas for bed-load transport**", Proceedings of the 2nd Meeting of the International Association for Hydraulic Structures Research, 39–64.
- Mia, M., Nago, H., (2003), "**Design Method of Time-Dependent Local Scour at Circular Bridge Pier**". Journal of Hydraulic Engineering, 129 (6), 420-427.
- Mohamed, T. (2005) "**Validation of some bridge pier scour formulae using field and laboratory data**", American Journal of Environmental Sciences, 1(2), 119-125, pp.119-125.
- Muzzammil, M., Gangadharaiah, T. and Gupta, A. K. (2004) "**An experimental investigation of a horseshoe vortex induced by a bridge pier**" ,in Proceedings of the institution of civil engineers-water management. Thomas Telford Ltd, pp. 109–119.
- Neill, C.R. (1964), **"River-bed scour—a review for engineers"**. Canadian Good Roads Association Technical Publication No. 23, Ottawa, Canada.
- Neill (1973) "**Guide to bridge hydraulics** ", Project Committee on Bridge Hydraulics, Roads and Transportation Association of Canada. University of Toronto Press, Toronto and Buffalo, p. 191.
- Nimnim, H. T. and Al-khaqani, M. A. J. (2017) "**Evaluation of local scour development around prismatic and non-prismitic bridge**", 8(2), pp. 88–104.
- Obeid, Z. H. (2016) "**Effect of Bridge Pier Shape on Depth and Configuration of Local Scour**", M.SC Thesis to the College of Engineering/ University of Babylon, pp. 5–34.
- Obeid, Z. H. (2016) "**3D numerical simulation of local scouring and velocity distributions around bridge piers with different shapes**", A Peer Reviewed International Journal of Asian Academic Research Associates, 20(16), p. 2801. doi: 10.1186/1757-7241-20-67.
- Olsen, N.R.B., and Melaaen, M.C. (1993) "**Three-dimensional calculation of scour around cylinders**", Journal of Hydraulic Engineering, 119(9), 1048-1054.
- Potter, M.C., Wiggert, D.C., Hondzo, M, Shih, T.I.-P. (2002) "**Mechanics of Fluids**". Brooks/Cole, Pacific Grove, CA.
- Raleigh, A. C. (2015) "**How to mitigate the effects of scour on bridge piers through the use of combined countermeasures**" ,University of Southern Queensland Faculty of Engineering and Surveying
- Raudkivi, A.J. and Ettema, R. (1977) "**Effect of sediment gradation on clear-water scour and measurement of scour depth** ", Journal of the Hydraulics Division, ASCE.
- Raudkivi, A. and Ettema, R., (1983), "**Clear Water Scour at Cylindrical Piers**", Journal of Hydraulic Engineering, 109(3), 338–350.
- Richardson, E. V., and, Davis, S. R. (2001) "**Evaluating scour at bridges 4th ed**", Federal Highway Administration Hydraulic Engineering Circular.
- Richardson, J. E. and Panchang, V. G. (1998) "**Three-Dimensional simulation of scour-inducing flow at bridge piers**", Journal of Hydraulic Engineering, 124(5), pp. 530–540. doi: 10.1061/(asce)0733-9429(1998)124:5(530).

- Salaheldin, T. M., Imran, J., and Chaudhry, M. H., (2004), "**Numerical modeling of three dimensional flow field around circular piers**", Journal of Hydraulic Engineering, 130(2), 91-100.
- Shen, H. W., Schneider, V. R. and Karaki, S. (1969) "**Local scour around bridge piers**", Journal of the Hydraulics Division.
- Sheppard, D.M., Odeh, M. and Glasser, T. (2004) "**Large scale clear-water local scour experiments** ", Journal of Hydraulic Engineering, ASCE, 130(10): 9.
- Soulsby, , R. L. and Whitehouse, R. J. S. W., (1997) "**Threshold of sediment motion in Coastal Environments**". Proc. Combined Australian Coastal Engineering and Port Conference, EA, pp. 149-154.
- Sumer, B. M., and Fredsoe, J. (2002) "**Hydrodynamics around cylindrical structures**", World Scientific, Singapore; River Edge, N.J.
- Tison, L.J. (1940) "**scour around bridge piers in river**". Ann. Des Travaux Publics de Beligique, 41 (6): 813-871.
- Tison, L.J. (1961) "**Local scour in rivers**". J. Geoph. Res., 66(12): 4427-4232.
- Vasquez, J. and Walsh, B. (2009) "**CFD simulation of local scour in complex piers under tidal flow**", Proceedings of the thirty-third IAHR Congress: Water Engineering for a Sustainable Environment, (604), pp. 913–920. Available at: http://flow3d2.propagation.net/pdfs/tp/wat_env_tp/cfd-simulation-of-local-scour-in-complex-piers-under-tidal-flow-23-09.pdf.
- Van Rijn, B. L. C. (1984) "**Sediment transport, part 1: bed load transport**", Journal of Hydraulic Engineering, 110(10), 1431-1456.
- Vincent, M. S., Ross, M. A., and Ross, B. E. (1993) "**Tidal inlet bridge scour assessment model**", Transportation Research Record, (1420).
- Williams (2009) "**Local scour viewed**" .
- Xiong, W. et al. (2016) "**Reliable bridge scour simulation using Eulerian Two-Phase flow theory**",Journal Comput. Civil. Engineering, m(5), pp. 1–11. doi: 10.1061/(ASCE)CP.1943-5487.0000570.
- Yakhot and Orszag (1986) "**Renormalization group analysis of turbulence, basic theory**", Journal of Scientific Computing, pp. 3–51.
- Yang,Q., (2005) "**Numerical Investigations of Scale Effects on Local Scour Around a Bridge Pier**", M.SC Thesis, Florida State University, FAMU-FSU College of Engineering.
- Zafer Bozkus, M.ASCE, 1 and Osman Yildiz (2004) "**Effects of inclination of bridge piers on scouring depth**", Journal of Hydraulic Engineering, 130(August), pp. 827–832. doi: 10.1061/(ASCE)0733-9429(2004)130:8(827).
- Zarrati, A.M., Gholami, H. and Mashahir, M.B, (2004), "**Application of collar to control scouring around rectangular bridge piers**", Journal of Hydraulic Research, IAHR,Vol. 42, No.1, pp.97-103

Appendix A- Results of Scour Depth

A.1- Table of results of scour depth

Table (A-1): Results of scour depth

Run no.	V/V$_C$	y/b	b/B	ks	Kθ	ds/b	shape
R1	0.55	2.95	0.11	1.00	1.00	0.28	circular
R2	0.55	2.95	0.11	0.84	1.00	0.16	elliptic
R3	0.55	2.95	0.11	1.16	1.00	0.28	square
R4	0.55	2.95	0.11	1.26	1.00	0.31	rectangle
R5	0.55	2.95	0.11	0.71	1.00	0.08	lenticular
R6	0.55	2.95	0.11	0.81	1.00	0.12	ogival
R7	0.55	2.95	0.11	0.87	1.00	0.14	oblong
R8	0.55	2.95	0.11	0.94	1.00	0.14	hexagonal
R9	0.55	2.95	0.11	1.03	1.00	0.22	octagonal
R10	0.76	2.95	0.11	1.00	1.00	0.71	circular
R11	0.76	2.95	0.11	0.84	1.00	0.51	elliptic
R12	0.76	2.95	0.11	1.16	1.00	0.71	square
R13	0.76	2.95	0.11	1.26	1.00	0.77	rectangle
R14	0.76	2.95	0.11	0.71	1.00	0.43	lenticular
R15	0.76	2.95	0.11	0.81	1.00	0.49	ogival
R16	0.76	2.95	0.11	0.87	1.00	0.53	oblong
R17	0.76	2.95	0.11	0.94	1.00	0.57	hexagonal
R18	0.76	2.95	0.11	1.03	1.00	0.63	octagonal
R19	1.00	2.95	0.11	1.00	1.00	1.08	circular
R20	1.00	2.95	0.11	0.84	1.00	1.00	elliptic
R21	1.00	2.95	0.11	1.16	1.00	1.18	square
R22	1.00	2.95	0.11	1.26	1.00	1.28	rectangle
R23	1.00	2.95	0.11	0.71	1.00	0.79	lenticular
R24	1.00	2.95	0.11	0.81	1.00	0.93	ogival
R25	1.00	2.95	0.11	0.87	1.00	0.93	oblong
R26	1.00	2.95	0.11	0.94	1.00	0.98	hexagonal
R27	1.00	2.95	0.11	1.03	1.00	1.08	octagonal
R28	0.55	0.98	0.11	1.00	1.00	0.31	circular
R29	0.55	0.98	0.11	0.84	1.00	0.28	elliptic
R30	0.55	0.98	0.11	1.16	1.00	0.35	square

Run no.	V/V$_C$	y/b	b/B	ks	kθ	ds/b	shape
R31	0.55	0.98	0.11	1.26	1.00	0.39	rectangle
R32	0.55	0.98	0.11	0.71	1.00	0.20	lenticular
R33	0.55	0.98	0.11	0.81	1.00	0.24	ogival
R34	0.55	0.98	0.11	0.87	1.00	0.33	oblong
R35	0.55	0.98	0.11	0.94	1.00	0.20	hexagonal
R36	0.55	0.98	0.11	1.03	1.00	0.31	octagonal
R37	0.76	0.98	0.11	1.00	1.00	0.49	circular
R38	0.76	0.98	0.11	0.84	1.00	0.41	elliptic
R39	0.76	0.98	0.11	1.16	1.00	0.53	square
R40	0.76	0.98	0.11	1.26	1.00	0.59	rectangle
R41	0.76	0.98	0.11	0.71	1.00	0.31	lenticular
R42	0.76	0.98	0.11	0.81	1.00	0.35	ogival
R43	0.76	0.98	0.11	0.87	1.00	0.43	oblong
R44	0.76	0.98	0.11	0.94	1.00	0.47	hexagonal
R45	0.76	0.98	0.11	1.03	1.00	0.51	octagonal
R46	1.00	0.98	0.11	1.00	1.00	0.79	circular
R47	1.00	0.98	0.11	0.84	1.00	0.67	elliptic
R48	1.00	0.98	0.11	1.16	1.00	0.83	square
R49	1.00	0.98	0.11	1.26	1.00	0.89	rectangle
R50	1.00	0.98	0.11	0.71	1.00	0.59	lenticular
R51	1.00	0.98	0.11	0.81	1.00	0.67	ogival
R52	1.00	0.98	0.11	0.87	1.00	0.65	oblong
R53	1.00	0.98	0.11	0.94	1.00	0.73	hexagonal
R54	1.00	0.98	0.11	1.03	1.00	0.81	octagonal
R55	0.55	0.20	0.11	1.00	1.00	0.01	circular
R56	0.55	0.20	0.11	0.84	1.00	0.01	elliptic
R57	0.55	0.20	0.11	1.16	1.00	0.02	square
R58	0.55	0.20	0.11	1.26	1.00	0.02	rectangle
R59	0.55	0.20	0.11	0.71	1.00	0.00	lenticular
R60	0.55	0.20	0.11	0.81	1.00	0.01	ogival
R61	0.55	0.20	0.11	0.87	1.00	0.01	oblong
R62	0.55	0.20	0.11	0.94	1.00	0.02	hexagonal
R63	0.55	0.20	0.11	1.03	1.00	0.02	octagonal
R64	0.76	0.20	0.11	1.00	1.00	0.02	circular
R65	0.76	0.20	0.11	0.84	1.00	0.02	elliptic
R66	0.76	0.20	0.11	1.16	1.00	0.04	square
R67	0.76	0.20	0.11	1.26	1.00	0.06	Rectangle

Run no.	V/V$_C$	y/b	b/B	ks	kθ	ds/b	shape
R68	0.76	0.20	0.11	0.71	1.00	0.00	lenticular
R69	0.76	0.20	0.11	0.81	1.00	0.03	ogival
R70	0.76	0.20	0.11	0.87	1.00	0.02	oblong
R71	0.76	0.20	0.11	0.94	1.00	0.04	hexagonal
R72	0.76	0.20	0.11	1.03	1.00	0.04	octagonal
R73	1.00	0.20	0.11	1.00	1.00	0.04	circular
R74	1.00	0.20	0.11	0.84	1.00	0.04	elliptic
R75	1.00	0.20	0.11	1.16	1.00	0.08	square
R76	1.00	0.20	0.11	1.26	1.00	0.10	rectangle
R77	1.00	0.20	0.11	0.71	1.00	0.04	lenticular
R78	1.00	0.20	0.11	0.81	1.00	0.06	ogival
R79	1.00	0.20	0.11	0.87	1.00	0.04	oblong
R80	1.00	0.20	0.11	0.94	1.00	0.06	hexagonal
R81	1.00	0.20	0.11	1.03	1.00	0.06	octagonal
R82	0.55	2.95	0.15	1.00	1.00	0.22	circular
R83	0.55	2.95	0.15	0.84	1.00	0.22	elliptic
R84	0.55	2.95	0.15	1.16	1.00	0.31	square
R85	0.55	2.95	0.15	1.26	1.00	0.35	rectangle
R86	0.55	2.95	0.15	0.71	1.00	0.22	lenticular
R87	0.55	2.95	0.15	0.81	1.00	0.33	ogival
R88	0.55	2.95	0.15	0.87	1.00	0.24	oblong
R89	0.55	2.95	0.15	0.94	1.00	0.28	hexagonal
R90	0.55	2.95	0.15	1.03	1.00	0.31	octagonal
R91	0.76	2.95	0.15	1.00	1.00	0.65	circular
R92	0.76	2.95	0.15	0.84	1.00	0.69	elliptic
R93	0.76	2.95	0.15	1.16	1.00	0.81	square
R94	0.76	2.95	0.15	1.26	1.00	0.89	rectangle
R95	0.76	2.95	0.15	0.71	1.00	0.53	lenticular
R96	0.76	2.95	0.15	0.81	1.00	0.83	ogival
R97	0.76	2.95	0.15	0.87	1.00	0.67	oblong
R98	0.76	2.95	0.15	0.94	1.00	0.79	hexagonal
R99	0.76	2.95	0.15	1.03	1.00	0.85	octagonal
R100	1.00	2.95	0.15	1.00	1.00	1.00	circular
R101	1.00	2.95	0.15	0.84	1.00	1.06	elliptic
R102	1.00	2.95	0.15	1.16	1.00	1.20	square
R103	1.00	2.95	0.15	1.26	1.00	1.34	rectangle
R104	1.00	2.95	0.15	0.71	1.00	0.87	Lenticular

Run no.	V/V$_C$	y/b	b/B	ks	kθ	ds/b	shape
R105	1.00	2.95	0.15	0.81	1.00	1.24	ogival
R106	1.00	2.95	0.15	0.87	1.00	1.02	oblong
R107	1.00	2.95	0.15	0.94	1.00	1.16	hexagonal
R108	1.00	2.95	0.15	1.03	1.00	1.18	octagonal
R109	0.55	0.98	0.15	1.00	1.00	0.30	circular
R110	0.55	0.98	0.15	0.84	1.00	0.35	elliptic
R111	0.55	0.98	0.15	1.16	1.00	0.49	square
R112	0.55	0.98	0.15	1.26	1.00	0.55	rectangle
R113	0.55	0.98	0.15	0.71	1.00	0.22	lenticular
R114	0.55	0.98	0.15	0.81	1.00	0.45	ogival
R115	0.55	0.98	0.15	0.87	1.00	0.35	oblong
R116	0.55	0.98	0.15	0.94	1.00	0.47	hexagonal
R117	0.55	0.98	0.15	1.03	1.00	0.51	octagonal
R118	0.76	0.98	0.15	1.00	1.00	0.59	circular
R119	0.76	0.98	0.15	0.84	1.00	0.61	elliptic
R120	0.76	0.98	0.15	1.16	1.00	0.67	square
R121	0.76	0.98	0.15	1.26	1.00	0.71	rectangle
R122	0.76	0.98	0.15	0.71	1.00	0.51	lenticular
R123	0.76	0.98	0.15	0.81	1.00	0.65	ogival
R124	0.76	0.98	0.15	0.87	1.00	0.61	oblong
R125	0.76	0.98	0.15	0.94	1.00	0.65	hexagonal
R125	0.76	0.98	0.15	1.03	1.00	0.67	octagonal
R127	1.00	0.98	0.15	1.00	1.00	0.71	circular
R128	1.00	0.98	0.15	0.84	1.00	0.77	elliptic
R129	1.00	0.98	0.15	1.16	1.00	0.91	square
R130	1.00	0.98	0.15	1.26	1.00	0.98	rectangle
R131	1.00	0.98	0.15	0.71	1.00	0.53	lenticular
R132	1.00	0.98	0.15	0.81	1.00	0.85	ogival
R133	1.00	0.98	0.15	0.87	1.00	0.73	oblong
R134	1.00	0.98	0.15	0.94	1.00	0.93	hexagonal
R135	1.00	0.98	0.15	1.03	1.00	0.94	octagonal
R136	0.55	0.20	0.15	1.00	1.00	0.01	circular
R137	0.55	0.20	0.15	0.84	1.00	0.01	elliptic
R138	0.55	0.20	0.15	1.16	1.00	0.02	square
R139	0.55	0.20	0.15	1.26	1.00	0.02	rectangle
R140	0.55	0.20	0.15	0.71	1.00	0.00	lenticular
R141	0.55	0.20	0.15	0.81	1.00	0.01	Ogival

Run no.	V/V$_C$	y/b	b/B	ks	kθ	ds/b	shape
R142	0.55	0.20	0.15	0.87	1.00	0.01	oblong
R143	0.55	0.20	0.15	0.94	1.00	0.01	hexagonal
R144	0.55	0.20	0.15	1.03	1.00	0.01	octagonal
R145	0.76	0.20	0.15	1.00	1.00	0.02	circular
R146	0.76	0.20	0.15	0.84	1.00	0.02	elliptic
R147	0.76	0.20	0.15	1.16	1.00	0.04	square
R148	0.76	0.20	0.15	1.26	1.00	0.04	rectangle
R149	0.76	0.20	0.15	0.71	1.00	0.01	lenticular
R150	0.76	0.20	0.15	0.81	1.00	0.04	ogival
R151	0.76	0.20	0.15	0.87	1.00	0.02	oblong
R152	0.76	0.20	0.15	0.94	1.00	0.04	hexagonal
R153	0.76	0.20	0.15	1.03	1.00	0.04	octagonal
R154	1.00	0.20	0.15	1.00	1.00	0.08	circular
R155	1.00	0.20	0.15	0.84	1.00	0.08	elliptic
R156	1.00	0.20	0.15	1.16	1.00	0.10	square
R157	1.00	0.20	0.15	1.26	1.00	0.10	rectangle
R158	1.00	0.20	0.15	0.71	1.00	0.04	lenticular
R159	1.00	0.20	0.15	0.81	1.00	0.06	ogival
R160	1.00	0.20	0.15	0.87	1.00	0.06	oblong
R161	1.00	0.20	0.15	0.94	1.00	0.08	hexagonal
R162	1.00	0.20	0.15	1.03	1.00	0.10	octagonal
R163	0.55	2.95	0.20	1.00	1.00	0.75	circular
R164	0.55	2.95	0.20	0.84	1.00	0.77	elliptic
R165	0.55	2.95	0.20	1.16	1.00	0.85	square
R166	0.55	2.95	0.20	1.26	1.00	0.94	rectangle
R167	0.55	2.95	0.20	0.71	1.00	0.31	lenticular
R168	0.55	2.95	0.20	0.81	1.00	0.89	ogival
R169	0.55	2.95	0.20	0.87	1.00	0.75	oblong
R170	0.55	2.95	0.20	0.94	1.00	0.83	hexagonal
R171	0.55	2.95	0.20	1.03	1.00	0.77	octagonal
R172	0.76	2.95	0.20	1.00	1.00	1.04	circular
R173	0.76	2.95	0.20	0.84	1.00	1.02	elliptic
R174	0.76	2.95	0.20	1.16	1.00	1.20	square
R175	0.76	2.95	0.20	1.26	1.00	1.26	rectangle
R176	0.76	2.95	0.20	0.71	1.00	0.71	lenticular
R177	0.76	2.95	0.20	0.81	1.00	1.22	ogival
R178	0.76	2.95	0.20	0.87	1.00	1.08	Oblong

Run no.	V/V$_C$	y/b	b/B	ks	kθ	ds/b	shape
R179	0.76	2.95	0.20	0.94	1.00	1.12	hexagonal
R180	0.76	2.95	0.20	1.03	1.00	1.14	octagonal
R181	1.00	2.95	0.20	1.00	1.00	1.36	circular
R182	1.00	2.95	0.20	0.84	1.00	1.26	elliptic
R183	1.00	2.95	0.20	1.16	1.00	1.42	square
R184	1.00	2.95	0.20	1.26	1.00	1.56	rectangle
R185	1.00	2.95	0.20	0.71	1.00	1.10	lenticular
R186	1.00	2.95	0.20	0.81	1.00	1.38	ogival
R187	1.00	2.95	0.20	0.87	1.00	1.34	oblong
R188	1.00	2.95	0.20	0.94	1.00	1.40	hexagonal
R189	1.00	2.95	0.20	1.03	1.00	1.38	octagonal
R190	0.55	0.98	0.20	1.00	1.00	0.47	circular
R191	0.55	0.98	0.20	0.84	1.00	0.51	elliptic
R192	0.55	0.98	0.20	1.16	1.00	0.69	square
R193	0.55	0.98	0.20	1.26	1.00	0.75	rectangle
R194	0.55	0.98	0.20	0.71	1.00	0.41	lenticular
R195	0.55	0.98	0.20	0.81	1.00	0.71	ogival
R196	0.55	0.98	0.20	0.87	1.00	0.53	oblong
R197	0.55	0.98	0.20	0.94	1.00	0.73	hexagonal
R198	0.55	0.98	0.20	1.03	1.00	0.75	octagonal
R199	0.76	0.98	0.20	1.00	1.00	0.71	circular
R200	0.76	0.98	0.20	0.84	1.00	0.85	elliptic
R201	0.76	0.98	0.20	1.16	1.00	0.94	square
R202	0.76	0.98	0.20	1.26	1.00	0.98	rectangle
R203	0.76	0.98	0.20	0.71	1.00	0.81	lenticular
R204	0.76	0.98	0.20	0.81	1.00	0.94	ogival
R205	0.76	0.98	0.20	0.87	1.00	0.87	oblong
R206	0.76	0.98	0.20	0.94	1.00	0.96	hexagonal
R207	0.76	0.98	0.20	1.03	1.00	1.00	octagonal
R208	1.00	0.98	0.20	1.00	1.00	1.34	circular
R209	1.00	0.98	0.20	0.84	1.00	1.36	elliptic
R210	1.00	0.98	0.20	1.16	1.00	1.46	square
R211	1.00	0.98	0.20	1.26	1.00	1.54	rectangle
R212	1.00	0.98	0.20	0.71	1.00	0.89	lenticular
R213	1.00	0.98	0.20	0.81	1.00	1.38	ogival
R214	1.00	0.98	0.20	0.87	1.00	1.34	oblong
R215	1.00	0.98	0.20	0.94	1.00	1.50	Hexagonal

Run no.	V/V$_C$	y/b	b/B	ks	kθ	ds/b	shape
R216	1.00	0.98	0.20	1.03	1.00	1.52	octagonal
R217	0.55	0.20	0.20	1.00	1.00	0.02	circular
R218	0.55	0.20	0.20	0.84	1.00	0.02	elliptic
R219	0.55	0.20	0.20	1.16	1.00	0.02	square
R220	0.55	0.20	0.20	1.26	1.00	0.04	rectangle
R221	0.55	0.20	0.20	0.71	1.00	0.01	lenticular
R222	0.55	0.20	0.20	0.81	1.00	0.02	ogival
R223	0.55	0.20	0.20	0.87	1.00	0.02	oblong
R224	0.55	0.20	0.20	0.94	1.00	0.02	hexagonal
R225	0.55	0.20	0.20	1.03	1.00	0.04	octagonal
R226	0.76	0.20	0.20	1.00	1.00	0.04	circular
R227	0.76	0.20	0.20	0.84	1.00	0.06	elliptic
R228	0.76	0.20	0.20	1.16	1.00	0.10	square
R229	0.76	0.20	0.20	1.26	1.00	0.12	rectangle
R230	0.76	0.20	0.20	0.71	1.00	0.02	lenticular
R231	0.76	0.20	0.20	0.81	1.00	0.10	ogival
R232	0.76	0.20	0.20	0.87	1.00	0.06	oblong
R233	0.76	0.20	0.20	0.94	1.00	0.08	hexagonal
R234	0.76	0.20	0.20	1.03	1.00	0.10	octagonal
R235	1.00	0.20	0.20	1.00	1.00	0.08	circular
R236	1.00	0.20	0.20	0.84	1.00	0.10	elliptic
R237	1.00	0.20	0.20	1.16	1.00	0.14	square
R238	1.00	0.20	0.20	1.26	1.00	0.16	rectangle
R239	1.00	0.20	0.20	0.71	1.00	0.08	lenticular
R240	1.00	0.20	0.20	0.81	1.00	0.12	ogival
R241	1.00	0.20	0.20	0.87	1.00	0.08	oblong
R242	1.00	0.20	0.20	0.94	1.00	0.14	hexagonal
R243	1.00	0.20	0.20	1.03	1.00	0.14	octagonal
R244	0.55	2.95	0.11	1.00	1.25	0.28	circular
R245	0.55	2.95	0.11	1.00	1.63	0.53	elliptic
R246	0.55	2.95	0.11	1.00	1.25	0.45	square
R247	0.55	2.95	0.11	1.00	1.63	0.49	rectangle
R248	0.55	2.95	0.11	1.00	1.63	0.41	lenticular
R249	0.55	2.95	0.11	1.00	1.63	0.47	ogival
R250	0.55	2.95	0.11	1.00	1.63	0.61	oblong
R251	0.55	2.95	0.11	1.00	1.63	0.51	hexagonal
R252	0.55	2.95	0.11	1.00	1.63	0.55	Octagonal

Run no.	V/V_C	y/b	b/B	ks	kθ	ds/b	shape
R253	0.76	2.95	0.11	1.00	1.25	0.61	circular
R254	0.76	2.95	0.11	1.00	1.63	0.63	elliptic
R255	0.76	2.95	0.11	1.00	1.25	0.96	square
R256	0.76	2.95	0.11	1.00	1.63	0.94	rectangle
R257	0.76	2.95	0.11	1.00	1.63	0.71	lenticular
R258	0.76	2.95	0.11	1.00	1.63	0.89	ogival
R259	0.76	2.95	0.11	1.00	1.63	0.67	oblong
R260	0.76	2.95	0.11	1.00	1.63	1.26	hexagonal
R261	0.76	2.95	0.11	1.00	1.63	1.32	octagonal
R262	1.00	2.95	0.11	1.00	1.25	1.08	circular
R263	1.00	2.95	0.11	1.00	1.63	1.10	elliptic
R264	1.00	2.95	0.11	1.00	1.25	1.04	square
R265	1.00	2.95	0.11	1.00	1.63	1.06	rectangle
R266	1.00	2.95	0.11	1.00	1.63	0.89	lenticular
R267	1.00	2.95	0.11	1.00	1.63	1.04	ogival
R268	1.00	2.95	0.11	1.00	1.63	1.12	oblong
R269	1.00	2.95	0.11	1.00	1.63	1.30	hexagonal
R270	1.00	2.95	0.11	1.00	1.63	1.36	octagonal
R271	0.55	0.98	0.11	1.00	1.25	0.31	circular
R272	0.55	0.98	0.11	1.00	1.68	0.35	elliptic
R273	0.55	0.98	0.11	1.00	1.63	0.43	square
R274	0.55	0.98	0.11	1.00	1.63	0.45	rectangle
R275	0.55	0.98	0.11	1.00	1.63	0.41	lenticular
R276	0.55	0.98	0.11	1.00	1.63	0.45	ogival
R277	0.55	0.98	0.11	1.00	1.63	0.43	oblong
R278	0.55	0.98	0.11	1.00	1.63	0.49	hexagonal
R279	0.55	0.98	0.11	1.00	1.63	0.55	octagonal
R280	0.76	0.98	0.11	1.00	1.25	0.49	circular
R281	0.76	0.98	0.11	1.00	1.68	0.51	elliptic
R282	0.76	0.98	0.11	1.00	1.25	0.67	square
R283	0.76	0.98	0.11	1.00	1.63	0.71	rectangle
R284	0.76	0.98	0.11	1.00	1.63	0.59	lenticular
R285	0.76	0.98	0.11	1.00	1.63	0.69	ogival
R286	0.76	0.98	0.11	1.00	1.63	0.57	oblong
R287	0.76	0.98	0.11	1.00	1.63	0.75	hexagonal
R288	0.76	0.98	0.11	1.00	1.63	0.81	octagonal
R289	1.00	0.98	0.11	1.00	1.25	0.79	Circular

Run no.	V/V$_C$	y/b	b/B	ks	kθ	ds/b	shape
R290	1.00	0.98	0.11	1.00	1.63	0.81	elliptic
R291	1.00	0.98	0.11	1.00	1.25	0.71	square
R292	1.00	0.98	0.11	1.00	1.63	0.75	rectangle
R293	1.00	0.98	0.11	1.00	1.63	0.87	lenticular
R294	1.00	0.98	0.11	1.00	1.63	0.77	ogival
R295	1.00	0.98	0.11	1.00	1.63	0.85	oblong
R296	1.00	0.98	0.11	1.00	1.63	0.89	hexagonal
R297	1.00	0.98	0.11	1.00	1.63	0.93	octagonal
R298	0.55	0.20	0.11	1.00	1.25	0.02	circular
R299	0.55	0.20	0.11	1.00	1.63	0.02	elliptic
R300	0.55	0.20	0.11	1.00	1.25	0.06	square
R301	0.55	0.20	0.11	1.00	1.63	0.08	rectangle
R302	0.55	0.20	0.11	1.00	1.63	0.04	lenticular
R303	0.55	0.20	0.11	1.00	1.63	0.10	ogival
R304	0.55	0.20	0.11	1.00	1.63	0.04	oblong
R305	0.55	0.20	0.11	1.00	1.63	0.12	hexagonal
R306	0.55	0.20	0.11	1.00	1.63	0.16	octagonal
R307	0.76	0.20	0.11	1.00	1.25	0.02	circular
R308	0.76	0.20	0.11	1.00	1.63	0.04	elliptic
R309	0.76	0.20	0.11	1.00	1.25	0.16	square
R310	0.76	0.20	0.11	1.00	1.63	0.20	rectangle
R311	0.76	0.20	0.11	1.00	1.63	0.10	lenticular
R312	0.76	0.20	0.11	1.00	1.63	0.18	ogival
R313	0.76	0.20	0.11	1.00	1.63	0.08	oblong
R314	0.76	0.20	0.11	1.00	1.63	0.24	hexagonal
R315	0.76	0.20	0.11	1.00	1.63	0.30	octagonal
R316	1.00	0.20	0.11	1.00	1.25	0.04	circular
R317	1.00	0.20	0.11	1.00	1.63	0.06	elliptic
R318	1.00	0.20	0.11	1.00	1.25	0.20	square
R319	1.00	0.20	0.11	1.00	1.63	0.24	rectangle
R320	1.00	0.20	0.11	1.00	1.63	0.18	lenticular
R321	1.00	0.20	0.11	1.00	1.63	0.22	ogival
R322	1.00	0.20	0.11	1.00	1.63	0.10	oblong
R323	1.00	0.20	0.11	1.00	1.63	0.26	hexagonal
R324	1.00	0.20	0.11	1.00	1.63	0.33	octagonal
R325	0.55	2.95	0.15	1.00	1.25	0.22	circular
R326	0.55	2.95	0.15	1.00	1.63	0.28	Elliptic

Run no.	V/V$_C$	y/b	b/B	ks	kθ	ds/b	shape
R327	0.55	2.95	0.15	1.00	1.25	0.87	square
R328	0.55	2.95	0.15	1.00	1.63	0.89	rectangle
R329	0.55	2.95	0.15	1.00	1.63	0.81	lenticular
R330	0.55	2.95	0.15	1.00	1.63	0.91	ogival
R331	0.55	2.95	0.15	1.00	1.63	0.39	oblong
R332	0.55	2.95	0.15	1.00	1.63	0.94	hexagonal
R333	0.55	2.95	0.15	1.00	1.63	0.98	octagonal
R334	0.76	2.95	0.15	1.00	1.25	0.65	circular
R335	0.76	2.95	0.15	1.00	1.63	0.75	elliptic
R336	0.76	2.95	0.15	1.00	1.25	1.44	square
R337	0.76	2.95	0.15	1.00	1.63	1.48	rectangle
R338	0.76	2.95	0.15	1.00	1.63	1.34	lenticular
R339	0.76	2.95	0.15	1.00	1.63	1.46	ogival
R340	0.76	2.95	0.15	1.00	1.63	0.85	oblong
R341	0.76	2.95	0.15	1.00	1.63	1.50	hexagonal
R342	0.76	2.95	0.15	1.00	1.63	1.54	octagonal
R343	1.00	2.95	0.15	1.00	1.25	1.00	circular
R344	1.00	2.95	0.15	1.00	1.63	1.04	elliptic
R345	1.00	2.95	0.15	1.00	1.25	1.52	square
R346	1.00	2.95	0.15	1.00	1.63	1.56	rectangle
R347	1.00	2.95	0.15	1.00	1.63	1.44	lenticular
R348	1.00	2.95	0.15	1.00	1.63	1.54	ogival
R349	1.00	2.95	0.15	1.00	1.63	1.12	oblong
R350	1.00	2.95	0.15	1.00	1.63	1.59	hexagonal
R351	1.00	2.95	0.15	1.00	1.63	1.63	octagonal
R352	0.55	0.98	0.15	1.00	1.25	0.30	circular
R353	0.55	0.98	0.15	1.00	1.63	0.39	elliptic
R354	0.55	0.98	0.15	1.00	1.25	0.75	square
R355	0.55	0.98	0.15	1.00	1.63	0.77	rectangle
R356	0.55	0.98	0.15	1.00	1.63	0.77	lenticular
R357	0.55	0.98	0.15	1.00	1.63	0.75	ogival
R358	0.55	0.98	0.15	1.00	1.63	0.67	oblong
R359	0.55	0.98	0.15	1.00	1.63	0.79	hexagonal
R360	0.55	0.98	0.15	1.00	1.63	0.85	octagonal
R361	0.76	0.98	0.15	1.00	1.25	0.59	circular
R362	0.76	0.98	0.15	1.00	1.63	0.69	elliptic
R363	0.76	0.98	0.15	1.00	1.25	1.06	Square

Run no.	V/V$_C$	y/b	b/B	ks	kθ	ds/b	shape
R364	0.76	0.98	0.15	1.00	1.63	1.10	rectangle
R365	0.76	0.98	0.15	1.00	1.63	1.00	lenticular
R366	0.76	0.98	0.15	1.00	1.63	1.08	ogival
R367	0.76	0.98	0.15	1.00	1.63	0.79	oblong
R368	0.76	0.98	0.15	1.00	1.63	1.14	hexagonal
R369	0.76	0.98	0.15	1.00	1.63	1.18	octagonal
R370	1.00	0.98	0.15	1.00	1.25	0.71	circular
R371	1.00	0.98	0.15	1.00	1.63	0.79	elliptic
R372	1.00	0.98	0.15	1.00	1.25	1.16	square
R373	1.00	0.98	0.15	1.00	1.63	1.18	rectangle
R374	1.00	0.98	0.15	1.00	1.63	1.10	lenticular
R375	1.00	0.98	0.15	1.00	1.63	1.20	ogival
R376	1.00	0.98	0.15	1.00	1.63	0.87	oblong
R377	1.00	0.98	0.15	1.00	1.63	1.24	hexagonal
R378	1.00	0.98	0.15	1.00	1.63	1.30	octagonal
R379	0.55	0.20	0.15	1.00	1.25	0.02	circular
R380	0.55	0.20	0.15	1.00	1.63	0.02	elliptic
R381	0.55	0.20	0.15	1.00	1.25	0.12	square
R382	0.55	0.20	0.15	1.00	1.63	0.16	rectangle
R383	0.55	0.20	0.15	1.00	1.63	0.08	lenticular
R384	0.55	0.20	0.15	1.00	1.63	0.14	ogival
R385	0.55	0.20	0.15	1.00	1.63	0.06	oblong
R386	0.55	0.20	0.15	1.00	1.63	0.18	hexagonal
R387	0.55	0.20	0.15	1.00	1.63	0.24	octagonal
R388	0.76	0.20	0.15	1.00	1.25	0.02	circular
R389	0.76	0.20	0.15	1.00	1.63	0.08	elliptic
R390	0.76	0.20	0.15	1.00	1.25	0.22	square
R391	0.76	0.20	0.15	1.00	1.63	0.24	rectangle
R392	0.76	0.20	0.15	1.00	1.63	0.16	lenticular
R393	0.76	0.20	0.15	1.00	1.63	0.24	ogival
R394	0.76	0.20	0.15	1.00	1.63	0.14	oblong
R395	0.76	0.20	0.15	1.00	1.63	0.28	hexagonal
R396	0.76	0.20	0.15	1.00	1.63	0.31	octagonal
R397	1.00	0.20	0.15	1.00	1.25	0.08	circular
R398	1.00	0.20	0.15	1.00	1.63	0.18	elliptic
R399	1.00	0.20	0.15	1.00	1.25	0.35	square
R400	1.00	0.20	0.15	1.00	1.63	0.39	Rectangle

Run no.	V/V$_C$	y/b	b/B	ks	kθ	ds/b	shape
R401	1.00	0.20	0.15	1.00	1.63	0.28	lenticular
R402	1.00	0.20	0.15	1.00	1.63	0.37	ogival
R403	1.00	0.20	0.15	1.00	1.63	0.24	oblong
R404	1.00	0.20	0.15	1.00	1.63	0.41	hexagonal
R405	1.00	0.20	0.15	1.00	1.63	0.49	octagonal
R406	0.55	2.95	0.20	1.00	1.25	0.75	circular
R407	0.55	2.95	0.20	1.00	1.63	0.85	elliptic
R408	0.55	2.95	0.20	1.00	1.25	1.14	square
R409	0.55	2.95	0.20	1.00	1.63	1.16	rectangle
R410	0.55	2.95	0.20	1.00	1.63	1.04	lenticular
R411	0.55	2.95	0.20	1.00	1.63	1.18	ogival
R412	0.55	2.95	0.20	1.00	1.63	0.91	oblong
R413	0.55	2.95	0.20	1.00	1.63	1.22	hexagonal
R414	0.55	2.95	0.20	1.00	1.63	1.28	octagonal
R415	0.76	2.95	0.20	1.00	1.25	1.04	circular
R416	0.76	2.95	0.20	1.00	1.63	1.08	elliptic
R417	0.76	2.95	0.20	1.00	1.25	1.52	square
R418	0.76	2.95	0.20	1.00	1.63	1.54	rectangle
R419	0.76	2.95	0.20	1.00	1.63	1.38	lenticular
R420	0.76	2.95	0.20	1.00	1.63	1.54	ogival
R421	0.76	2.95	0.20	1.00	1.63	1.18	oblong
R422	0.76	2.95	0.20	1.00	1.63	1.56	hexagonal
R423	0.76	2.95	0.20	1.00	1.63	1.63	octagonal
R424	1.00	2.95	0.20	1.00	1.25	1.36	circular
R425	1.00	2.95	0.20	1.00	1.63	1.38	elliptic
R426	1.00	2.95	0.20	1.00	1.25	1.63	square
R427	1.00	2.95	0.20	1.00	1.63	1.65	rectangle
R428	1.00	2.95	0.20	1.00	1.63	1.56	lenticular
R429	1.00	2.95	0.20	1.00	1.63	1.67	ogival
R430	1.00	2.95	0.20	1.00	1.63	1.46	oblong
R431	1.00	2.95	0.20	1.00	1.63	1.67	hexagonal
R432	1.00	2.95	0.20	1.00	1.63	1.71	octagonal
R433	0.55	0.98	0.20	1.00	1.25	0.47	circular
R434	0.55	0.98	0.20	1.00	1.63	0.53	elliptic
R435	0.55	0.98	0.20	1.00	1.25	0.91	square
R436	0.55	0.98	0.20	1.00	1.63	0.96	rectangle
R437	0.55	0.98	0.20	1.00	1.63	0.85	Lenticular

Run no.	V/V$_C$	y/b	b/B	ks	kθ	ds/b	shape
R438	0.55	0.98	0.20	1.00	1.63	0.94	ogival
R439	0.55	0.98	0.20	1.00	1.63	0.61	oblong
R440	0.55	0.98	0.20	1.00	1.63	1.00	hexagonal
R441	0.55	0.98	0.20	1.00	1.63	1.06	octagonal
R442	0.76	0.98	0.20	1.00	1.25	0.75	circular
R443	0.76	0.98	0.20	1.00	1.63	0.79	elliptic
R444	0.76	0.98	0.20	1.00	1.25	1.26	square
R445	0.76	0.98	0.20	1.00	1.63	1.30	rectangle
R446	0.76	0.98	0.20	1.00	1.63	1.14	lenticular
R447	0.76	0.98	0.20	1.00	1.63	1.28	ogival
R448	0.76	0.98	0.20	1.00	1.63	0.85	oblong
R449	0.76	0.98	0.20	1.00	1.63	1.34	hexagonal
R450	0.76	0.98	0.20	1.00	1.63	1.38	octagonal
R451	1.00	0.98	0.20	1.00	1.25	1.34	circular
R452	1.00	0.98	0.20	1.00	1.63	1.38	elliptic
R453	1.00	0.98	0.20	1.00	1.25	1.42	square
R454	1.00	0.98	0.20	1.00	1.63	1.46	rectangle
R455	1.00	0.98	0.20	1.00	1.63	1.24	lenticular
R456	1.00	0.98	0.20	1.00	1.63	1.44	ogival
R457	1.00	0.98	0.20	1.00	1.63	1.42	oblong
R458	1.00	0.98	0.20	1.00	1.63	1.52	hexagonal
R459	1.00	0.98	0.20	1.00	1.63	1.57	octagonal
R460	0.55	0.20	0.20	1.00	1.25	0.02	circular
R461	0.55	0.20	0.20	1.00	1.63	0.02	elliptic
R462	0.55	0.20	0.20	1.00	1.25	0.20	square
R463	0.55	0.20	0.20	1.00	1.63	0.22	rectangle
R464	0.55	0.20	0.20	1.00	1.63	0.12	lenticular
R465	0.55	0.20	0.20	1.00	1.63	0.24	ogival
R466	0.55	0.20	0.20	1.00	1.63	0.20	oblong
R467	0.55	0.20	0.20	1.00	1.63	0.24	hexagonal
R468	0.55	0.20	0.20	1.00	1.63	0.28	octagonal
R469	0.76	0.20	0.20	1.00	1.25	0.04	circular
R470	0.76	0.20	0.20	1.00	1.63	0.08	elliptic
R471	0.76	0.20	0.20	1.00	1.25	0.26	square
R472	0.76	0.20	0.20	1.00	1.63	0.30	rectangle
R473	0.76	0.20	0.20	1.00	1.63	0.20	lenticular
R474	0.76	0.20	0.20	1.00	1.63	0.28	Ogival

Run no.	V/V$_C$	y/b	b/B	ks	kθ	ds/b	shape
R475	0.76	0.20	0.20	1.00	1.63	0.31	oblong
R476	0.76	0.20	0.20	1.00	1.63	0.35	hexagonal
R477	0.76	0.20	0.20	1.00	1.63	0.39	octagonal
R478	1.00	0.20	0.20	1.00	1.25	0.08	circular
R479	1.00	0.20	0.20	1.00	1.63	0.14	elliptic
R480	1.00	0.20	0.20	1.00	1.25	0.37	square
R481	1.00	0.20	0.20	1.00	1.63	0.39	rectangle
R482	1.00	0.20	0.20	1.00	1.63	0.31	lenticular
R483	1.00	0.20	0.20	1.00	1.63	0.41	ogival
R484	1.00	0.20	0.20	1.00	1.63	0.39	oblong
R485	1.00	0.20	0.20	1.00	1.63	0.45	hexagonal
R486	1.00	0.20	0.20	1.00	1.63	0.53	octagonal
R487	0.55	2.95	0.11	1.00	1.23	0.28	circular
R488	0.55	2.95	0.11	1.00	1.50	0.31	elliptic
R489	0.55	2.95	0.11	1.00	1.23	0.39	square
R490	0.55	2.95	0.11	1.00	1.50	0.45	rectangle
R491	0.55	2.95	0.11	1.00	1.50	0.37	lenticular
R492	0.55	2.95	0.11	1.00	1.50	0.43	ogival
R493	0.55	2.95	0.11	1.00	1.50	0.30	oblong
R494	0.55	2.95	0.11	1.00	1.50	0.47	hexagonal
R495	0.55	2.95	0.11	1.00	1.50	0.53	octagonal
R496	0.76	2.95	0.11	1.00	1.23	0.61	circular
R497	0.76	2.95	0.11	1.00	1.50	0.65	elliptic
R498	0.76	2.95	0.11	1.00	1.23	0.79	square
R499	0.76	2.95	0.11	1.00	1.50	0.83	rectangle
R500	0.76	2.95	0.11	1.00	1.50	0.67	lenticular
R501	0.76	2.95	0.11	1.00	1.50	0.81	ogival
R502	0.76	2.95	0.11	1.00	1.50	0.69	oblong
R503	0.76	2.95	0.11	1.00	1.50	0.87	hexagonal
R504	0.76	2.95	0.11	1.00	1.50	0.91	octagonal
R505	1.00	2.95	0.11	1.00	1.23	1.08	circular
R506	1.00	2.95	0.11	1.00	1.50	1.12	elliptic
R507	1.00	2.95	0.11	1.00	1.23	0.93	square
R508	1.00	2.95	0.11	1.00	1.50	0.96	rectangle
R509	1.00	2.95	0.11	1.00	1.50	0.73	lenticular
R510	1.00	2.95	0.11	1.00	1.50	0.94	ogival
R511	1.00	2.95	0.11	1.00	1.50	1.14	Oblong

Run no.	V/V_C	y/b	b/B	ks	kθ	ds/b	shape
R512	1.00	2.95	0.11	1.00	1.50	0.98	hexagonal
R513	1.00	2.95	0.11	1.00	1.50	1.04	octagonal
R514	0.55	0.98	0.11	1.00	1.23	0.31	circular
R515	0.55	0.98	0.11	1.00	1.50	0.33	elliptic
R516	0.55	0.98	0.11	1.00	1.23	0.35	square
R517	0.55	0.98	0.11	1.00	1.50	0.39	rectangle
R518	0.55	0.98	0.11	1.00	1.50	0.31	lenticular
R519	0.55	0.98	0.11	1.00	1.50	0.37	ogival
R520	0.55	0.98	0.11	1.00	1.50	0.35	oblong
R521	0.55	0.98	0.11	1.00	1.50	0.41	hexagonal
R522	0.55	0.98	0.11	1.00	1.50	0.47	octagonal
R523	0.76	0.98	0.11	1.00	1.23	0.49	circular
R524	0.76	0.98	0.11	1.00	1.50	0.39	elliptic
R525	0.76	0.98	0.11	1.00	1.23	0.59	square
R526	0.76	0.98	0.11	1.00	1.50	0.65	rectangle
R527	0.76	0.98	0.11	1.00	1.50	0.47	lenticular
R528	0.76	0.98	0.11	1.00	1.50	0.63	ogival
R529	0.76	0.98	0.11	1.00	1.50	0.43	oblong
R530	0.76	0.98	0.11	1.00	1.50	0.67	hexagonal
R531	0.76	0.98	0.11	1.00	1.50	0.71	octagonal
R532	1.00	0.98	0.11	1.00	1.23	0.79	circular
R533	1.00	0.98	0.11	1.00	1.50	0.83	elliptic
R534	1.00	0.98	0.11	1.00	1.23	0.65	square
R535	1.00	0.98	0.11	1.00	1.50	0.69	rectangle
R536	1.00	0.98	0.11	1.00	1.50	0.59	lenticular
R537	1.00	0.98	0.11	1.00	1.50	0.73	ogival
R538	1.00	0.98	0.11	1.00	1.50	0.85	oblong
R539	1.00	0.98	0.11	1.00	1.50	0.75	hexagonal
R540	1.00	0.98	0.11	1.00	1.50	0.87	octagonal
R541	0.55	0.20	0.11	1.00	1.23	0.02	circular
R542	0.55	0.20	0.11	1.00	1.50	0.02	elliptic
R543	0.55	0.20	0.11	1.00	1.23	0.04	square
R544	0.55	0.20	0.11	1.00	1.50	0.08	rectangle
R545	0.55	0.20	0.11	1.00	1.50	0.02	lenticular
R546	0.55	0.20	0.11	1.00	1.50	0.06	ogival
R547	0.55	0.20	0.11	1.00	1.50	0.02	oblong
R548	0.55	0.20	0.11	1.00	1.50	0.10	Hexagonal

Run no.	V/V_C	y/b	b/B	ks	kθ	ds/b	shape
R549	0.55	0.20	0.11	1.00	1.50	0.28	octagonal
R550	0.76	0.20	0.11	1.00	1.23	0.02	circular
R551	0.76	0.20	0.11	1.00	1.50	0.06	elliptic
R552	0.76	0.20	0.11	1.00	1.23	0.10	square
R553	0.76	0.20	0.11	1.00	1.50	0.12	rectangle
R554	0.76	0.20	0.11	1.00	1.50	0.04	lenticular
R555	0.76	0.20	0.11	1.00	1.50	0.10	ogival
R556	0.76	0.20	0.11	1.00	1.50	0.08	oblong
R557	0.76	0.20	0.11	1.00	1.50	0.14	hexagonal
R558	0.76	0.20	0.11	1.00	1.50	0.18	octagonal
R559	1.00	0.20	0.11	1.00	1.23	0.04	circular
R560	1.00	0.20	0.11	1.00	1.50	0.06	elliptic
R561	1.00	0.20	0.11	1.00	1.23	0.16	square
R562	1.00	0.20	0.11	1.00	1.50	0.20	rectangle
R563	1.00	0.20	0.11	1.00	1.50	0.12	lenticular
R564	1.00	0.20	0.11	1.00	1.50	0.18	ogival
R565	1.00	0.20	0.11	1.00	1.50	0.08	oblong
R566	1.00	0.20	0.11	1.00	1.50	0.22	hexagonal
R567	1.00	0.20	0.11	1.00	1.50	0.28	octagonal
R568	0.55	2.95	0.15	1.00	1.23	0.22	circular
R569	0.55	2.95	0.15	1.00	1.50	0.24	elliptic
R570	0.55	2.95	0.15	1.00	1.23	0.63	square
R571	0.55	2.95	0.15	1.00	1.50	0.67	rectangle
R572	0.55	2.95	0.15	1.00	1.50	0.59	lenticular
R573	0.55	2.95	0.15	1.00	1.50	0.65	ogival
R574	0.55	2.95	0.15	1.00	1.50	0.28	oblong
R575	0.55	2.95	0.15	1.00	1.50	0.69	hexagonal
R576	0.55	2.95	0.15	1.00	1.50	0.75	octagonal
R577	0.76	2.95	0.15	1.00	1.23	0.65	circular
R578	0.76	2.95	0.15	1.00	1.50	0.69	elliptic
R579	0.76	2.95	0.15	1.00	1.23	1.24	square
R580	0.76	2.95	0.15	1.00	1.50	1.30	rectangle
R581	0.76	2.95	0.15	1.00	1.50	1.20	lenticular
R582	0.76	2.95	0.15	1.00	1.50	1.26	ogival
R583	0.76	2.95	0.15	1.00	1.50	0.71	oblong
R584	0.76	2.95	0.15	1.00	1.50	1.32	hexagonal
R585	0.76	2.95	0.15	1.00	1.50	1.36	Octagonal

Run no.	V/V$_C$	y/b	b/B	ks	kθ	ds/b	shape
R586	1.00	2.95	0.15	1.00	1.23	1.00	circular
R587	1.00	2.95	0.15	1.00	1.50	1.08	elliptic
R588	1.00	2.95	0.15	1.00	1.23	1.34	square
R589	1.00	2.95	0.15	1.00	1.50	1.36	rectangle
R590	1.00	2.95	0.15	1.00	1.50	1.28	lenticular
R591	1.00	2.95	0.15	1.00	1.50	1.34	ogival
R592	1.00	2.95	0.15	1.00	1.50	1.08	oblong
R593	1.00	2.95	0.15	1.00	1.50	1.38	hexagonal
R594	1.00	2.95	0.15	1.00	1.50	1.40	octagonal
R595	0.55	0.98	0.15	1.00	1.23	0.30	circular
R596	0.55	0.98	0.15	1.00	1.50	0.31	elliptic
R597	0.55	0.98	0.15	1.00	1.23	0.67	square
R598	0.55	0.98	0.15	1.00	1.50	0.69	rectangle
R599	0.55	0.98	0.15	1.00	1.50	0.53	lenticular
R600	0.55	0.98	0.15	1.00	1.50	0.69	ogival
R601	0.55	0.98	0.15	1.00	1.50	0.33	oblong
R602	0.55	0.98	0.15	1.00	1.50	0.71	hexagonal
R603	0.55	0.98	0.15	1.00	1.50	0.77	octagonal
R604	0.76	0.98	0.15	1.00	1.23	0.59	circular
R605	0.76	0.98	0.15	1.00	1.50	0.63	elliptic
R606	0.76	0.98	0.15	1.00	1.23	1.00	square
R607	0.76	0.98	0.15	1.00	1.50	1.04	rectangle
R608	0.76	0.98	0.15	1.00	1.50	0.85	lenticular
R609	0.76	0.98	0.15	1.00	1.50	1.00	ogival
R610	0.76	0.98	0.15	1.00	1.50	0.67	oblong
R611	0.76	0.98	0.15	1.00	1.50	1.08	hexagonal
R612	0.76	0.98	0.15	1.00	1.50	1.12	octagonal
R613	1.00	0.98	0.15	1.00	1.23	0.71	circular
R614	1.00	0.98	0.15	1.00	1.50	0.73	elliptic
R615	1.00	0.98	0.15	1.00	1.23	1.10	square
R616	1.00	0.98	0.15	1.00	1.50	1.14	rectangle
R617	1.00	0.98	0.15	1.00	1.50	0.94	lenticular
R618	1.00	0.98	0.15	1.00	1.50	1.10	ogival
R619	1.00	0.98	0.15	1.00	1.50	0.75	oblong
R620	1.00	0.98	0.15	1.00	1.50	1.14	hexagonal
R621	1.00	0.98	0.15	1.00	1.50	1.18	octagonal
R622	0.55	0.20	0.15	1.00	1.23	0.02	Circular

Run no.	V/V$_C$	y/b	b/B	ks	kθ	ds/b	shape
R623	0.55	0.20	0.15	1.00	1.50	0.02	elliptic
R624	0.55	0.20	0.15	1.00	1.23	0.06	square
R625	0.55	0.20	0.15	1.00	1.50	0.10	rectangle
R626	0.55	0.20	0.15	1.00	1.50	0.02	lenticular
R627	0.55	0.20	0.15	1.00	1.50	0.08	ogival
R628	0.55	0.20	0.15	1.00	1.50	0.04	oblong
R629	0.55	0.20	0.15	1.00	1.50	0.12	hexagonal
R630	0.55	0.20	0.15	1.00	1.50	0.16	octagonal
R631	0.76	0.20	0.15	1.00	1.23	0.02	circular
R632	0.76	0.20	0.15	1.00	1.50	0.06	elliptic
R633	0.76	0.20	0.15	1.00	1.23	0.14	square
R634	0.76	0.20	0.15	1.00	1.50	0.18	rectangle
R635	0.76	0.20	0.15	1.00	1.50	0.12	lenticular
R636	0.76	0.20	0.15	1.00	1.50	0.14	ogival
R637	0.76	0.20	0.15	1.00	1.50	0.10	oblong
R638	0.76	0.20	0.15	1.00	1.50	0.20	hexagonal
R639	0.76	0.20	0.15	1.00	1.50	0.24	octagonal
R640	1.00	0.20	0.15	1.00	1.23	0.08	circular
R641	1.00	0.20	0.15	1.00	1.50	0.12	elliptic
R642	1.00	0.20	0.15	1.00	1.23	0.26	square
R643	1.00	0.20	0.15	1.00	1.50	0.30	rectangle
R644	1.00	0.20	0.15	1.00	1.50	0.22	lenticular
R645	1.00	0.20	0.15	1.00	1.50	0.28	ogival
R646	1.00	0.20	0.15	1.00	1.50	0.14	oblong
R647	1.00	0.20	0.15	1.00	1.50	0.31	hexagonal
R648	1.00	0.20	0.15	1.00	1.50	0.35	octagonal
R649	0.55	2.95	0.20	1.00	1.23	0.75	circular
R650	0.55	2.95	0.20	1.00	1.50	0.77	elliptic
R651	0.55	2.95	0.20	1.00	1.23	0.98	square
R652	0.55	2.95	0.20	1.00	1.50	1.02	rectangle
R653	0.55	2.95	0.20	1.00	1.50	0.93	lenticular
R654	0.55	2.95	0.20	1.00	1.50	0.98	ogival
R655	0.55	2.95	0.20	1.00	1.50	0.81	oblong
R656	0.55	2.95	0.20	1.00	1.50	1.06	hexagonal
R657	0.55	2.95	0.20	1.00	1.50	1.10	octagonal
R658	0.76	2.95	0.20	1.00	1.23	1.04	circular
R659	0.76	2.95	0.20	1.00	1.50	1.06	elliptic

Run no.	V/V$_C$	y/b	b/B	ks	1.00	ds/b	shape
R660	0.76	2.95	0.20	1.00	1.23	1.38	square
R661	0.76	2.95	0.20	1.00	1.50	1.40	rectangle
R662	0.76	2.95	0.20	1.00	1.50	1.28	lenticular
R663	0.76	2.95	0.20	1.00	1.50	1.40	ogival
R664	0.76	2.95	0.20	1.00	1.50	1.10	oblong
R665	0.76	2.95	0.20	1.00	1.50	1.42	hexagonal
R666	0.76	2.95	0.20	1.00	1.50	1.46	octagonal
R667	1.00	2.95	0.20	1.00	1.23	1.36	circular
R668	1.00	2.95	0.20	1.00	1.50	1.40	elliptic
R669	1.00	2.95	0.20	1.00	1.23	1.54	square
R670	1.00	2.95	0.20	1.00	1.50	1.56	rectangle
R671	1.00	2.95	0.20	1.00	1.50	1.44	lenticular
R672	1.00	2.95	0.20	1.00	1.50	1.54	ogival
R673	1.00	2.95	0.20	1.00	1.50	1.42	oblong
R674	1.00	2.95	0.20	1.00	1.50	1.59	hexagonal
R675	1.00	2.95	0.20	1.00	1.50	1.63	octagonal
R676	0.55	0.98	0.20	1.00	1.23	0.47	circular
R677	0.55	0.98	0.20	1.00	1.50	0.49	elliptic
R678	0.55	0.98	0.20	1.00	1.23	0.83	square
R679	0.55	0.98	0.20	1.00	1.50	0.87	rectangle
R680	0.55	0.98	0.20	1.00	1.50	0.71	lenticular
R681	0.55	0.98	0.20	1.00	1.50	0.85	ogival
R682	0.55	0.98	0.20	1.00	1.50	0.53	oblong
R683	0.55	0.98	0.20	1.00	1.50	0.89	hexagonal
R684	0.55	0.98	0.20	1.00	1.50	0.93	octagonal
R685	0.76	0.98	0.20	1.00	1.23	0.75	circular
R686	0.76	0.98	0.20	1.00	1.50	0.79	elliptic
R687	0.76	0.98	0.20	1.00	1.23	1.20	square
R688	0.76	0.98	0.20	1.00	1.50	1.28	rectangle
R689	0.76	0.98	0.20	1.00	1.50	0.94	lenticular
R690	0.76	0.98	0.20	1.00	1.50	1.22	ogival
R691	0.76	0.98	0.20	1.00	1.50	0.83	oblong
R692	0.76	0.98	0.20	1.00	1.50	0.98	hexagonal
R693	0.76	0.98	0.20	1.00	1.50	1.00	octagonal
R694	1.00	0.98	0.20	1.00	1.23	1.34	circular
R695	1.00	0.98	0.20	1.00	1.50	1.36	elliptic
R696	1.00	0.98	0.20	1.00	1.23	1.38	Square

Run no.	V/V_C	y/b	b/B	ks	$k\theta$	ds/b	shape
R697	1.00	0.98	0.20	1.00	1.50	1.44	rectangle
R698	1.00	0.98	0.20	1.00	1.50	1.12	lenticular
R699	1.00	0.98	0.20	1.00	1.50	1.40	ogival
R700	1.00	0.98	0.20	1.00	1.50	1.36	oblong
R701	1.00	0.98	0.20	1.00	1.50	1.48	hexagonal
R702	1.00	0.98	0.20	1.00	1.50	1.50	octagonal
R703	0.55	0.20	0.20	1.00	1.23	0.02	circular
R704	0.55	0.20	0.20	1.00	1.50	0.02	elliptic
R705	0.55	0.20	0.20	1.00	1.23	0.10	square
R706	0.55	0.20	0.20	1.00	1.50	0.12	rectangle
R707	0.55	0.20	0.20	1.00	1.50	0.06	lenticular
R708	0.55	0.20	0.20	1.00	1.50	0.12	ogival
R709	0.55	0.20	0.20	1.00	1.50	0.04	oblong
R710	0.55	0.20	0.20	1.00	1.50	0.14	hexagonal
R711	0.55	0.20	0.20	1.00	1.50	0.18	octagonal
R712	0.76	0.20	0.20	1.00	1.23	0.04	circular
R713	0.76	0.20	0.20	1.00	1.50	0.08	elliptic
R714	0.76	0.20	0.20	1.00	1.23	0.22	square
R715	0.76	0.20	0.20	1.00	1.50	0.26	rectangle
R716	0.76	0.20	0.20	1.00	1.50	0.12	lenticular
R717	0.76	0.20	0.20	1.00	1.50	0.24	ogival
R718	0.76	0.20	0.20	1.00	1.50	0.14	oblong
R719	0.76	0.20	0.20	1.00	1.50	0.30	hexagonal
R720	0.76	0.20	0.20	1.00	1.50	0.31	octagonal
R721	1.00	0.20	0.20	1.00	1.23	0.08	circular
R722	1.00	0.20	0.20	1.00	1.50	0.10	elliptic
R723	1.00	0.20	0.20	1.00	1.23	0.28	square
R724	1.00	0.20	0.20	1.00	1.50	0.31	rectangle
R725	1.00	0.20	0.20	1.00	1.50	0.18	lenticular
R726	1.00	0.20	0.20	1.00	1.50	0.31	ogival
R727	1.00	0.20	0.20	1.00	1.50	0.16	oblong
R728	1.00	0.20	0.20	1.00	1.50	0.33	hexagonal
R729	1.00	0.20	0.20	1.00	1.50	0.37	octagonal

A.2- Scour depth at different rate of flow intensity V/V$_C$
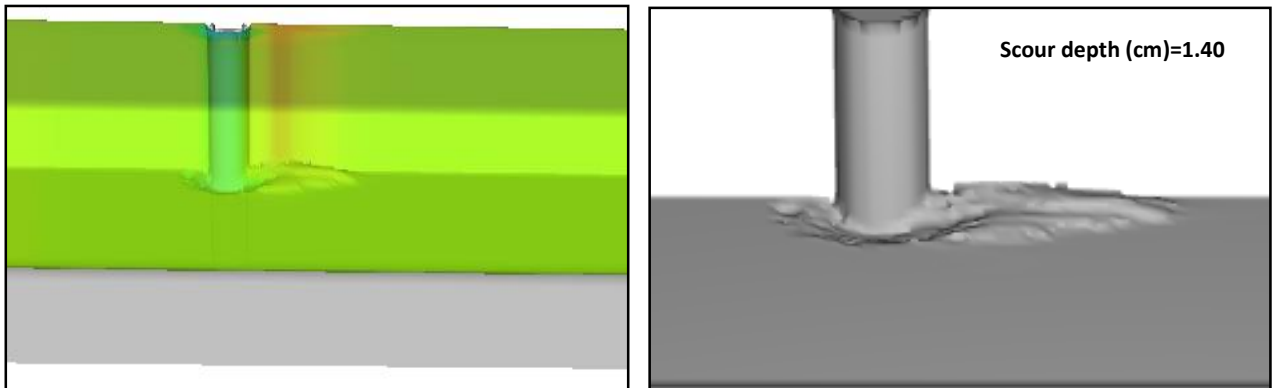
Figure (A-1): Scour depth around circular pier at V/V$_C$=0.55, y/b=2.95,
b/B=0.11, Ks=1.00, Kθ=1.00 for run no.1
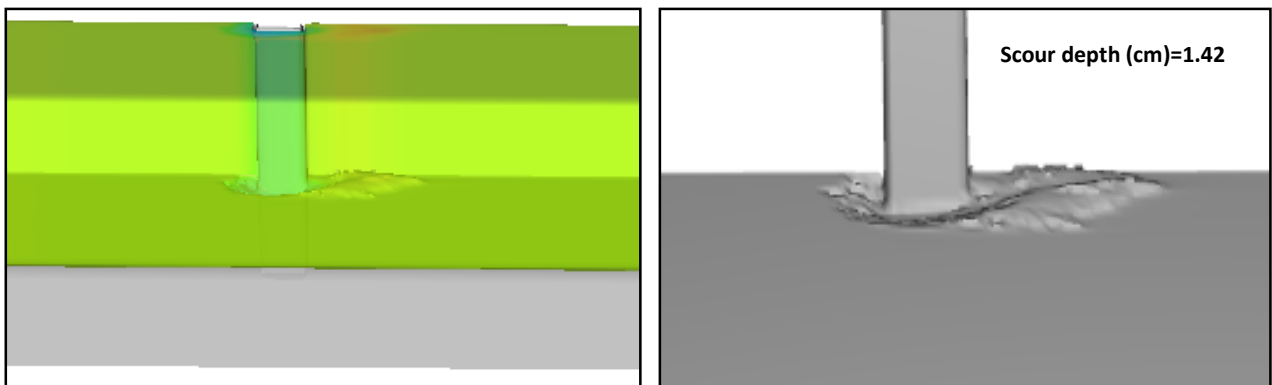
Figure (A-2): Scour depth around square pier at V/V$_C$=0.55, y/b=2.95,
b/B=0.11, Ks=1.16, Kθ=1.00 for run no.3
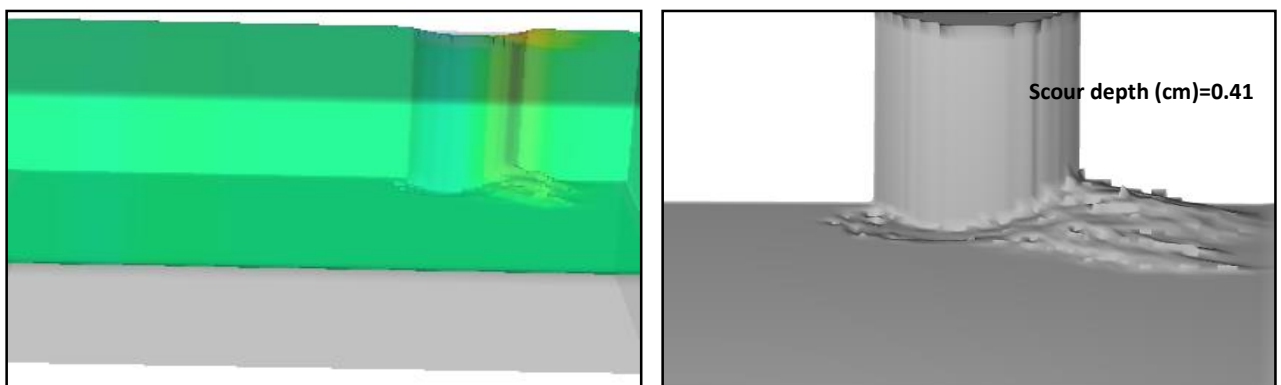
Figure (A-3): Scour depth around lenticular pier at V/V$_C$=0.55, y/b=2.95,
b/B=0.11, Ks=0.71, Kθ=1.00 for run no.5
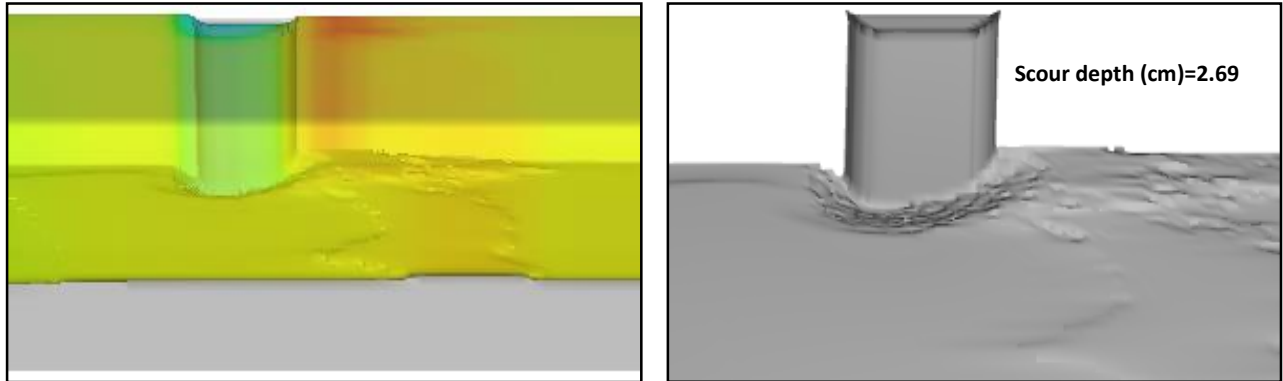
Figure (A-4): Scour depth around oblong pier at V/V$_C$=0.76, y/b=2.95, b/B=0.11, Ks=0.87, Kθ=1.00 for run no.16
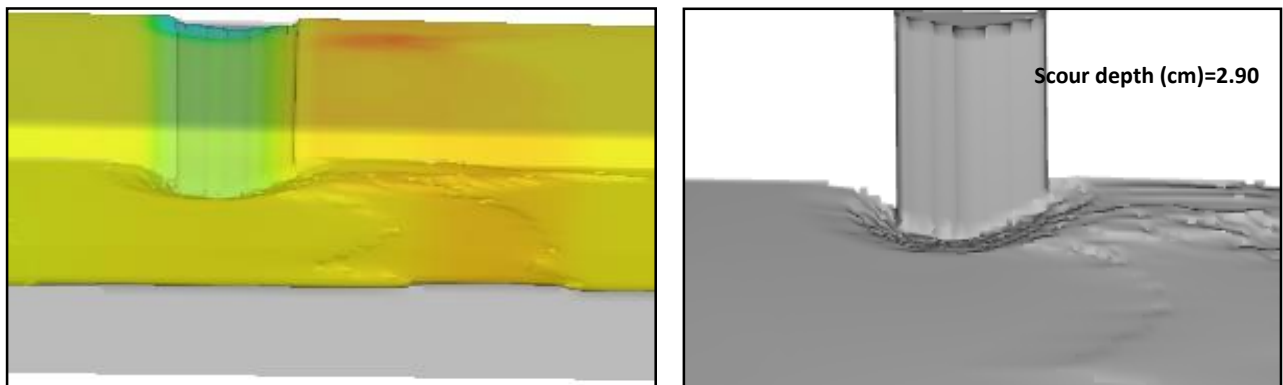
Figure (A-5): Scour depth around hexagonal pier at V/V$_C$=0.76, y/b=2.95, b/B=0.11, Ks=0.94, Kθ=1.00 for run no.17
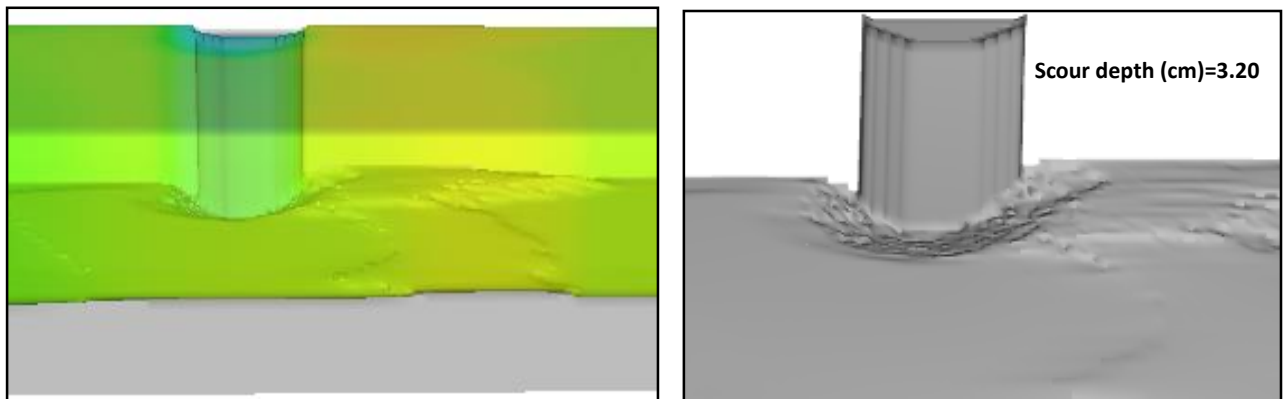
Figure (A-6): Scour depth around octagonal pier at V/V$_C$=0.76, y/b=2.95, b/B=0.11, Ks=1.03, Kθ=1.00 for run no.18
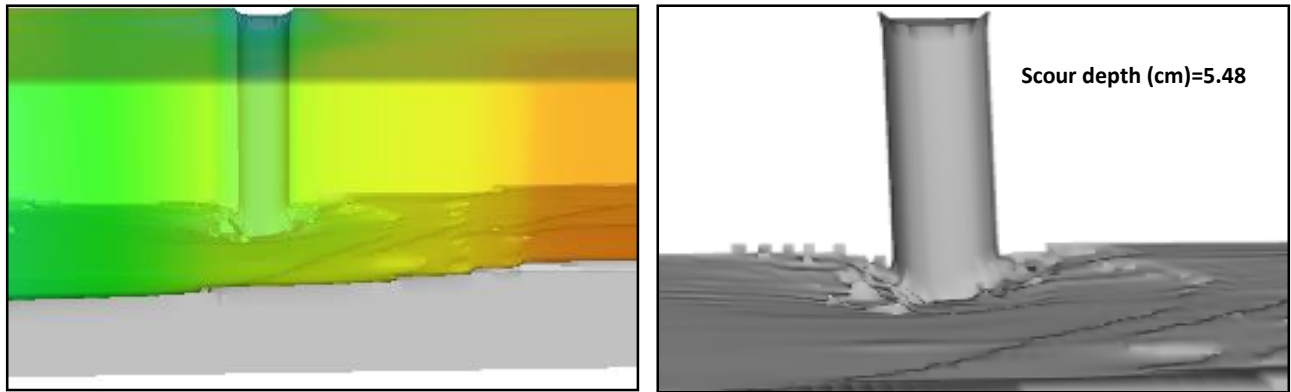
Figure (A-7): Scour depth around circular pier at V/V_C=1.00, y/b=2.95, b/B=0.11, Ks=1.00, Kθ=1.00 for run no.19
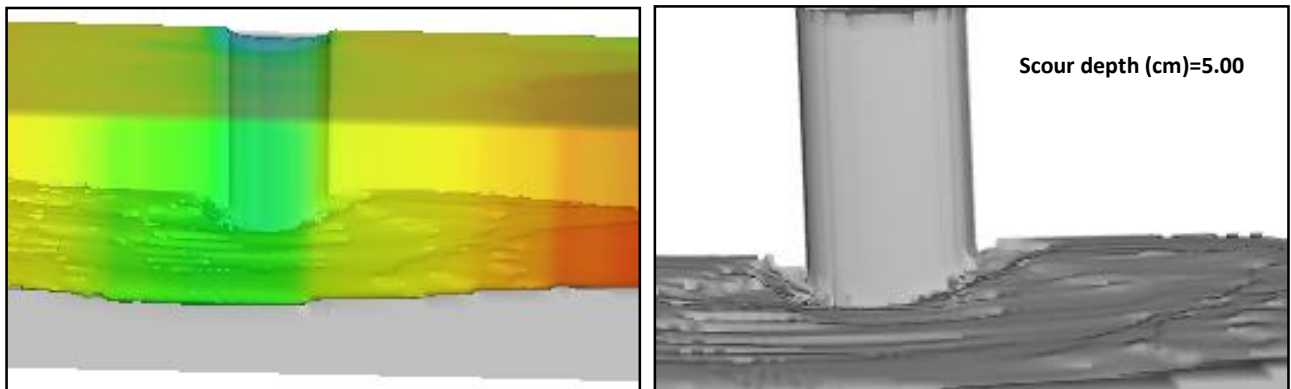
Figure (A-8): Scour depth around elliptic pier at V/V_C=1.00, y/b=2.95, b/B=0.11, Ks=0.84, Kθ=1.00 for run no.20

A.3- Scour depth at different rate of flow depth ratio y/b
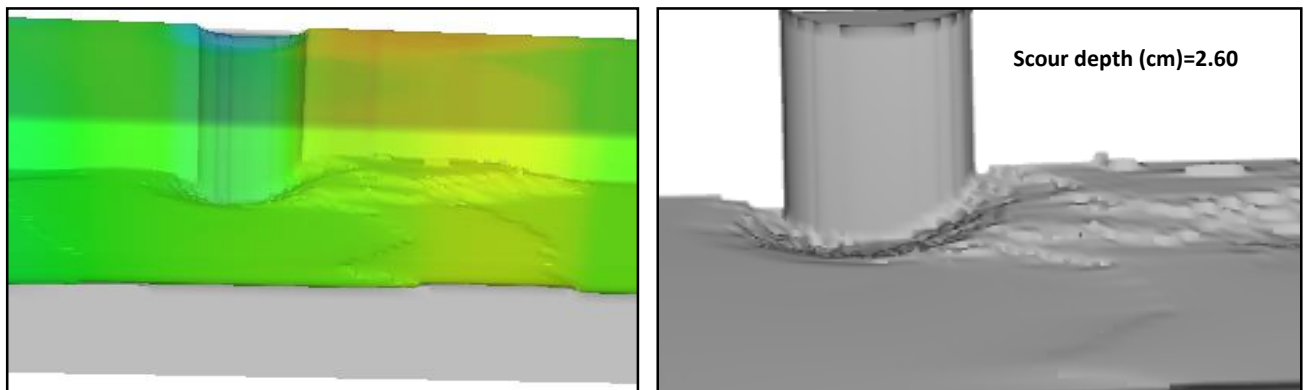
Figure (A-9): Scour depth around elliptic pier at y/b=2.95, V/V_C=0.76, b/B=0.11, Ks=0.84, Kθ=1.00 for run no.11
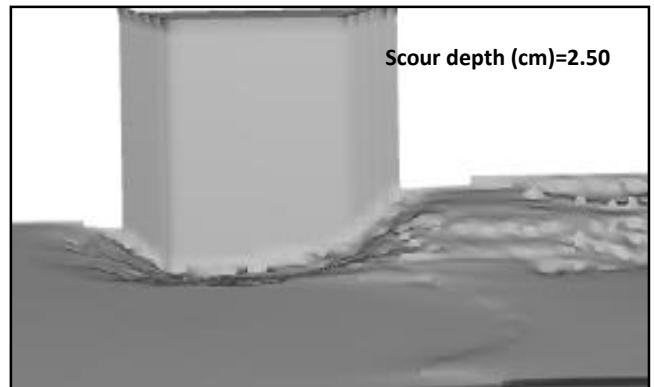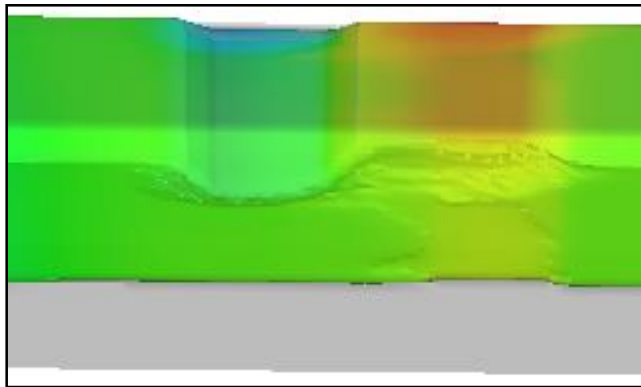
Figure (A-10): Scour depth around ogival pier at y/b=2.95, V/V$_C$=0.76,
b/B=0.11, Ks=0.81, Kθ=1.00 for run no.15
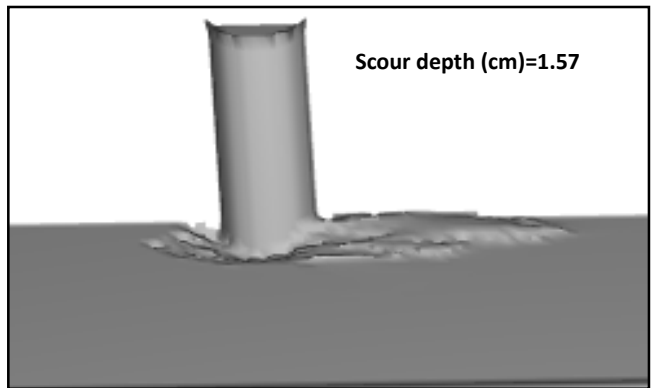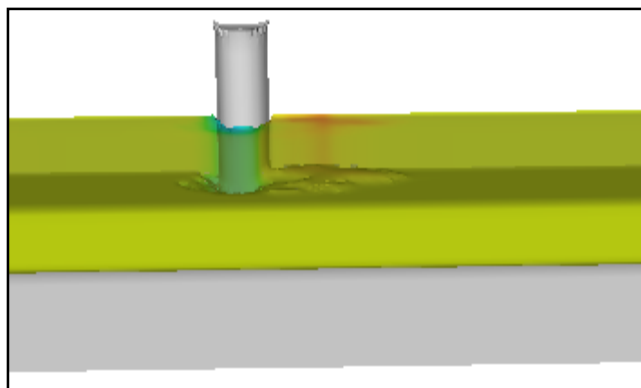
Figure (A-11): Scour depth around circular pier at y/b=0.98, V/V$_C$=0.55,
b/B=0.11, Ks=1.00, Kθ=1.00 for run no.28
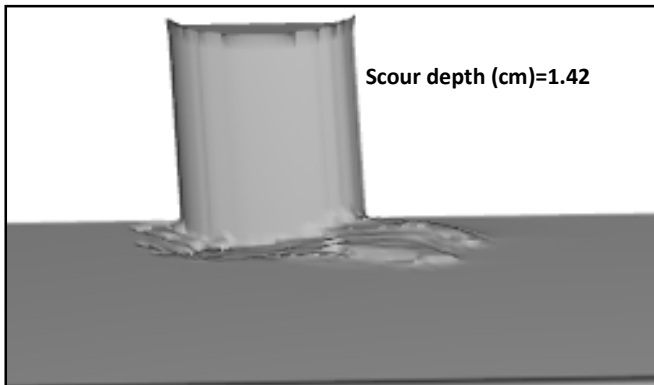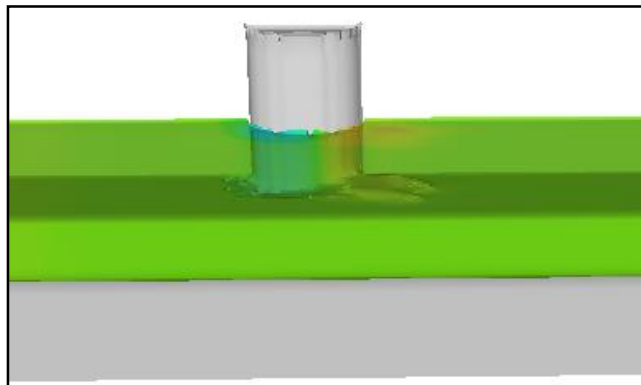
Figure (A-12): Scour depth around elliptic pier at y/b=0.98, V/V$_C$=0.55,
b/B=0.11, Ks=0.84, Kθ=1.00 for run no.29
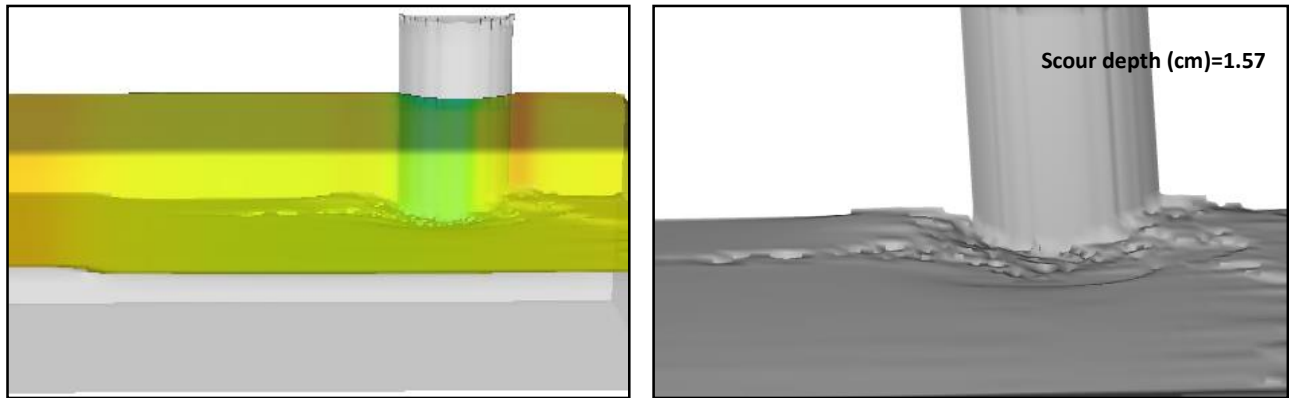
Figure (A-13): Scour depth around lenticular pier at y/b=0.98, V/V$_C$=0.76, b/B=0.11, Ks=0.71, Kθ=1.00 for run no.41
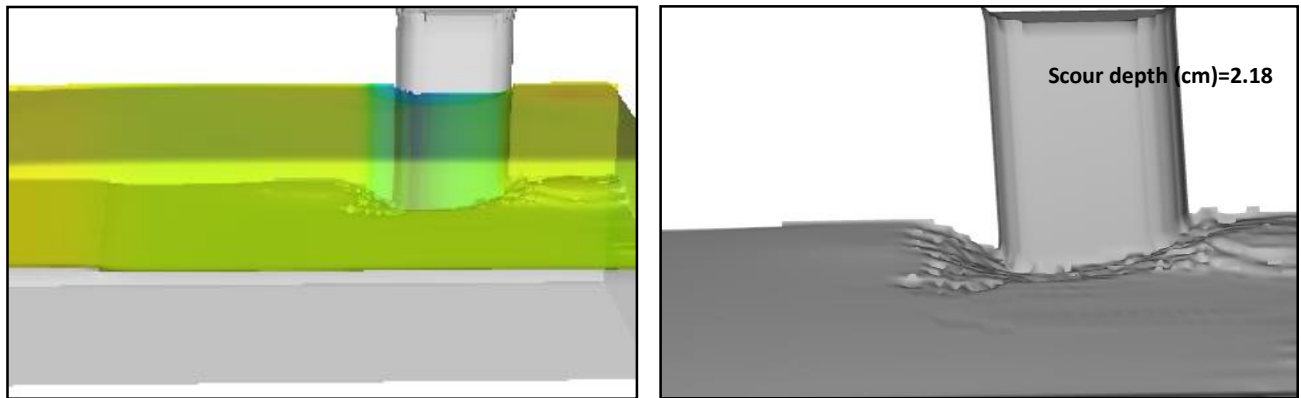
Figure (A-14): Scour depth around oblong pier at y/b=0.98, V/V$_C$=0.76, b/B=0.11, Ks=0.87, Kθ=1.00 for run no.43
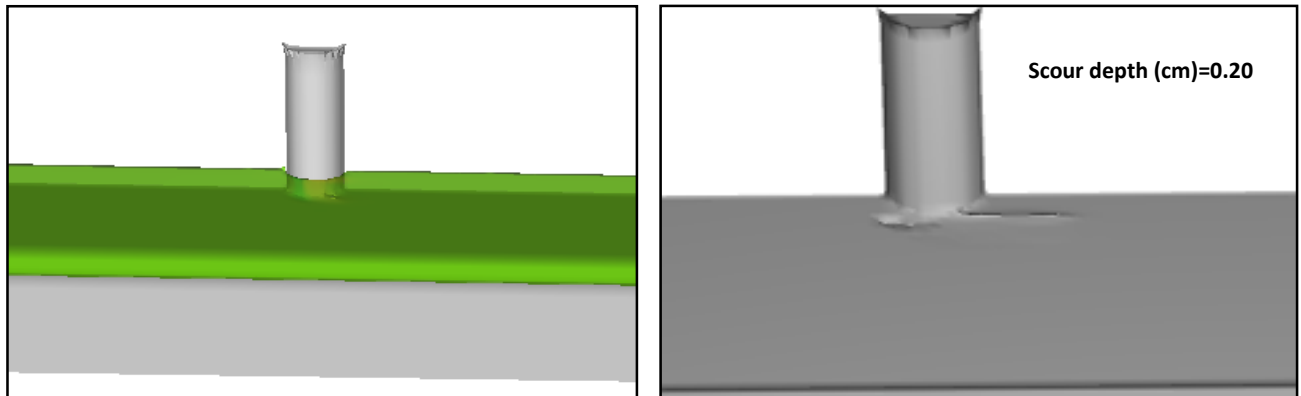
Figure (A-15): Scour depth around circular pier at y/b=0.20, V/V$_C$=1.00, b/B=0.11, Ks=1.00, Kθ=1.00 for run no.73

A.4- Scour depth at different rate of flow depth ratio b/B

Scour depth (cm)=2.50
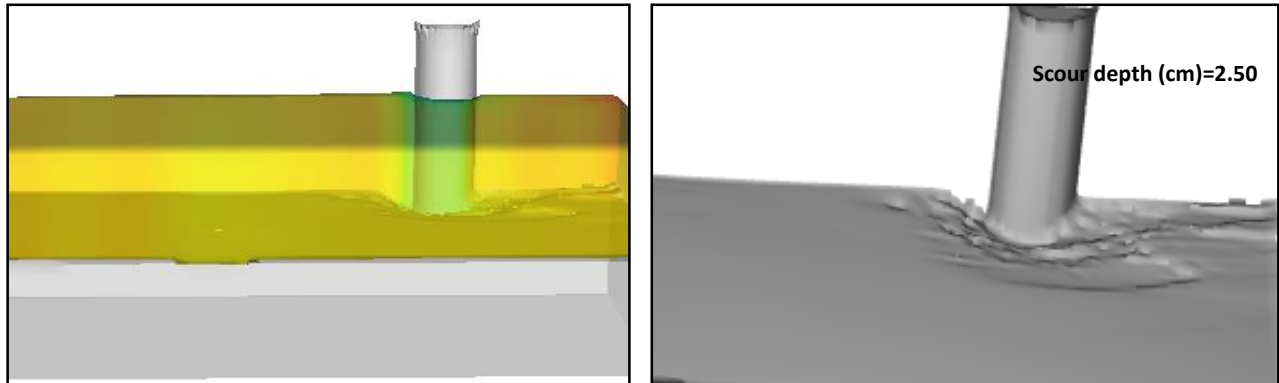
Figure (A-16): Scour depth around circular pier at b/B=0.11, y/b=0.98,
V/V$_C$=0.76, Ks=1.00, Kθ=1.00 for run no.37

Scour depth (cm)=2.10
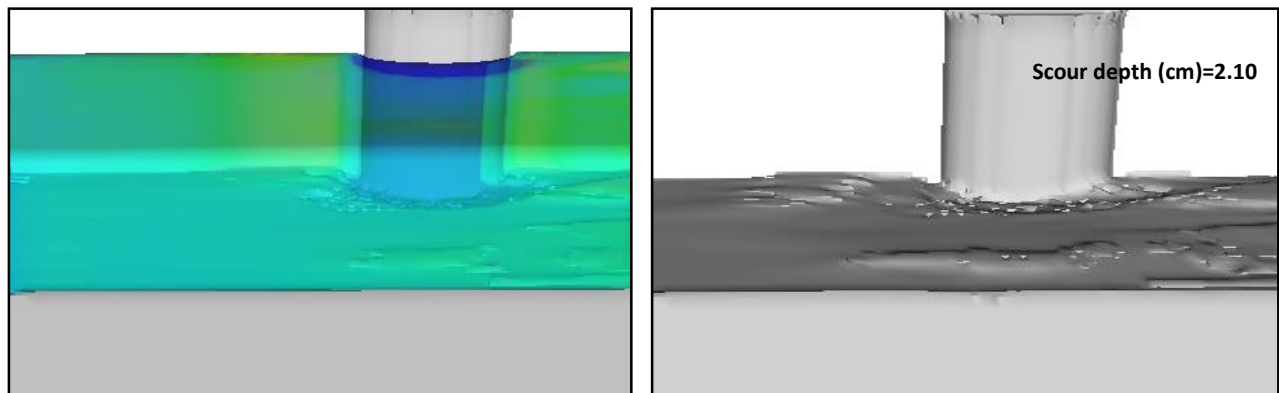
Figure (A-17): Scour depth around elliptic pier at b/B=0.11, y/b=0.98,
V/V$_C$=0.76, Ks=0.84, Kθ=1.00 for run no.38

Scour depth (cm)=3.30
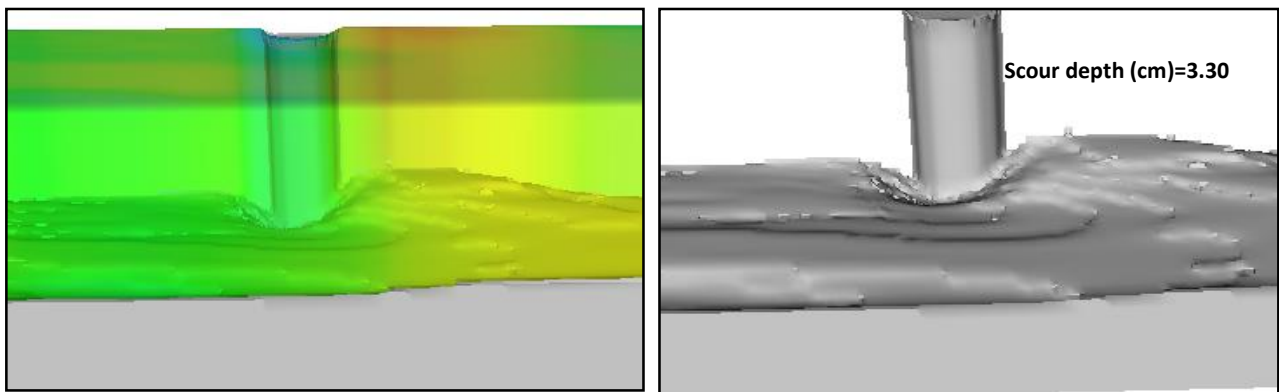
Figure (A-18): Scour depth around circular pier at b/B=0.15, y/b=2.95,
V/V$_C$=0.76, Ks=1.00, Kθ=1.00 for run no.91
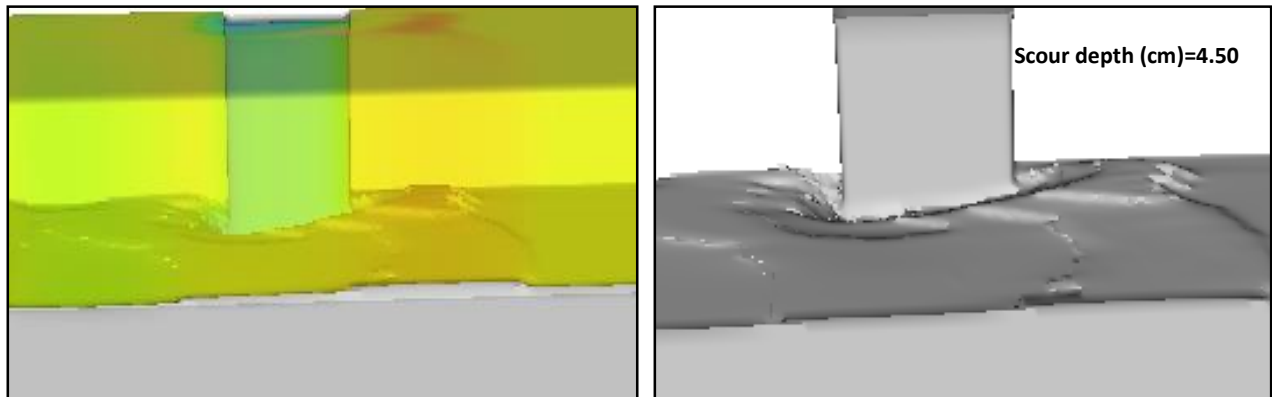
Figure (A-19): Scour depth around rectangular pier at b/B=0.15, y/b=2.95, V/V$_C$=0.76, Ks=1.26, Kθ=1.00 for run no.94
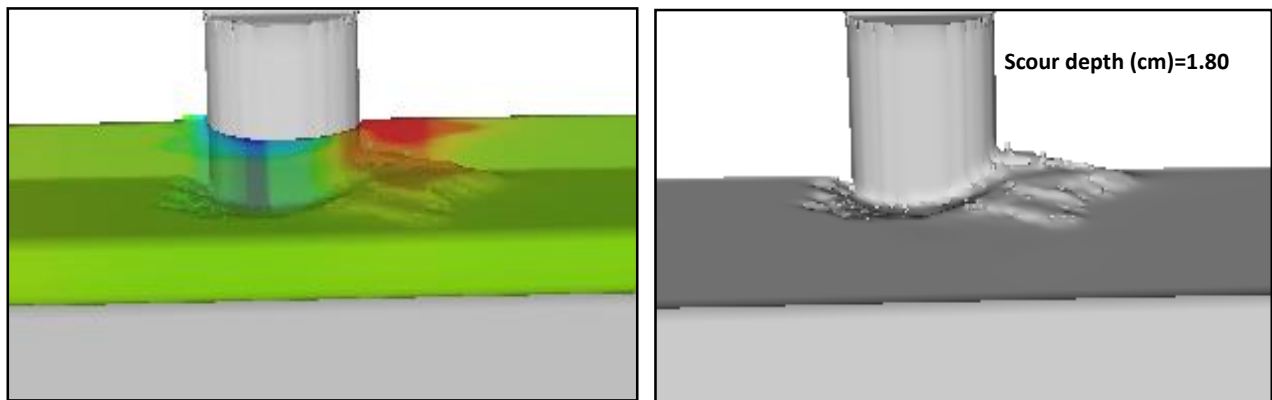
Figure (A-20): Scour depth around elliptic pier at b/B=0.15, y/b=0.98, V/V$_C$=0.55, Ks=0.84, Kθ=1.00 for run no.110
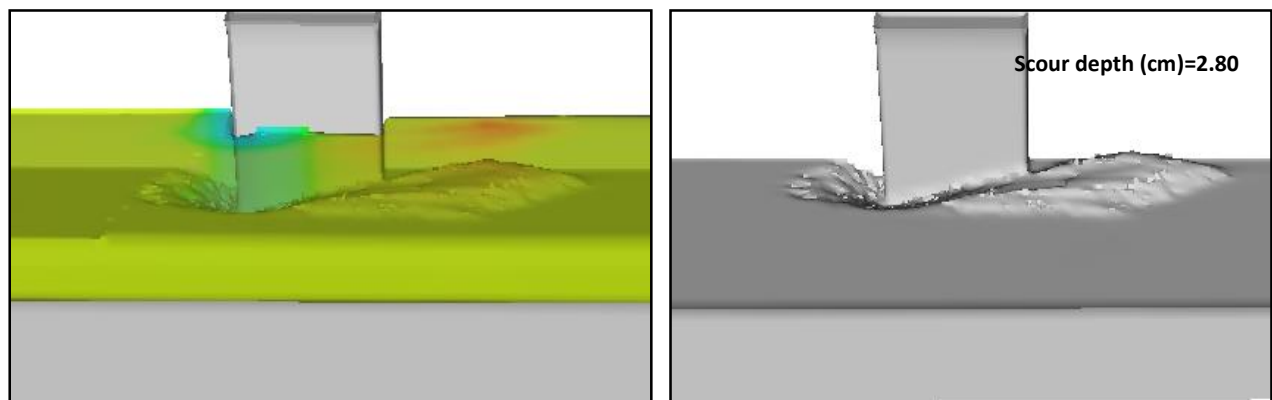
Figure (A-21): Scour depth around rectangular pier at b/B=0.15, y/b=0.98, V/V$_C$=0.55, Ks=1.26, Kθ=1.00 for run no.112

Scour depth (cm)=5.58
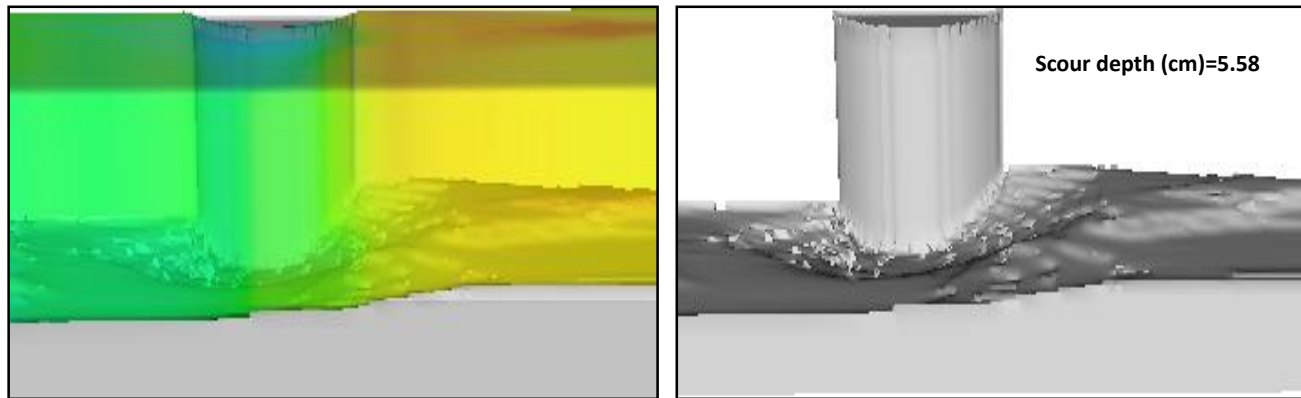
Figure (A-22): Scour depth around lenticular pier at b/B=0.2, y/b=2.95,
V/V$_C$=1.00, Ks=0.71, Kθ=1.00 for run no.185

Scour depth (cm)=6.81
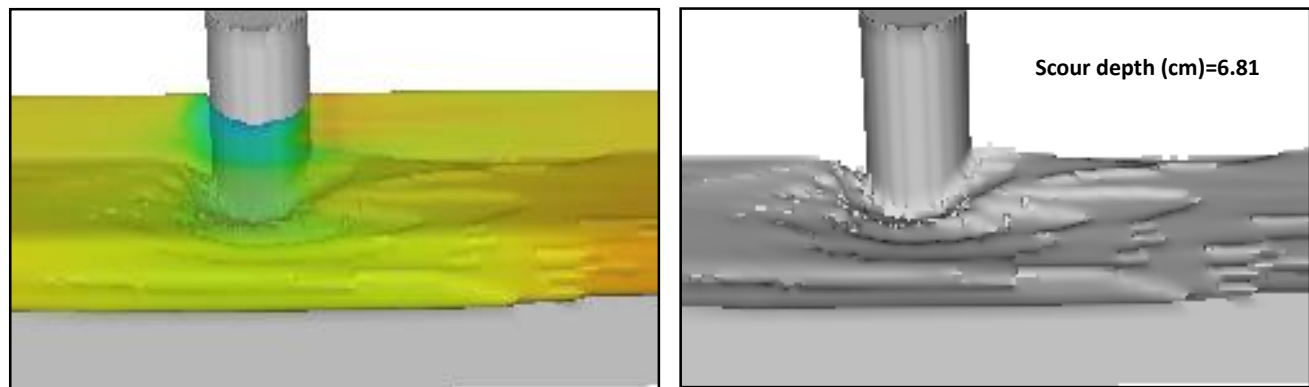
Figure (A-23): Scour depth around circular pier at b/B=0.2, y/b=0.98,
V/V$_C$=1.00, Ks=1.00, Kθ=1.00 for run no.208

A.5- Scour depth at different rate of angle of alignment θ°

Scour depth (cm)=4.20
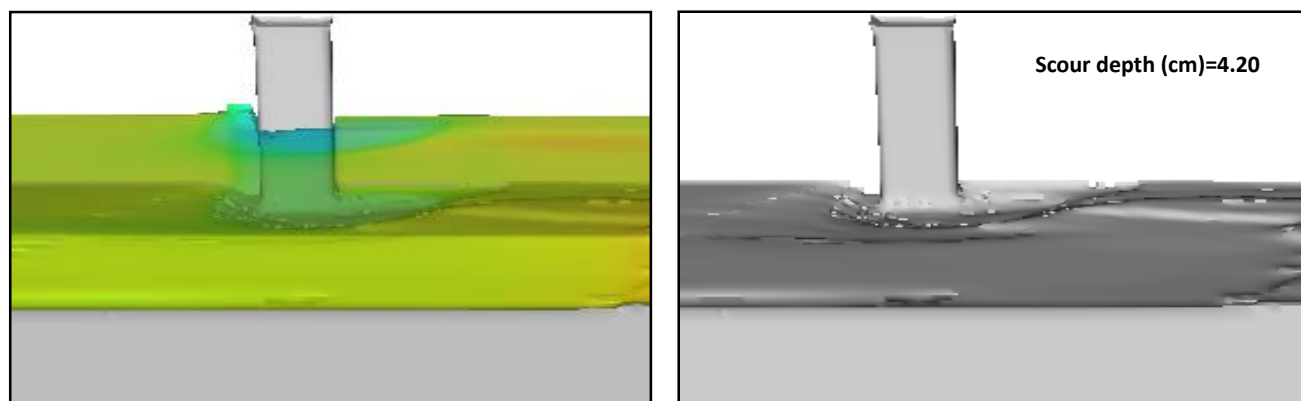
Figure (A-24): Scour depth around square pier at angle 0º of Kθ =1.00,
V/V$_C$=1.00, y/b=0.98, b/B=0.11, Ks=1.16 for run no.48
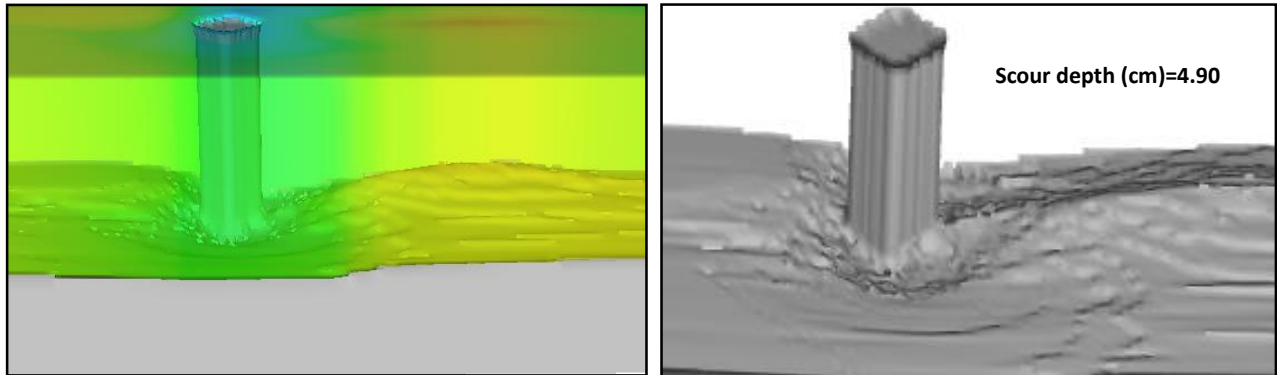
Figure (A-25): Scour depth around square pier at θ°=45 of Kθ =1.25, V/V$_C$=0.76, y/b=2.95, b/B=0.11, Ks=1.00 for run no.255
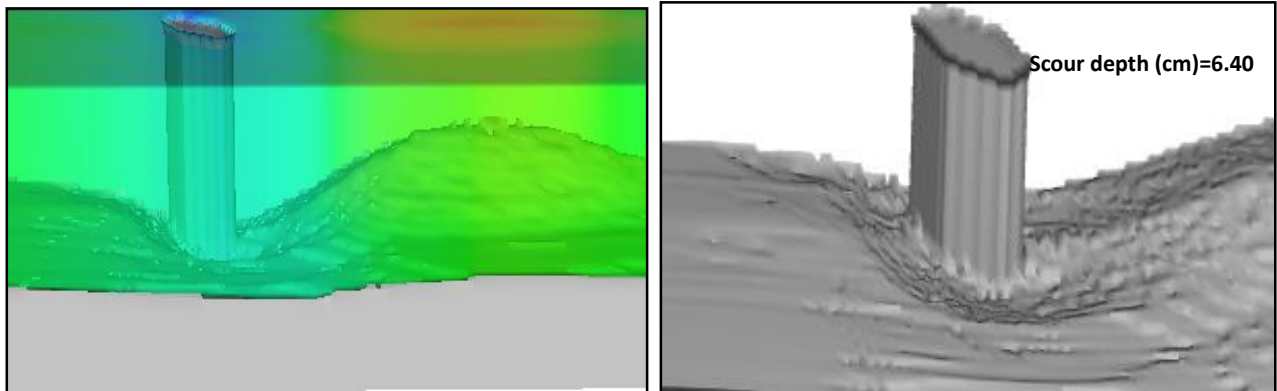

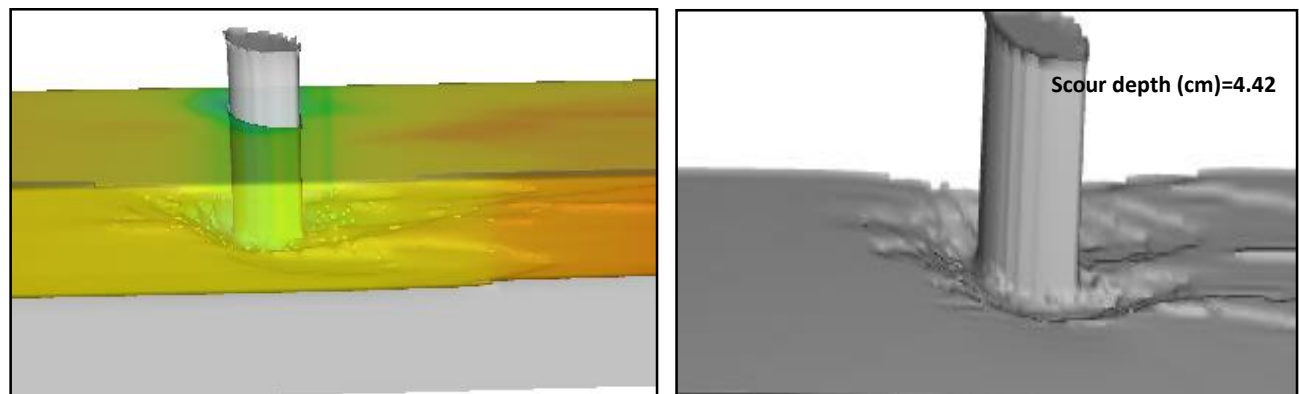Figure (A-26): Scour depth around hexagonal pier at θ°=45 of Kθ =1.63, V/V$_C$=0.76, y/b=2.95, b/B=0.11, Ks=1.00 for run no.260

Figure (A-27): Scour depth around lenticular pier at θ°=45 of Kθ =1.63, V/V$_C$=1.00, y/b=0.98, b/B=0.11, Ks=1.00 for run no.293
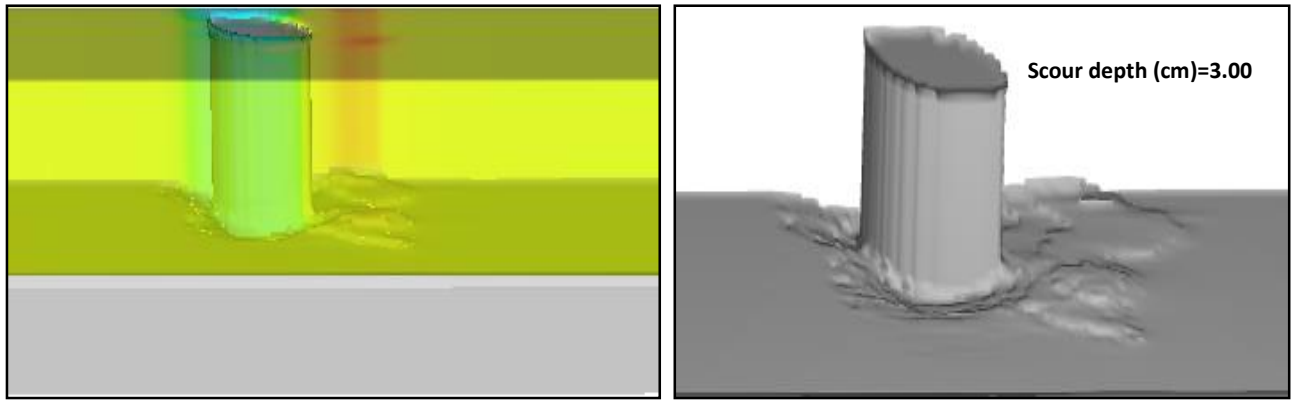
Figure (A-28): Scour depth around lenticular pier at θ°=30 of Kθ =1.50,
V/V$_C$=0.55, y/b=2.95, b/B=0.15 for run no.572

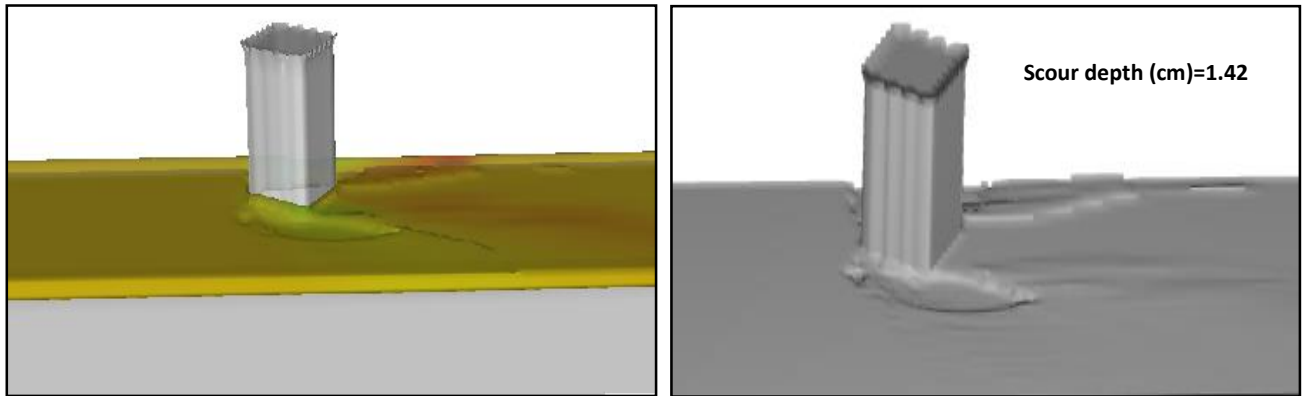Figure (A-29): Scour depth around square pier at θ°=30 of Kθ =1.23,
V/V$_C$=1.00, y/b=0.20, b/B=0.20, Ks=1.00 for run no.723

المستخلص

يعد الانجراف الموقعي (local scouring) حول دعامات الجسور أحد الأسباب الرئيسية لفشل الجسور في جميع أنحاء العالم ، مما يؤثر بشكل كبير على إجمالي تكاليف البناء والصيانة. اظهرت الابحاث التي أجريت على الانجراف الموقعي حول دعامات الجسور أنه لا يزال هناك نقص في فهم تأثيرات العوامل الرئيسية مثل شكل الدعامة على عمق الانجراف الموقعي.

أن الهدف الرئيسي من هذه الدراسة هو التحري عن تأثير شكل دعامة الجسر على عمق الانجراف لتحديد التصميم الهيدروليكي الأمثل الذي يحقق الحد الأدنى من عمق الانجراف . بالإضافة الى ذلك ، تم تطوير معادلة جديدة للتنبؤ بعمق الانجراف استنادا إلى المحددات التي تم الحصول عليها من التحليل البعدي من حيث عامل الشكل ،عمق المائع ,شدة التدفق ،عرض الدعامة وزاوية المحاذاة من خلال استخدام برمجه التعبير الجيني(GEP) و برنامج التحليل الاحصائي (SPSS) . تم استخدام اشكال مختلفة للدعامة في هذه الدراسه بما في ذلك الدائري, المربع, المستطيل, البيضوي, مستطيل برأس دائري, ثماني الاضلاع, سداسي الاضلاع, الحاد, العدسي او الأنسيابي لتقليل تأثير الانجراف حول الدعامة. تم الاستخدام في هذه الدراسة منهجية محاكاة تعتمد على ديناميكيا الموائع الحسابية (CFD) لحساب عمق الانجراف الموقعي حول دعامة الجسر باستخدام برنامج ال Flow-3D. لاختبار فعالية النموذج العددي ، تمت معايرة النموذج العددي لبرنامج Flow-3D مع البيانات التي تم الحصول عليها مختبريا من Melville 1975. وبعد عملية التحقق تم إجراء 729 محاكاة عددية لكل أشكال الدعامة بثلاث قيم مختلفة لشدة التدفق (0.55,0.76,1) V/V_C, ولنسب عمق المائع y/b (0.2,0.98,2.95), ولنسبة عرض الدعامة b/B (0.11, 0.15, 0.2) وبزاوية محاذاة (°0, 30°, 45°)، وتم اجراء كل المحاكاة العدديه في ترب رمليه غير متماسكة تحت ظروف الجريان الخالي من حمل الرسوبيات (clear-water).

أظهرت نتائج مقارنة النتائج العددية للتنبؤ بعمق الانجراف حول الدعامة الدائرية مع النتائج المختبرية لـ Melville 1975 ان النموذج العددي يتوافق بصوره جيدة مع النموذج المختبري بنسبة خطأ بين النموذجين العددي والمختبري لا تتجاوز 10٪. و كشفت نتائج الموديلات العدديه أن اعلى عمق للانجراف لوحظ حول شكل الدعامة المستطيله في حين اقل عمق للانجراف لوحظ حول الشكل العدسي للدعامة. اظهرت النتائج التي تم الحصول عليها من محاكاة اربعة اشكال للدعامة وهي الدائري, المربع, البيضوي والعدسي لهم نفس الحجم من الخرسانة ولهم نفس المساحة السطحية, انه تم ملاحظة اقل عمق للانجراف حول الدعامة عدسية الشكل بحوالي 70% اقل من الدعامة مربعه الشكل. بناءً على النتائج ، يمكن القول ان الشكل العدسي يوفر التصميم

الهيدروليكي الأمثل للدعامة. بالإضافة إلى ذلك ، اظهرت النتائج ان عمق الانجراف يزداد مع زيادة شدة تدفق عمق المائع, عرض الدعامة وزاوية المحاذاة.

استنادًا إلى نتائج المحاكاة, أدت المعادلة التي تم الحصول عليها من نموذج GEP على تنبؤ أفضل لعمق الانجراف مقارنة مع البرنامج الاحصائي SPSS مع معامل التحديد (R^2) وجذر متوسط مربع الخطأ (RMSE) 0.89 و 0.152 على التوالي . المعادلة التجريبية الناتجة للتنبؤ بعمق الانجراف مبنية على عامل الشكل ،عمق المائع ,شدة التدفق ،عرض الدعامة وزاوية المحاذاة. تشير نتائج تحليل الحساسية إلى أن عمق التدفق له تأثير كبير في التنبؤ بعمق الانجراف مقارنة بمعايير الإدخال الأخرى.

دراسة عددية لشكل الدعامة الأمثل للحصول على جسور آمنة

الرسالة مقدمة إلى

قسم الهندسة المدنية / كلية الهندسة في جامعة كربلاء كجزء من متطلبات نيل درجة الماجستير في علوم الهندسة المدنية (البنى التحتية)

من قبل

هالة قيس جلال

(بكالوريوس هندسة مدني 2016)

بأشراف

الاستاذ الدكتور

واقد حميد حسن

محرم (1441)

أيلول (2019)